

LEVEL

DC
NRL Memorandum Report 4506

10A103897

Cosmic Ray Effects on Microelectronics, Part I: The Near-Earth Particle Environment

J. H. ADAMS, JR., R. SILBERBERG, AND C. H. TSAO

Laboratory for Cosmic Ray Physics

SEP 8 1981

August 25, 1981



NAVAL RESEARCH LABORATORY
Washington, D.C.

Approved for public release; distribution unlimited.

81 9 08 246

Best Available Copy

(P) N
10
SECURITY CLASSIFICATION OF THIS PAGE (When Data Entered)

REPORT DOCUMENTATION PAGE		READ INSTRUCTIONS BEFORE COMPLETING FORM
1. REPORT NUMBER <i>(1) NRL-MF</i>	2. GOVT ACCESSION NO. <i>NRL Memorandum Report 4506-PN-1AD-A103 897</i>	3. RECIPIENT'S CATALOG NUMBER
4. TITLE (and Subtitle) COSMIC RAY EFFECTS ON MICROELECTRONICS, PART I: THE NEAR-EARTH PARTICLE ENVIRONMENT.		5. TYPE OF REPORT & PERIOD COVERED Interim report on a continuing problem.
6. AUTHOR(s) <i>J.H. Adams, Jr., R. Silberberg, and C.H. Tsao</i>		7. CONTRACT OR GRANT NUMBER(s) <i>(1) 25 111-824</i>
8. PERFORMING ORGANIZATION NAME AND ADDRESS Naval Research Laboratory Washington, D.C. 20375		9. PROGRAM ELEMENT, PROJECT, TASK AREA & WORK UNIT NUMBERS RR34-06-43; 42-1279-A1 & 42-0309-01
10. CONTROLLING OFFICE NAME AND ADDRESS Naval Electronic Systems Office of Naval Research Command, Arlington, VA 20380 Arlington, VA 22217		11. REPORT DATE August 25, 1981
12. MONITORING AGENCY NAME & ADDRESS (if different from Controlling Office) <i>(1) 25</i>		13. NUMBER OF PAGES 94
14. SECURITY CLASS. (of this report) UNCLASSIFIED		15. DECLASSIFICATION/DOWNGRADING SCHEDULE
16. DISTRIBUTION STATEMENT (of this Report) Approved for public release; distribution unlimited. <i>(1) 25 111-824</i>		
17. DISTRIBUTION STATEMENT (of the abstract entered in Block 20, if different from Report) <i>(1) 25 111-824 43</i>		
18. SUPPLEMENTARY NOTES		
19. KEY WORDS (Continue on reverse side if necessary and identify by block number) Cosmic rays Heavy ions Single-event upsets Solar flares Microelectronics Trapped radiation Soft errors Radiation belts Soft upsets		
20. ABSTRACT (Continue on reverse side if necessary and identify by block number) It has recently been recognized that a single intensely ionizing particle can alter the information stored in a modern semiconductor memory and possibly do permanent damage to the microelectronic circuit involved. Such particles are common in nature and abundant in space. This report describes the natural particle environment in which modern space-borne electronics must operate, and provides a simple but accurate empirical model of that environment.		

DD FORM 1 JAN 73 1473 EDITION OF 1 NOV 68 IS OBSOLETE
S/N 0102-014-6501

SECURITY CLASSIFICATION OF THIS PAGE (When Data Entered)

10
B
25 111-824

CONTENTS

1.0 Introduction	1
2.0 The Galactic Cosmic Ray Model	6
2.1 The Nucleonic Component of Cosmic Rays	6
2.2 The Relative Abundances of Cosmic Rays	8
2.3 Nuclei Heavier than Nickel	11
2.4 Cosmic Ray Electrons	12
2.5 Solar Modulation	13
2.6 The Analytic Model for Galactic Cosmic Rays	14
3.0 Particles from the Interplanetary Medium	33
3.1 Co-rotating Events	33
3.2 The Anomalous Component	33
4.0 Solar Flare Particles	37
4.1 The Sizes and Frequencies of Flares	37
4.2 Solar Proton Spectra	38
4.3 Solar Energetic Particle Composition	40
4.4 Recommendations	42
5.0 The Geomagnetic Cutoff	48
5.1 Methods for Computing the Cutoff	48
5.2 The Effect of Magnetic Storms	50
5.3 Recommended Procedure	51
6.0 Particles from the Magnetosphere	55
6.1 Protons	55
6.2 Alpha Particles	55
6.3 Heavy Nuclei	57
6.4 Other Particles in the Magnetosphere	61
7.0 Cosmic Ray Effects on Space-Borne Microelectronics	64
7.1 Cosmic Ray Transport Through the Spacecraft Walls	64
7.2 The Effects of Intense Ionization	65
7.3 Efforts to Reduce Cosmic Ray Effects	66
7.4 Shielding Against Cosmic Rays	66
7.5 The Relative Importance of the Various Components in the Near-Earth Particle Environment	68
8.0 Conclusions and Recommendations	71
8.1 Galactic Cosmic Rays	71
8.2 The Anomalous Component	72
8.3 Solar Flares	72
8.4 Trapped Particles	73
9.0 Acknowledgements	75
References	76
Appendix 1: The Analytic Model for the Charged Particle Environment	85

COSMIC RAY EFFECTS ON MICROELECTRONICS,
PART I: THE NEAR-EARTH PARTICLE ENVIRONMENT

1.0 Introduction

A number of ground-based experiments have recently shown that a single intensely-ionizing particle can change the logic state of modern electronic circuits of the kind used as memories on satellites. Soft errors (also called soft upsets or single event upsets) have been observed on more than a dozen satellites. The soft errors on three of these satellites have been conclusively attributed to single intensely-ionizing particles. Besides soft errors, single intensely ionizing particles have been shown, in laboratory experiments, to cause latchup and even to do permanent damage to the microcircuits.

Intensely-ionizing particles may be produced locally, in the electronic device itself, as a product of nuclear reactions or they may come directly from outside the spacecraft. Even when the intensely-ionizing particle is the product of a nuclear reaction, that reaction is usually initiated by a more lightly ionizing particle that came from outside the spacecraft.

The objective of this study is to begin addressing this problem by developing the tools needed to estimate the rate at which soft errors can be expected to occur on various spacecraft exposed to the natural space environment. The first step is to develop a model of the energetic particle environment near earth that is accurate and yet easy to use.

This report will be followed by additional reports. One will describe the way in which the earth's magnetic field has modulated the energy spectra of particles reaching any satellite. A second report will describe how the energy spectra and elemental composition of these particles are modified in passing through spacecraft walls to reach the electronic components inside. The results of these three reports can then be combined with measured or estimated operational cross sections for the various single-particle effects on microelectronics to compute their expected rates on various spacecraft.

This report describes simple analytic models for the energy spectra and elemental compositions of the various components of ionizing particle radiation in the vicinity of the earth that are as accurate as the data will allow. The models are based on an exhaustive review of the available data. From the length of this report, it can be seen that a substantial data base exists on the energetic particle environment. Even so there are deficiencies in the data base required to accurately estimate the rates of single particle effects.

This situation has led us to adopt the following philosophy in modeling the environment. Where the data base is adequate, the model gives "most-probable" spectra and compositions. When the component is variable, a worst case, at a 90 per cent confidence level, is given. In those cases where the data base is inadequate, we can only speculate what the conditions might be. Such speculation would lead us to construct credible worst-case models that are quite severe and therefore pessimistic from the spacecraft designers point of view. To avoid provoking undue expense in spacecraft design, we have adopted an optimistic philosophy. In cases where the data base is inadequate, we have modeled whatever data actually exist, ignoring the untested possibilities. This guarantees the user that his

spacecraft will actually experience an environment as severe as the one described here. The design effort expended by using this model will then not have been wasted. It is, of course, possible that some of the untested speculations may prove correct, leading to a far more hostile environment than described here. Until the necessary experiments can be carried out, the spacecraft designer must simply take some risks.

Spacecraft operating near earth may be bombarded by energetic charged particles that are trapped in the earth's radiation belts. Spacecraft may also be bombarded by cosmic rays, particles from solar flares and particles accelerated in the interplanetary medium, all of which come from great distances.

The contribution each component makes to the total particle flux bombarding a spacecraft is complicated by the presence of the earth's magnetosphere shown in Figure 1.1. The intensity, energy and elemental composition of the trapped radiation varies enormously with position in the radiation belts. To reach a spacecraft inside the magnetosphere, particles coming from great distances must penetrate the earth's magnetic field. Their ability to do so depends on their momentum divided by their electrical charge. The larger this ratio, the deeper they can penetrate.

In the models presented here, we will describe the trapped radiation as it is found in the radiation belts. The cosmic rays, solar flare particles and particles from the interplanetary medium will be described as they are found outside the magnetosphere in the interplanetary medium near the orbit of the earth. A later report will describe how these components are modulated prior to reaching the orbit of a satellite in the magnetosphere.

As pointed out in the beginning paragraphs of this introduction, it is the intensely-ionizing particles that cause single particle effects on microelectronics. The intensity with which a charged energetic particle ionizes matter varies approximately as the square of the particle's electrical charge divided by the square of its velocity. When a particle is ionizing intensely enough to produce a single particle effect directly, it will be far more effective in doing so than a particle that must produce a nearby nuclear reaction with an intensely-ionizing product. This difference in effectiveness is about 10^6 , so the energy spectra and elemental compositions of energetic particles in the natural environment are very important for the estimation of these effects.

The energy spectra presented here are differential energy spectra. They give the particle flux per unit energy as a function of the particle's energy. The units of energy are millions of electron volts per atomic mass unit (MeV/u) or billions of electron volts per atomic mass unit (GeV/u) (see Rossi, 1964, Appendix E for an explanation of electron volt). This way of expressing energy is useful because it means that particles with the same energy also have the same velocity regardless of their atomic mass. Many of the properties of the various elemental spectra are identical when this energy scale is used. The units of flux are particles per square meter - second - steradian - MeV/u ($m^2 \cdot sec \cdot ster \cdot MeV/u$). The steradian is a unit of solid angle.

The elemental composition of most of the energetic particle components is similar to the universal composition of matter as determined from the study of meteorites, the sun and the stars. Figure 1.2 shows the relative abundances of the elements in nature (Cameron, 1980). As can be seen in Figure 1.2 the elements are ~ 93.6 per cent hydrogen ~ 0.3 per cent helium and ~ 0.14 per cent elements carbon and heavier. Iron is about 5 per cent of oxygen and the elements beyond nickel are very rare. This is approximately the composition seen in solar flare particles, though the actual composition varies a lot from flare to flare. The galactic cosmic ray composition is qualitatively similar to Figure 2.1, but differs considerably in detail. The compositions of particles accelerated in the interplanetary medium and trapped in the magnetosphere are profoundly altered by special physical effects.

For those who do not have a background in space science, but wish to know more about the subject, we recommend, "Cosmic Rays" by Bruno Rossi (1964), "Space Physics" by Steve White (1970), and "Introduction to Space Science" by Willmont Hess and Gilbert Mead (1968).

For users of this report who are interested only in the model itself, the details have been collected in Appendix 1. This appendix gives all the equations required to compute the flux levels expected under various conditions in the near-earth environment. Only the trapped proton environment has not been included, since it has already been described by the AP-8 model of Sawyer and Vette (1976).

Sections 2.0, 3.0 and 4.0 present the data base for particles in the interplanetary medium and describe how this environment has been modeled.

Section 5.0 discusses the geomagnetic cutoff and describes, qualitatively, how it modifies the particle spectra from the interplanetary medium. The second report of this study will describe an accurate method for modulating the interplanetary spectra to obtain the orbit-averaged spectra incident on any spacecraft in any orbit.

The composition of particles trapped in the earth's magnetosphere is described in Section 6.0. The heavy ion composition of trapped radiation at energies above 10 MeV/u is the least well known part of the particle environment. The few measurements that exist show heavy ion fluxes higher than those in the interplanetary medium.

Section 7.0 discusses, in a qualitative way, how shielding alters the particle spectra. Cosmic ray transport theory in condensed media will be the subject of a third report. This section also reviews the work that has been published to date on soft errors and gives a general discussion of the environment and its effects on electronics in various orbits.

The status of the data base for this first part of the study is reviewed in Section 8.0 and recommendations are made for additional work that would allow the particle environment model to be improved.

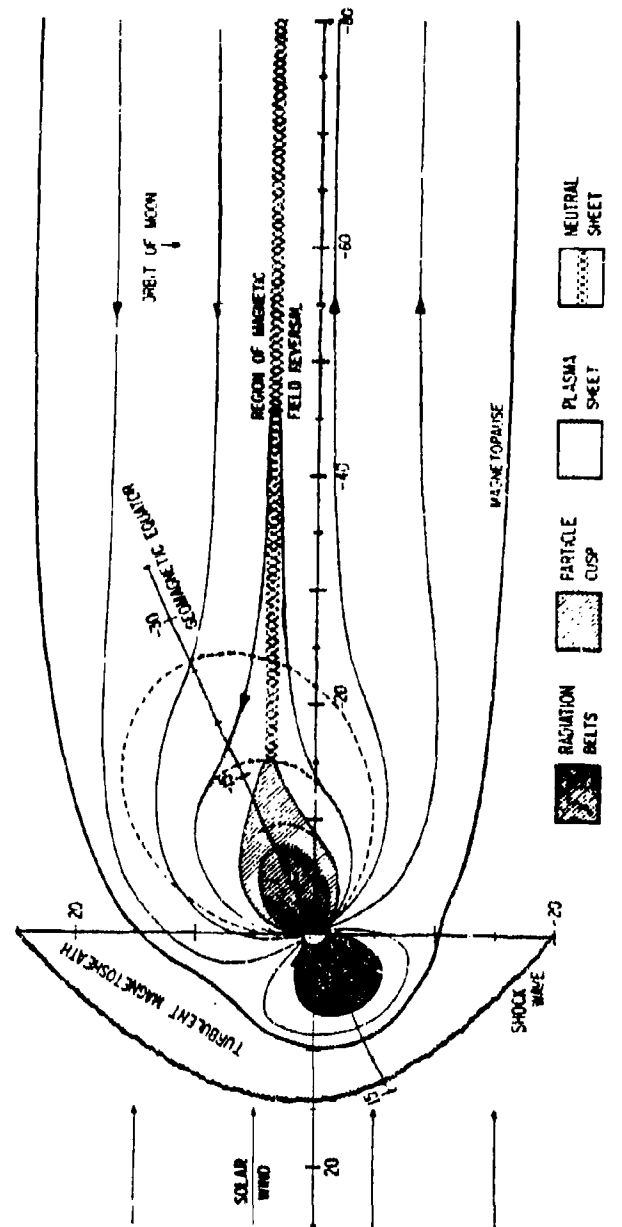


Fig. 1.1 — A cross section of the earth's magnetosphere in the noon-midnight plane perpendicular to the geomagnetic equatorial plane. The locations of the radiation belts and several other magnetospheric features are shown (taken from White, 1970).

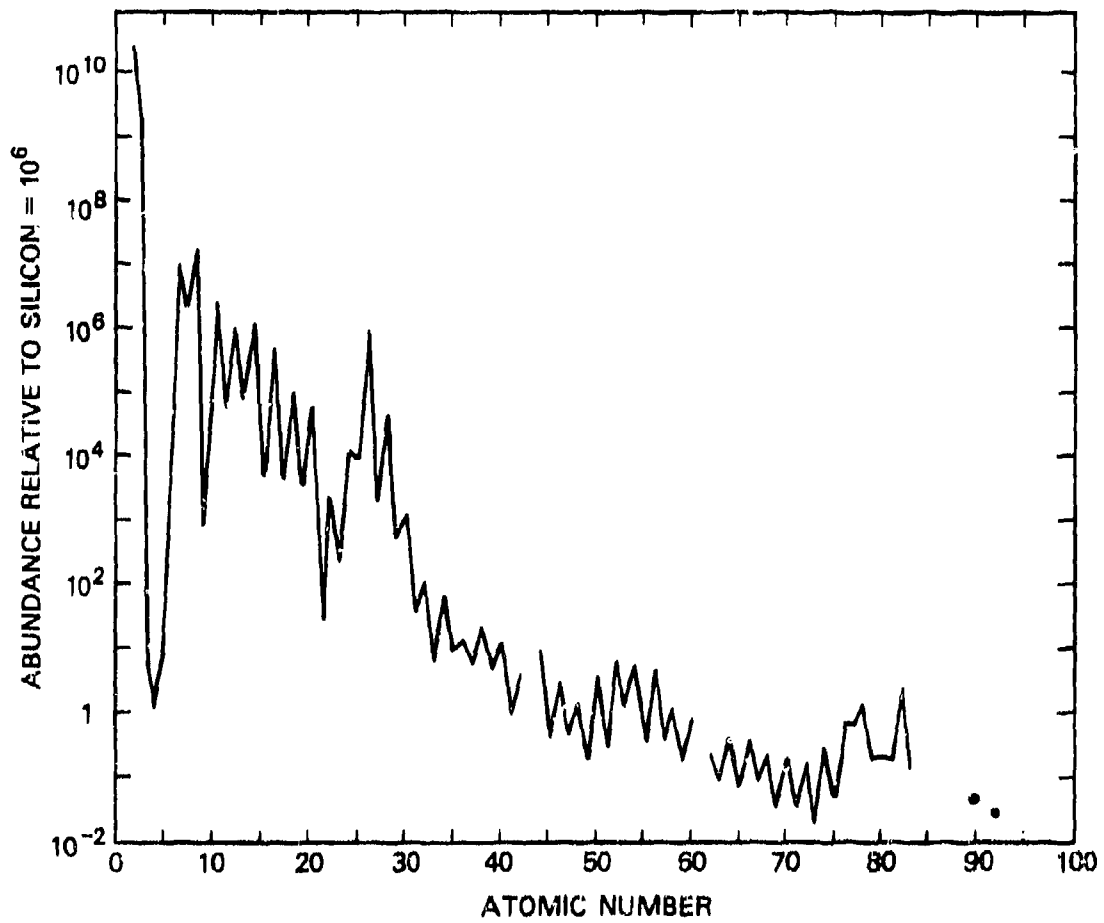


Fig. 1.2 — The universal abundance of the chemical elements in nature relative to silicon $\approx 10^6$. These results are obtained from studies of meteorites, our sun and other stars (taken from Cameron, 1980).

2.0 The Galactic Cosmic Ray Model

Most of the energetic charged particles usually found in the vicinity of earth are cosmic rays, particles which come from outside our solar system. The sources of these cosmic rays are as yet unknown. The existing evidence suggests that, except for the highest energies, these particles come from sources within our galaxy. Cosmic rays arriving in our solar system consist of the nuclei of all the elements in the periodic table and electrons.

2.1 The Nucleonic Component of Cosmic Rays

By studying the differences between the chemical composition of nucleonic cosmic rays and material in our universe generally, we have been able to learn some things about the cosmic ray population in our galaxy. As cosmic rays travel through the galaxy, they occasionally collide with nuclei of interstellar gas. The resulting nuclear reactions modify the composition of cosmic rays. A detailed recent estimate of these modifications has been given by Silberberg et al (1976). These authors have found that, by assuming cosmic rays traverse $\sim 5.5 \text{ g/cm}^2$ of interstellar gas on the average, they can account for almost all the differences in chemical composition. These results are further supported by the measured cosmic ray abundances of electron-capture isotopes such as ^{10}Be that could only have been produced in collisions with interstellar gas (see for example, Wiedenbeck and Greiner, 1980). By measuring the cosmic ray abundance of the radioactive isotope ^{10}Be ($T_{1/2} = 1.6 \times 10^6$ years), Wiedenbeck and Cretner (1980) have shown that cosmic rays reaching earth have wandered about in our galaxy for $\sim 8 \times 10^6$ years, on the average. Their measurements are consistent with the results of a number of earlier investigators.

These results and others have led to a model for cosmic ray confinement in the galaxy. The standard model assumes that the galaxy is uniformly populated with cosmic ray sources. These sources emit cosmic rays into the galaxy where they diffuse through the random magnetic fields of the galaxy, but are contained, with some leakage at the galactic boundary.

In the context of the standard model, Figure 2.1 shows how the cosmic ray composition is transformed by fragmentation as cosmic rays wander through the galaxy on their way to earth, Adams, et al. (1980a). The abundances at earth are plotted on a scale relative to arriving carbon = 100. The abundances are broken down according to the fraction that have survived collisions (open bars) with interstellar gas to reach us and those that were produced by collisions of heavier cosmic rays with interstellar gas (filled bars). Also shown are the inferred source abundances (dashed bars). It should be noted that about half of the heavy ($Z > 6$) cosmic ray nuclei have collided with interstellar gas nuclei.

The most abundant element in cosmic rays is hydrogen. Figure 2.2 shows the differential energy spectrum of hydrogen (for the most part protons).

The data shown in this figure are only the most recent measurements of cosmic ray protons. They are consistent with the much larger number of measurements carried out in the 50's and 60's. We have selected the data presented below 10^3 MeV to show only those measurements made during periods of maximum and minimum solar activity. The smooth solid curve is an analytic function fit to the data.

At the highest energies, the proton spectrum has the mathematical form of a power law, i.e. $dJ/dE \sim E^{-\alpha}$, with a spectral index, $\alpha \sim 2.75$. Power law spectra can be produced by particle acceleration in random moving magnetic fields as shown by Fermi (1949). The conditions for Fermi acceleration occur in a variety of astrophysical settings. We believe that outside the solar system, cosmic rays obey a power law to much lower energies than shown in Figure 2.2. The deviation from a power law below 5000 MeV/u in Figure 2.2 is largely due to solar modulation. The power-law fit is better in the case of a rigidity spectrum; some of the deviation is due to the transformation from rigidity to kinetic energy. To reach the vicinity of earth, cosmic rays must "swim" upstream in the solar wind. The process of diffusion inward against the outward-flowing solar wind (see Webb and Gleason, 1980; Jokipii, et al. 1977; Fisk, 1976; Jokipii, 1971) reduces the energy of the cosmic rays an average ~ 300 -400 MeV/u. It also attenuates the flux arriving near earth in an energy dependent way. The amount of solar modulation depends on the general level of solar activity. When the sun is quiet and especially during the minimum of the 11-year solar activity cycle, cosmic rays have the easiest access to the earth's orbit. These periods account for the upper branch of the spectrum in Figure 2.2. The lower branch corresponds to a quiet (no flares) period during the maximum of the 11-year cycle. Solar modulation is a complex subject and still an area of active research. We will describe our model for dealing with it in a later section.

At the lowest energies shown in Figure 2.2, the cosmic ray flux varies considerably even when no large solar flare is in progress. These variations take the form of short term increases above a lower limit that varies slowly with the solar cycle. These increases are due to small solar flares, flares poorly connected to the earth (i.e. on the backside of the sun) and particles accelerated by the solar wind in co-rotating interaction regions (CIR) in the interplanetary medium (to be discussed in section 3.0).

These variations have been observed on IMP-8, an interplanetary probe orbiting the earth at 24 to 26 earth radii. Figure 2.3 shows six-hour averages of the proton flux observed on IMP-8 (Pyle, 1981) as a function of flux level. These protons had energies between 11.24 MeV and 29.75 MeV and the data span the period from Oct 30, 1973 to July 2, 1980. The most common flux level measured was in the range of the galactic cosmic ray background (CCR) and corresponds to the range between the solar minimum and solar maximum spectra in Figure 2.2. The tail-off in measurements below this flux level is due to temporary increases in solar modulation called Forbush Decreases (Forbush, 1938). Above the flux-level of galactic cosmic rays, there is a long tail extending up for many orders of magnitude. The smallest of these increases is due to the addition of protons from co-rotating interaction regions, Fan, et al. (1965) (also discussed in section 3.1) or small solar flares. Flux levels observed between 3 and 60,000 protons/m²ster sec MeV/u are due to medium-size flares or larger ones that were poorly-connected to IMP-8 by the interplanetary magnetic fields. The flux levels above this range are due to large flares which are treated separately in section 4.0. Also shown in Figure 2.3 is a 90 per cent confidence level, that is a flux level which was exceeded in only 10 per cent of the six-hour intervals.

Figure 2.2 shows a worst case proton spectrum (with 90 per cent confidence), based on four energy intervals spanning the range $11.24 \text{ MeV} \leq E \leq 94.78 \text{ MeV}$.

2.2 The Relative Abundances of Cosmic Rays

It would be convenient to simply scale the hydrogen spectrum, Figure 2.2, according to the ratio of hydrogen with respect to the other elements. Unfortunately the ratio of hydrogen to the other elements depends on particle energy and the level of solar modulation. Basically, this is because the charge to mass ratio for hydrogen is ~ 1 while it is ~ 0.5 for the other elements. This leads to different responses of the spectra to magnetic rigidity dependent and velocity dependent phenomena. It is better to treat hydrogen as a special case and proceed to helium.

The helium differential energy spectrum is shown in Figure 2.4. The data points shown in this spectrum are only a representative sample of the data we examined. The density of points plotted precluded the identification of each data point with its author. To avoid cluttering the figure we have shown error bars on only a sampling of the data points. The data shown come from measurements made throughout the solar cycle, though we included as many data points as possible near solar maximum and minimum. The helium data we have used in the figure came from Ryan et al. (1972), Smith et al. (1973), Verma et al. (1972), Anand et al. (1968), Ormes and Webber (1965), Von Rosenvinge et al. (1969), Webber et al. (1973a), Fan et al. (1965), Balasubrahmanyam et al. (1965), Freier and Waddington (1965), Hofmann and Winckler (1966), Cleghorn et al. (1971), Leech and O'Gallagher (1978), Webber and Lezniak (1973), Bhatia et al. (1977), Rygg and Earl (1971), Webber and Ormes (1968), Badhwar et al. (1969), Ormes and Webber (1968), Balasubrahmanyam et al (1967), Mason (1972) and Garcia-Munoz et al. (1975), though the data of other authors was also consulted. The smooth solid curve is from an analytic function we have fit through the data points.

As in the case of the proton spectra discussed earlier, the helium flux levels at low energies are sometimes measured to be considerably different from those predicted by the analytic spectral functions in Figure 2.4. Figure 2.5 shows 6-hour averages of the helium flux measured on IMP-8, (Pyle, 1981). The helium nuclei had energies of $10.9 \text{ MeV/u} < E < 25.36 \text{ MeV/u}$, and the data set spans the same period as the proton data shown earlier.

During most of the period covered by these observations, the low energy helium spectrum was dominated by the addition of anomalous component (to be discussed later in section 3.2). This accounts for the location of the most common flux level measured in this period. Lower flux levels were measured after the spring of 1978 when the anomalous component no longer contributed to the flux near earth. These two conditions are smeared together by Forbush decreases.

As in the case of protons the enhanced flux levels are the result of particles accelerated in co-rotating interaction regions (CIR's) and flares of varying sizes.

Figure 2.4 shows a worst case spectrum (with a 90 per cent confidence level). This spectrum is chosen so that fluxes above this level are observed only 10 per cent of the time. These data are based on four energy intervals between 10.9 MeV/u and 94.81 MeV/u.

Comparing Figures 2.2 and 2.4 we see that the cosmic-ray He abundance is ~ 15 per cent of the H abundance in the energy range 200-700 MeV/u, and ~ 5 per cent above 10^4 MeV/u. Helium is the best element to choose for measuring the differential energy spectrum because it is distinct from all the singly charged particles (i.e. protons, electrons, muons, and pions all have one charge); it is plentiful; and it has a charge to mass ratio similar to the heavier elements.

As mentioned in Section 2.1, cosmic rays spend $\sim 10^7$ years diffusing around the galaxy and being broken up in collisions with the interstellar gas. Not surprisingly, this diffusion process is energy dependent and the higher energy cosmic rays have not travelled as far, or as long as the lower energy ones. This means that, at higher energies, there will be fewer arriving secondaries and more surviving primordial cosmic rays.

Cosmic ray helium is mostly surviving primordial material in the context of Figure 2.1; only ~ 10 per cent of He is secondary. This places it in the same class with hydrogen, carbon, oxygen, neon, magnesium, silicon, sulfur, calcium and iron; a list which includes the most abundant nuclei. We would expect, as Figure 2.6 shows, that the helium to carbon plus oxygen ratio is nearly independent of energy at 21 + 2 for the 1-5 GeV/u range.* Figure 2.7 (from Caldwell, 1977) shows, based on less data, that the ratio of (neon + magnesium + silicon)/helium does not vary much with energy. Figure 2.8 however shows that the Fe/He ratio is energy dependent. To some extent, this merely reflects the relatively larger fraction of surviving Fe at high energies. In this way, the ratio can increase by a factor of ~ 3 as can be inferred from Figure 2.1. The Fe/He ratio could increase even more, if the source spectra of Fe and He differ as well. It appears that Fe will have to be treated separately from helium. Figure 2.9 shows the differential energy spectrum of Fe. The data base for the Fe spectrum is rather limited. Figure 2.9 shows all the published data for iron from 10 MeV/u to 100 MeV/u. Between 100 MeV/u and 10^3 MeV/u there is an adequate set of measurements during solar minimum conditions, but there are no published measurements during solar maximum (experiments are in progress at NRL and elsewhere to obtain these data). For the present, we have used the general shapes of the solar maximum and minimum helium spectra as a guide to obtain the smooth solid curve shown in Figure 2.9. By analogy with the flux enhancements found for helium, we have suggested a worst case spectrum for iron shown as a dashed line.

The differential energy spectra of all the elements between helium and nickel will be obtained by scaling the helium or iron spectra. Figure 2.10 shows the data on elemental composition of lithium through sulfur, normalized to helium = 1000. The data in Figures 2.6 and 2.7 together with

*If the He, C and O source spectra are identical, this ratio is ~ 15 for a path length, $X < 1 \text{ g/cm}^2$, i.e. for $E > 50 \text{ GeV/nucl}$. and may go to ~ 23 for $X \sim 8 \text{ g/cm}^2$, which is plausible at energies of 200 to 600 MeV/u. We have adopted a ratio of 21, for the complete integral energy spectrum.

that of Juliusson (1974), Lezniak and Webber (1978), Orth et al (1978) and Caldwell (1977) show that the ratios of C, O, Ne, Mg, and Si to He are approximately independent of particle energy. This is to be expected since as Figure 2.1 shows these nuclei are principally surviving primordial material. Table 2.1 shows the relative abundances we have adopted for these elements as well as sulfur.

TABLE 2.1 The Elemental ratios for Elements having Helium-like and Iron-like Spectra Respectively

Element	Ratio to He	Element	Ratio to Fe
C	2.5×10^{-2}	Ca	2.3×10^{-1}
O	2.3×10^{-2}	Co	6.0×10^{-3}
F	4.1×10^{-4}	Ni	4.8×10^{-2}
Ne	3.5×10^{-3}		
Na	7.0×10^{-4}		
Mg	4.7×10^{-3}		
Al	8.3×10^{-4}		
Si	3.5×10^{-3}		
P	2.0×10^{-4}		
S	7.4×10^{-4}		

Figure 2.11 shows the energy dependence of the ratio of $(Li + Be + B)/He$. Since all three elements Li, Be and B are entirely secondary, we believe that each of them displays this energy dependence. Table 2.2 shows the ratios $Li/(Li + Be + B)$, $Be/(Li + Be + B)$ and $B/(Li + Be + B)$. Using these ratios, we can scale Figure 2.11 to obtain the ratios Li/He , Be/He and B/He as a function of energy. The differential energy spectra of these elements can then be obtained from Figure 2.4.

The ratio N/He is shown in Figure 2.12. It is also clearly energy dependent, but in a different way. Figure 2.12 can be used to scale Figure 2.4 to obtain the nitrogen differential energy spectrum.

From Figure 2.1, we can guess that F, Na, Al and P will also have energy dependent ratios relative to He. The available experimental data (see Orth et al., 1978; Juliusson, 1974; and Lezniak and Webber, 1978) are not of sufficient accuracy to define this energy dependence, so we will use constant ratios. The adopted values are shown in Table 2.1

Figure 2.13 shows the ratios of the elements $17 \leq Z \leq 25$ to Fe as a function of energy. While this ratio is energy dependent, it's not clear

that all the elements in the numerator display this dependence. Figure 2.1 shows that calcium is mostly primordial material, we would therefore expect Ca/Fe to be independent of energy. The abundances of the elements Cl through Ni are shown in Figure 2.14 normalized to Fe = 100. The adopted value for Ca/Fe is shown in Table 2.1

The adopted ratios, at low energies, of the other elements in the $17 \leq z \leq 25$ range to the sum of the elements in that range are shown in Table 2.2. These ratios are used to scale the energy dependent ratio in Figure 2.13 so as to obtain the ratios Cl/Fe, etc. which in turn are used to scale the Fe spectrum, Figure 2.9, to the spectra of these elements.

TABLE 2.2 The Elemental Ratios Required to obtain the Individual Elemental Spectra from Figures 2.11 and 2.13 Combined with Figures 2.4 and 2.9 respectively.

Ratio	Relative Abundances
Li/(Li + Be + B)	0.33
Be/(Li + Be + B)	0.175
B/(Li + Be + B)	0.50
Cl/(17 \leq z \leq 25)	0.07
Ar/(17 \leq z \leq 25)	0.13
K/(17 \leq z \leq 25)	0.09
Sc/(17 \leq z \leq 25)	0.05
Ti/(17 \leq z \leq 25)	0.14
V/(17 \leq z \leq 25)	0.07
Cr/(17 \leq z \leq 25)	0.14
Mn/(17 \leq z \leq 25)	0.10

2.3 Nuclei Heavier than Nickel

The galactic cosmic rays consist of every element in the periodic table. So far we have only dealt with the first 28, which are the most abundant. The abundances of the remaining elements relative to ^{106}Fe are shown in Table 2.3, (Adams, et al., 1980b).

TABLE 2.3 Abundances of Trans-iron Nuclei in Galactic Cosmic Rays

Atomic Number	Relative Abundance
26	10^6
$29 \leq Z \leq 34$	1.7×10^3
$35 \leq Z \leq 39$	1.7×10^2
$Z \geq 40$	8×10^1

For the purposes of this particle environment model, these very rare, but very damaging nuclei will be ignored. It should be noted, however, that should a microelectronic component be struck by one of these rare nuclei, an enormous amount of charge would be liberated, leading to a soft error even in devices commonly thought to be insensitive to this effect!

2.4 Cosmic Ray Electrons

There appear to be two plausible methods by which electrons can produce soft errors. The first is by directly depositing enough energy in the critical volume to produce the required critical charge. The second is by producing bremsstrahlung photons that, in turn, undergo photo-nuclear interactions with the silicon in the device.

We will consider the direct method first. Electrons deposit energy most densely near the end of their range. Because of their low rest mass, electrons undergo large angle scattering before their stopping power has risen much above its minimum value. This causes the practical range (displacement distance) of a stopping electron to be much shorter than its path length with the result that the electron deposits all its energy in a relatively small volume. The practical range of an electron in aluminum is given by:

$$r = 5.37 \times 10^{-1} E [1 - 0.9815/(1 - 3.123E)] \text{ g/cm}^2 \quad (2.1)$$

where E is in MeV (see Klobetich and Katz, 1968). Without introducing much error we may use this equation for silicon and compute the electron energy corresponding to any practical range. If this practical range is taken to be the diameter of a collection volume, then the corresponding energy is roughly the energy one might expect an electron to deposit in that volume. Using 3.6 eV per electron-hole pair, we can estimate the charge, Q, that the electron produces.

Figure 2.15 shows Q in electron-hole pairs as a function of the mean device diameter. This figure suggests that devices such as the 256K CCD described by Ziegler and Lanford (1979) will have soft errors due to stopping electrons. It should be noted that these need not be cosmic ray electrons; trapped electrons, air shower electrons and electrons from terrestrial γ -ray interactions would be equally effective!

While electrons seem to be capable of producing errors directly in devices sensitive to $< 10^4$ electron-hole pairs, they are unable to produce

errors when $> 10^5$ electron-hole pairs are required. Devices being considered for satellite applications are much less sensitive than 256K CCD's and cannot be directly upset by stopping electrons.

The second way in which electrons can cause errors is effective for less sensitive devices. Electrons must produce photons that, in turn, undergo $\text{Si}(\gamma, n)$, $\text{Si}(\gamma, p)$, or $\text{Si}(\gamma, \alpha)$ reactions in the devices. Because of the thresholds for these reactions, electrons with energies below 20 MeV will not cause these reactions. Webber (1973) has reviewed the cosmic ray electron differential energy spectra. He shows that the electron flux is comparable to the proton flux at 10 MeV, but falls rapidly to $\sim 10^{-2}$ of the proton flux at 100 MeV. Clearly, low energy protons produced by electrons will always be out-numbered by cosmic ray protons. As was shown in section 2.2, the alpha flux is ~ 15 per cent of the proton flux, so electron-produced alpha particles will always be overwhelmed by cosmic ray alphas.

In general, we conclude that low energy electrons (< 20 MeV) will not cause errors in the relatively insensitive components considered for satellite applications. Higher energy electrons can cause errors by the three stage process described above, but this process will be important only if the electron flux is enormously larger than the elemental flux.

2.5 Solar Modulation

As can be seen in Figures 2.2, 2.4, and 2.9, the differential energy spectra are spread between two extremes below $\sim 10^3$ MeV. This is due to solar modulation of the differential energy spectra incident on the solar cavity and depends on the level of solar activity.

Figure 2.16 shows the annual average cosmic ray flux for the past four decades, measured for most of that period by the neutron monitor at Deep River (Rao, 1972, and Ahluwalia, 1979). This monitor detects hadrons, primarily neutrons, which are secondary products of cosmic rays incident on the atmosphere. In this way it measures the cosmic ray flux at earth continuously. The valleys in 1947, 1958 and 1969 correspond to maxima in solar activity. The detailed shape of the curve over several solar cycles is quite variable, though crudely sinusoidal.

To estimate the low energy spectra at any time in the past, it is best to peg the modulation level by the measured intensity in experiments carried out at that time or, at best another time when the solar neutron monitor levels were similar. The solar modulation level in the near future may also be predicted by extrapolating the present solar neutron monitor level, using a sine curve with the same period as that shown in Figure 2.16. This method is probably only reliable for predictions less than one year into the future.

In modeling the spectra of cosmic rays for satellite planning, we must be able to predict the level of solar modulation years into the future. It seems that a simple sine function:

$$M = A \sin W(t-t_0)+B \quad (2.2)$$

is the best choice. The function, eq. (2.2) with $W = 2\pi/10.9$ years = 0.576/year and $t_0 = 1950.06$ is shown as the smooth curve in Figure 2.16.

The values of A and B were chosen to best fit the data in Figure 2.16. As we can see, the cosmic ray flux is quite variable from one solar cycle to the next, and only crudely predicted by eq. 2.2. The Deep River neutron monitor responds mostly to very energetic cosmic rays, so the amplitude of the solar cycle variation is much greater at lower energies (see Figure 2.2, 2.4 and 2.9), and probably less predictable. We feel that our present inability to predict the level of solar modulation in the future is the principal source of uncertainty in the estimates of future cosmic ray flux levels below ~ 1000 MeV/u.

2.6 The Analytic Model for Galactic Cosmic Rays

In the preceding sections we have discussed the nature of the cosmic ray energy spectra and chemical composition. In this section we present a simple analytic recipe that may be used to estimate the differential energy spectrum of each of the first 28 elements in cosmic rays between 10 and 10^5 MeV/u.

The solid curves in Figures 2.2, 2.4 and 2.9 are chosen to form an envelope around the data at low energies and blend to a single curve at high energies. The analytic form of these is:

$$F(E,t) = A(E)\sin W(t-t_0) + B(E) \text{ in particles/m}^2\text{ster.sec.MeV/u} \quad (2.3)$$

where $W = 0.576/\text{year}$, $t_0 = 1950.6$,

$$A(E) = 0.5[f_{\min}(E) - f_{\max}(E)],$$

$$B(E) = 0.5[f_{\min}(E) + f_{\max}(E)]$$

The spectral shapes f_{\max} and f_{\min} are both obtained from the equation:

$$f(E) = 10^m (E/E_0)^a \quad (2.4)$$

where

$$a = a_0 \{1 - \exp[-X_1(\log_{10}E)^b]\} \quad (2.5)$$

and

$$m = C_1 \exp[-X_2(\log_{10}E)^2] - C_2 \quad (2.6)$$

The constants a_0 , E_0 , b , X_1 , X_2 , C_1 and C_2 are given in Table 2.4 for the solar maximum and solar minimum cases of the proton, helium and iron spectra.

TABLE 2.4 Parameter Values used in Eq. (2.4) to Reproduce the solar maximum and solar minimum envelopes (solid curves) shown in Figures 2.2, 2.4 and 2.9 for hydrogen, helium and iron respectively

Element	Solar Activity	a_0	E_0	b	x_1	x_2	c_1	c_2
hydrogen	min	-2.2	117500	2.75	.117	.80	6.52	4.0
hydrogen	max	-2.2	117500	2.75	.079	.80	6.52	4.0
helium	min	-2.25	79400	2.30	.22	.83	5.0	5.0
helium	max	-2.25	79400	2.30	.155	.83	5.0	5.0
iron	min	-2.70	110000	2.30	.140	.65	7.0	8.0
iron	max	-2.70	110000	2.30	.117	.65	7.0	8.0

As discussed in section 2.2, flux levels well above the cosmic ray background level often occur at energies below 100 MeV/u. We recommend that these results be treated as follows: 1) large solar flares be treated as random events obeying the probability distribution, spectra and compositions discussed in Section 4.0; 2) smaller enhancements be handled on a worst-case basis, using the worst case spectra (dashed curves) in Figures 2.2, 2.4 and 2.9. These are obtained from the solar minimum cosmic ray spectra discussed above. For protons,

$$F_{\text{worst}}(E) = f_{\text{min}}(E)[1897e^{-E/9.66} + 1.64]$$

For helium and iron nuclei,

$$F_{\text{worst}}(E) = f_{\text{min}}(E)[28.4e^{-E/13.84} + 1.64]$$

The spectra for the elements C, O, F, Ne, Na, Mg, Al, Si, P and S are all obtained by scaling Eq. 2.3 for helium. That is, just compute the helium spectra for solar maximum and solar minimum using Eqs. 2.3, 2.4 and Table 2.4, then multiply the result by the appropriate entry in Table 2.1. In the same manner, the spectra of the elements Ca, Co and Ni are all obtained from Eqs. 2.3 and 2.4 evaluated for iron and multiplied by the appropriate entry from Table 2.1.

The spectra of the remaining elements are more complicated to obtain since they involve energy dependent charge ratios. Figure 2.11 shows the ratio of (Li + Be + B) to He. The smooth curve in the figure is the ratio we have adopted. Specifically the helium spectrum is modified as shown below to obtain the (Li + Be + B) spectrum:

$$F^* = \begin{cases} 0.0142 F_{\text{He}}, & E < 6 \times 10^3 \text{ MeV/u} \\ & \\ 0.67e^{-0.443} F_{\text{He}}, & E \geq 6 \times 10^3 \text{ MeV/u} \end{cases} \quad (2.7)$$

The spectra of Li, Be and B are obtained by multiplying Eq. (2.7) by the appropriate ratios in Table 2.2

The nitrogen (N) spectrum must also be obtained by an energy dependent modification of the helium spectrum, Figure 2.12, i.e.

$$F_N = \{6.4 \times 10^{-3} \exp[-0.4(\log_{10}E - 3.15)^2] + 5.6 \times 10^{-3} \exp[-0.9(\log_{10}E - 0.8)^2]\} F_{He} \quad (2.6)$$

where E is in MeV/u.

The spectra of the elements chlorine (Cl), argon (Ar), potassium (K), scandium (Sc), titanium (Ti), vanadium (V), chromium (Cr) and manganese (Mn) are all obtained by modifying the iron (Fe) spectrum with the function Q(E) to obtain the spectrum of these combined elements, i.e.

$$Q(E) = 16[1 - \exp(-.126E^{0.4})]E^{-0.33} \quad (2.9)$$

$$F_{comb} = Q(E) F_{iron}(E)$$

The spectra of the individual elements are obtained by multiplying F_{comb} by the appropriate entry from Table 2.2.

If there is an interest in the spectra of the elements heavier than nickel, they can be obtained by multiplying F_{iron} , Eqs. 2.3 and 2.4, by the appropriate entry in Table 2.3.

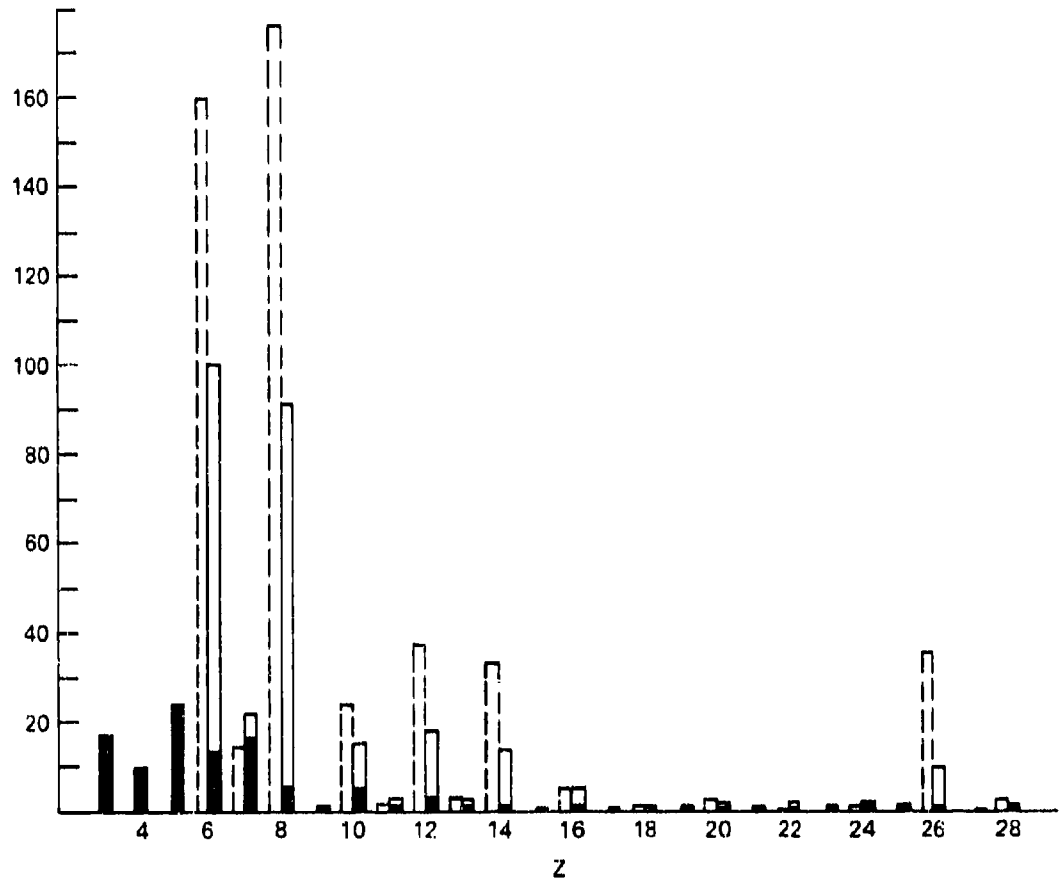


Fig. 2.1 — This figure shows how the cosmic ray composition is transformed by fragmentation as the cosmic rays we detect wander through the galaxy on their way to earth. The dashed bars show the source composition. The adjacent bars show the arriving composition with the filled portion of the bar being nuclei produced by fragmentation and the open portion surviving primordial nuclei.

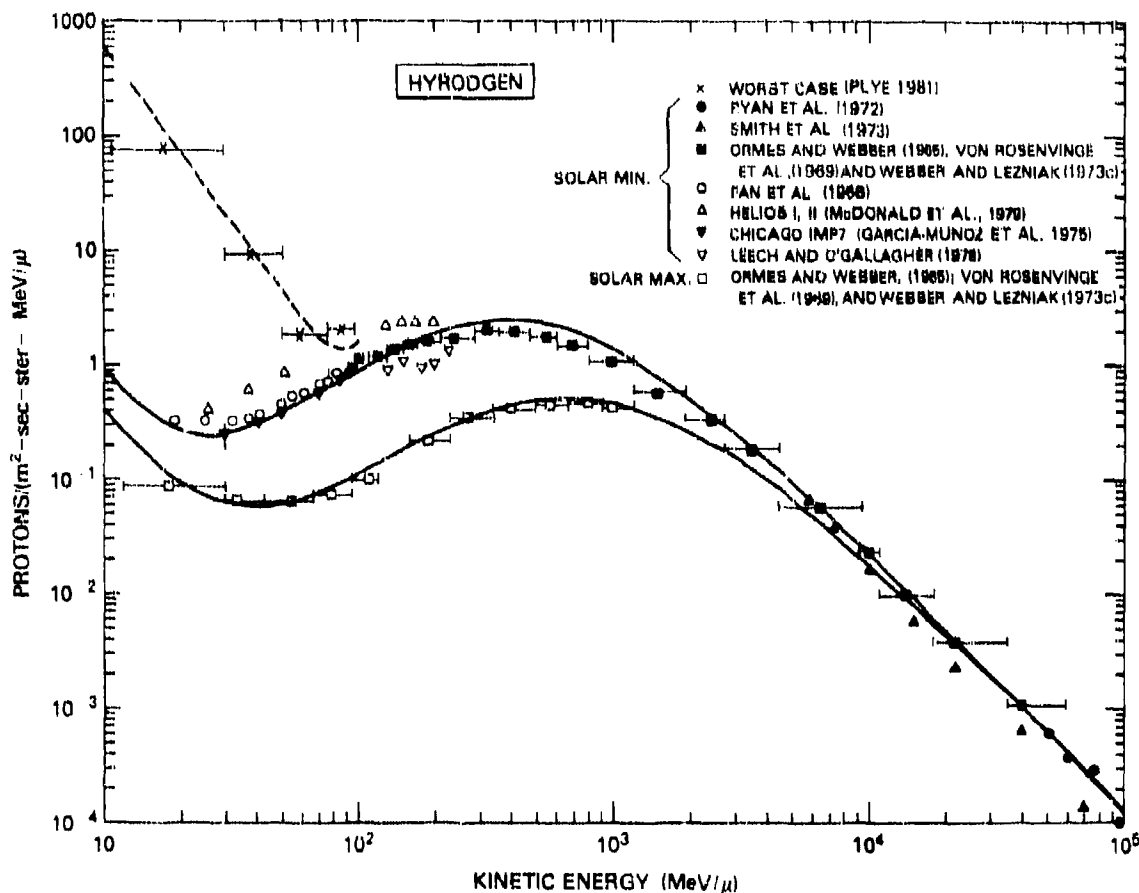


Fig. 2.2 — The differential energy spectrum of hydrogen (mostly protons). The data are selected to show the solar maximum and solar minimum forks. The smooth curve is an analytic function contrived to fit the data. The dashed curve is a worst-case spectrum.

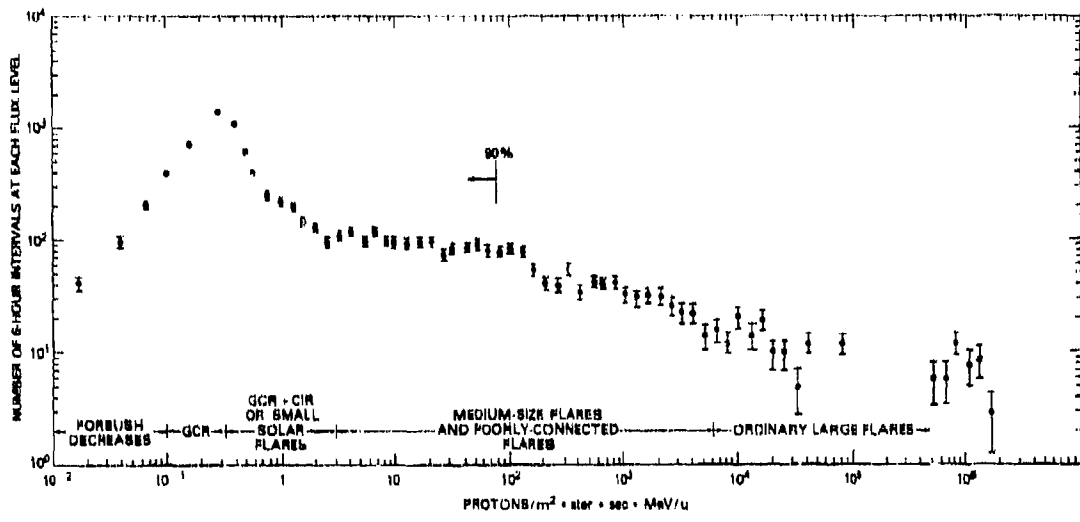


Fig. 2.3 - A sample-size distribution of six-hour average flux measurements of protons ($11.24 \text{ MeV} \leq E \leq 29.75 \text{ MeV}$). The measurements were made by the University of Chicago instrument on IMP-8 at 24 to 28 earth radii between Oct. 30, 1973 and July 2, 1980 (Pyle, 1981). Shown among the bottom are the sources of the particles that contributed to the flux levels above. In addition to solar flare protons, those sources include galactic cosmic rays (GCR) and protons accelerated in co-rotating interaction regions (CIR).

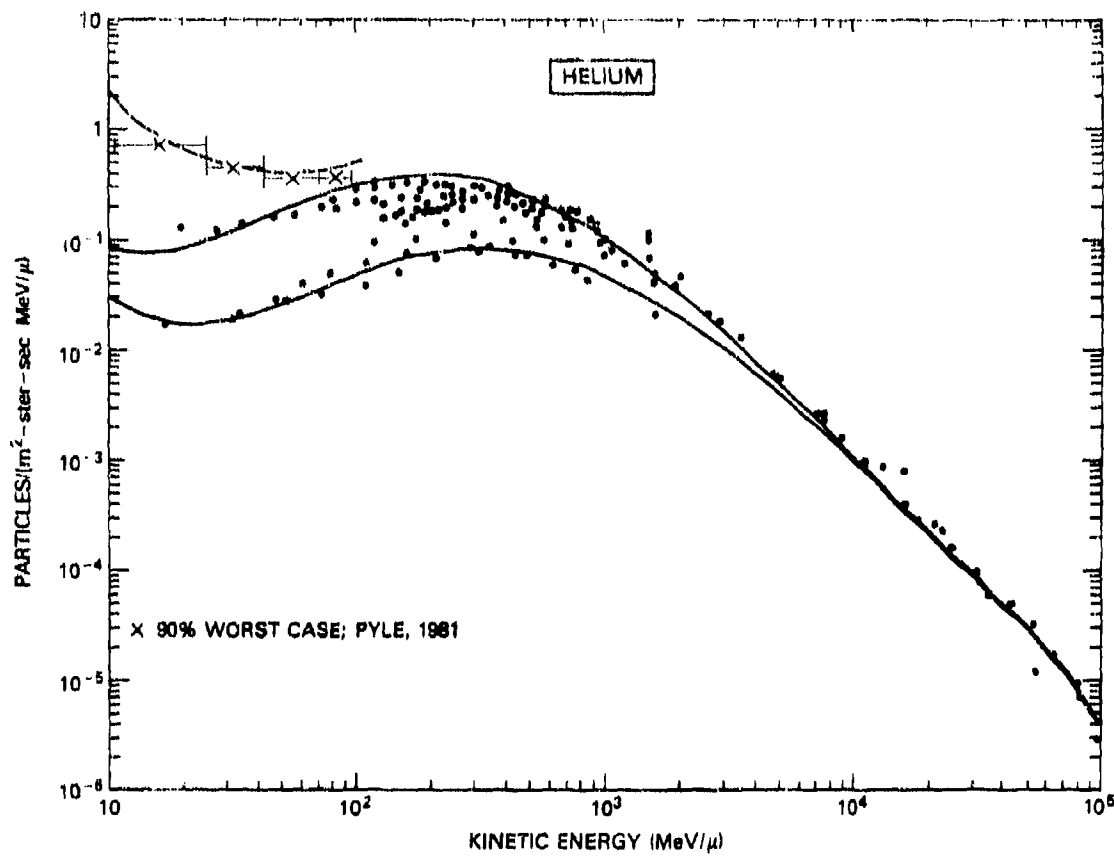


Fig. 2.4 — The differential energy spectrum of helium (mostly alphas). The data are so extensive that it was not possible to individually attribute the data points. The smooth curve is an analytic function contrived to fit the data for solar maximum and solar minimum conditions. The dashed curve is a worst case spectrum.

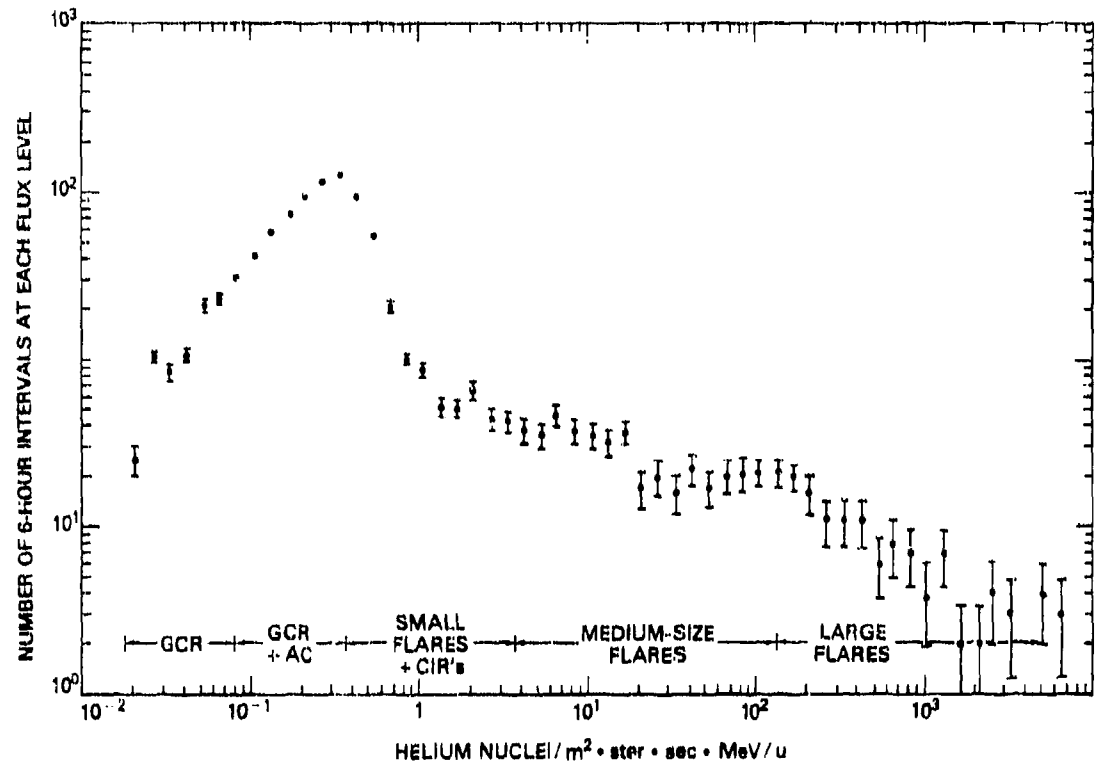


Fig. 2.5 — A sample-size distribution of six-hour average flux measurements of helium nuclei $10.9 \text{ MeV/u} \leq E \leq 28.36 \text{ MeV/u}$). The measurements were made by the University of Chicago instrument on IMP-8 at 24-26 earth radii between Oct. 30, 1973 and July 2, 1980 (Pyle, 1981). AC in this figure refers to the anomalous component, refer to Fig. 2.3 for additional details.

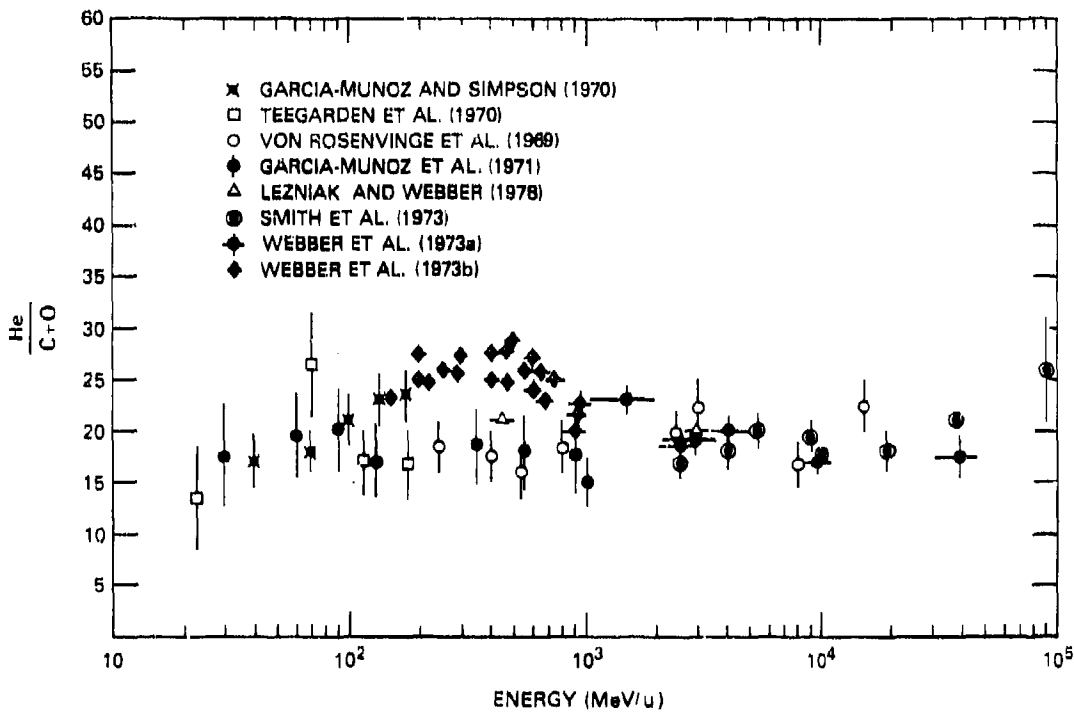


Fig. 2.6 — The He/(C+O) ratio as a function of energy. This ratio is nearly energy independent, permitting us to scale the He spectrum to obtain carbon and oxygen spectra. Some of the data points are based on measured ratios like He/CNO, He/O, or He/C. These were corrected to obtain He/(C+O) ratio. We adopt the value 21 ± 2 for this ratio at all energies.

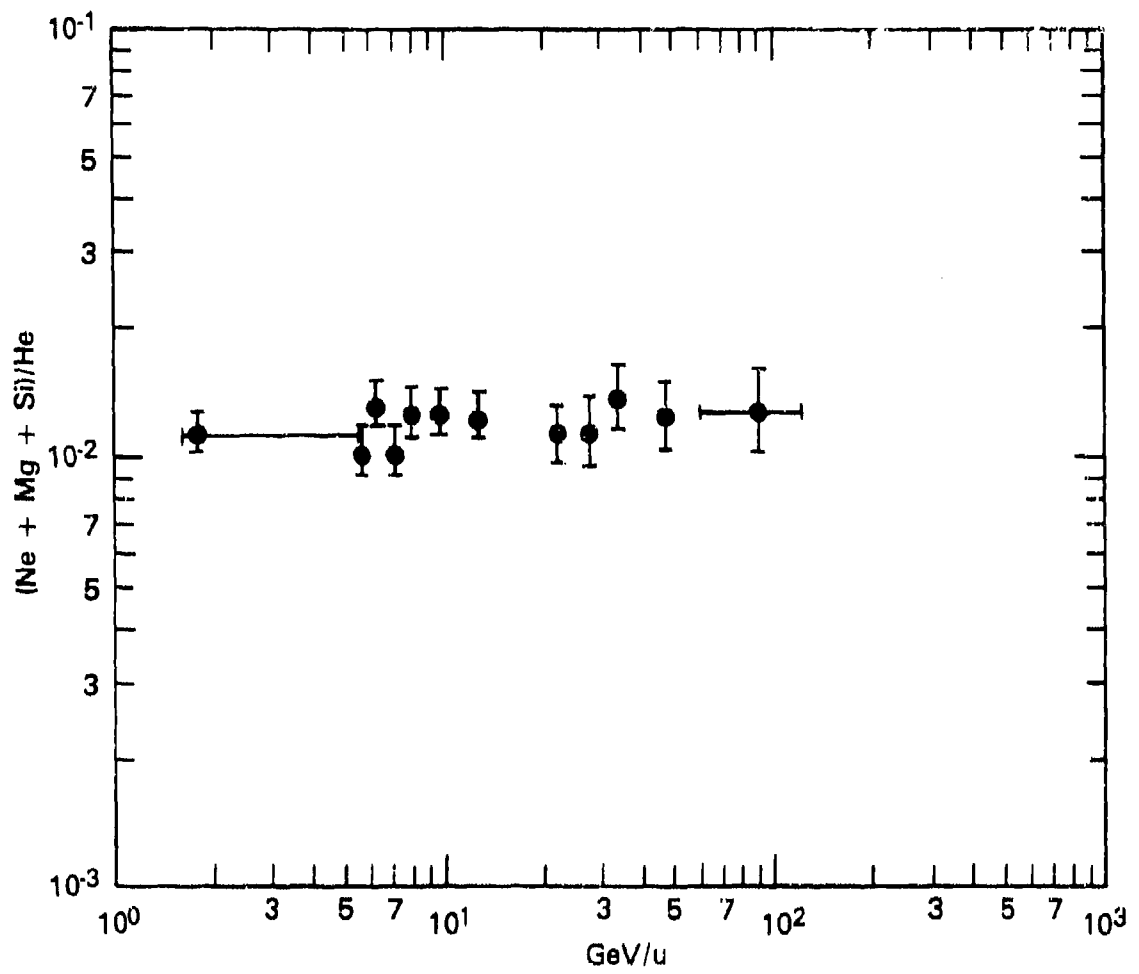


Fig. 2.7 — The $(\text{Ne} + \text{Mg} + \text{Si})/\text{He}$ ratio. This data was taken from Caldwell (1977) and corrected using $\text{He}/\text{C} + \text{O} = 21$ from Fig. 2.6. This figure shows that this ratio is nearly energy independent.

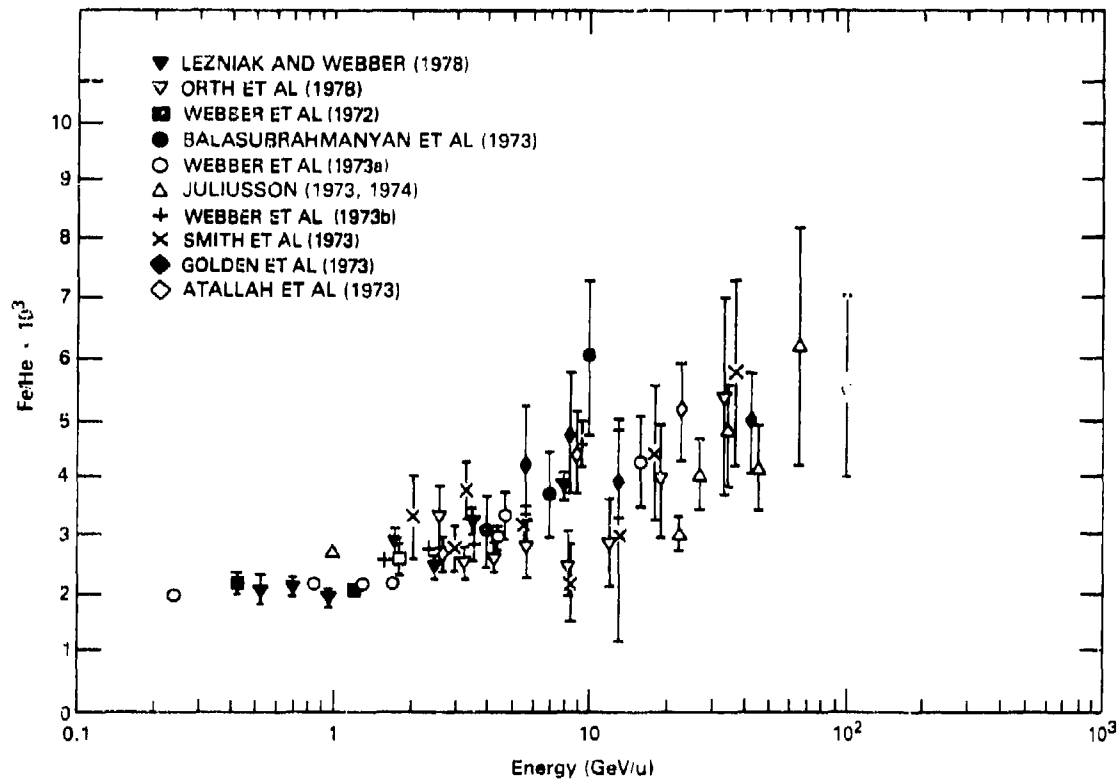


Fig. 2.8 — The Fe/He ratio. These data had to be converted from Fe/(C+O), and similar ratios to Fe/He using the He/(C+O) ratio from Fig. 2.6. This figure demonstrates that the He and Fe spectra do not have the same shape.

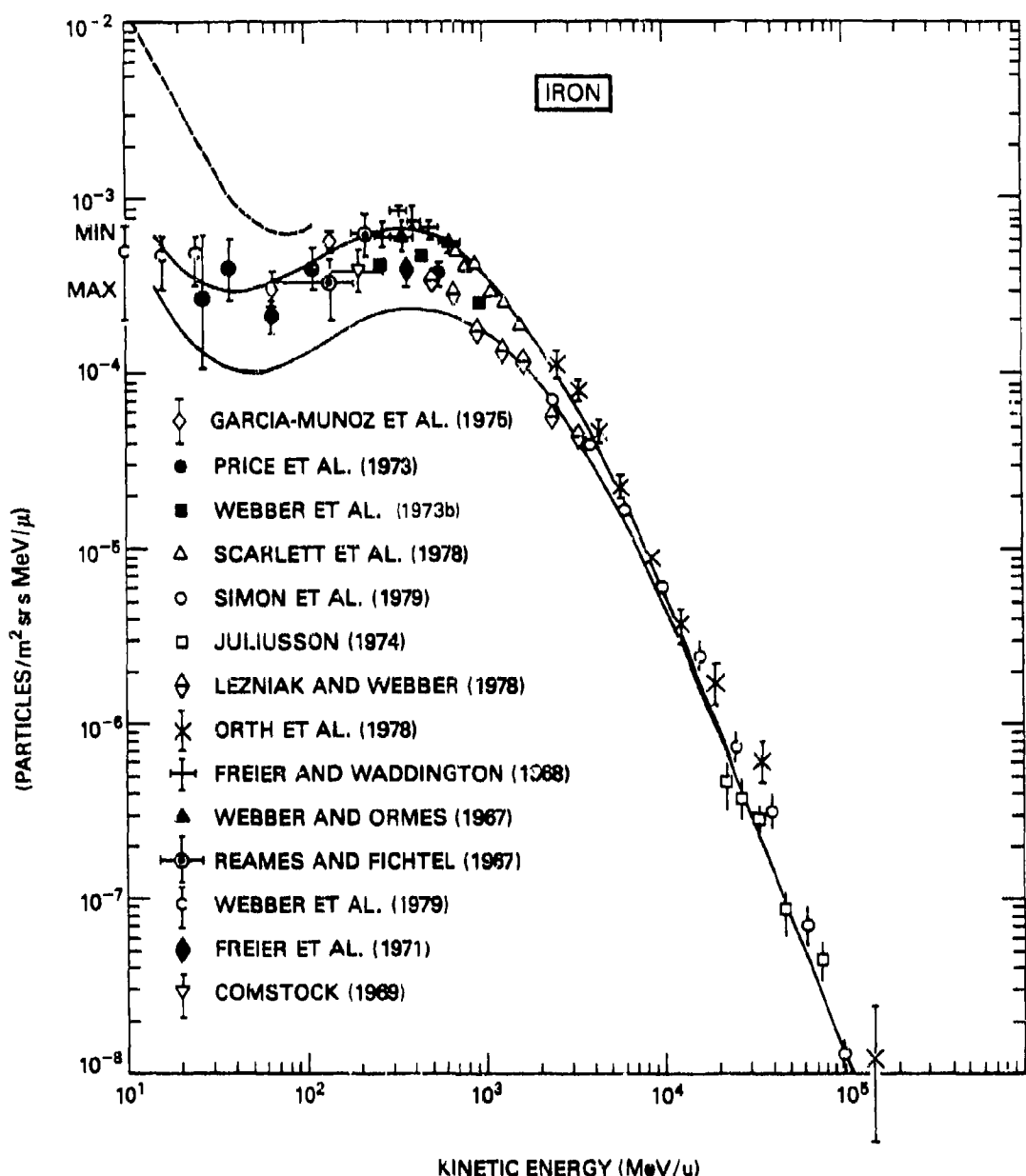


Fig. 2.9 — The differential energy spectrum for Fe. This spectrum has not been defined well at low energies and no measurements exist during solar maximum. As a result the smooth curves were defined using the data shown here as well as the He/Fe data shown in Fig. 2.8 and the helium spectrum, Fig. 2.4. The smooth curve is an analytic function, describing the iron spectrum at the extremes of solar activity. The dashed curve is a worst-case spectrum.

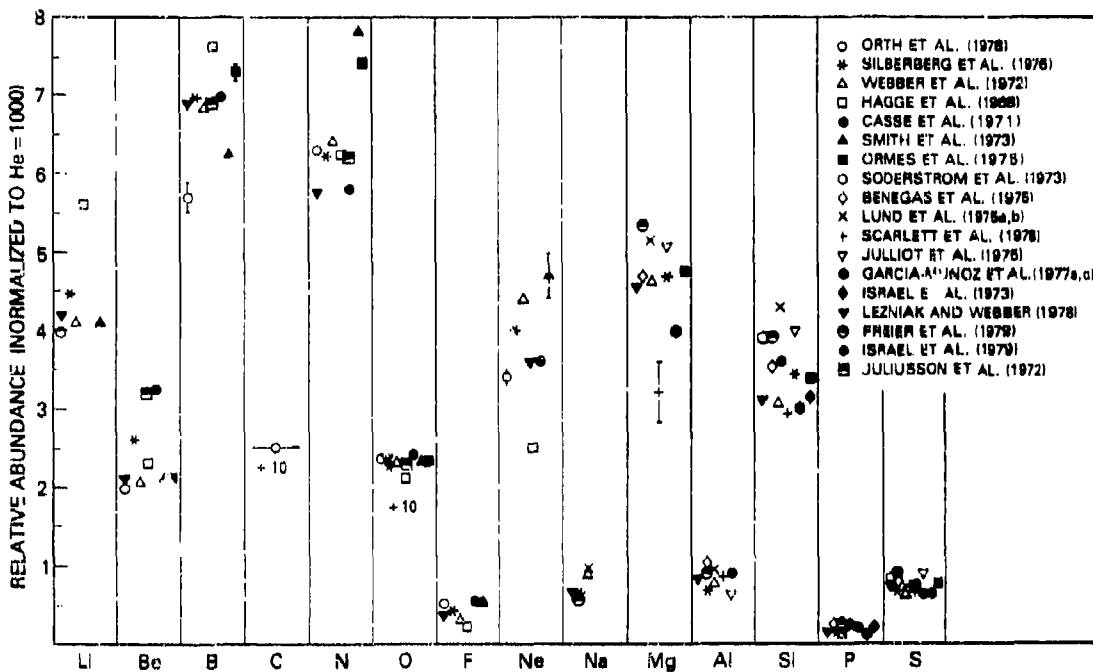


Fig. 2.10 — The abundances of the elements Li through S relative to He are shown. These data were used to obtain the charge ratios given in Tables 2.1 and 2.2 and the total arriving abundances in Fig. 2.1. Note that the abundances of C and O are plotted 1/10 scale.

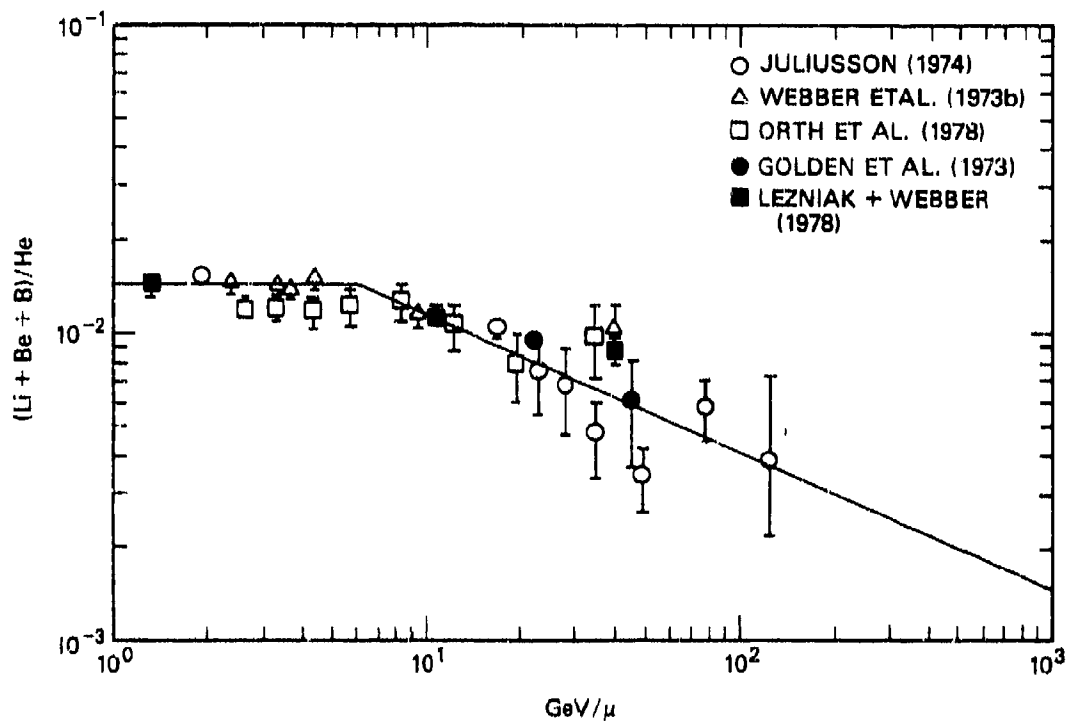


Fig. 2.11 — The $(\text{Li} + \text{Be} + \text{B})/\text{He}$ ratio; the data shown here are, for the most part ratios to $\text{C} + \text{O}$. These were corrected to He using the results of Fig. 2.6. The solid curve is an analytic fit through the data.

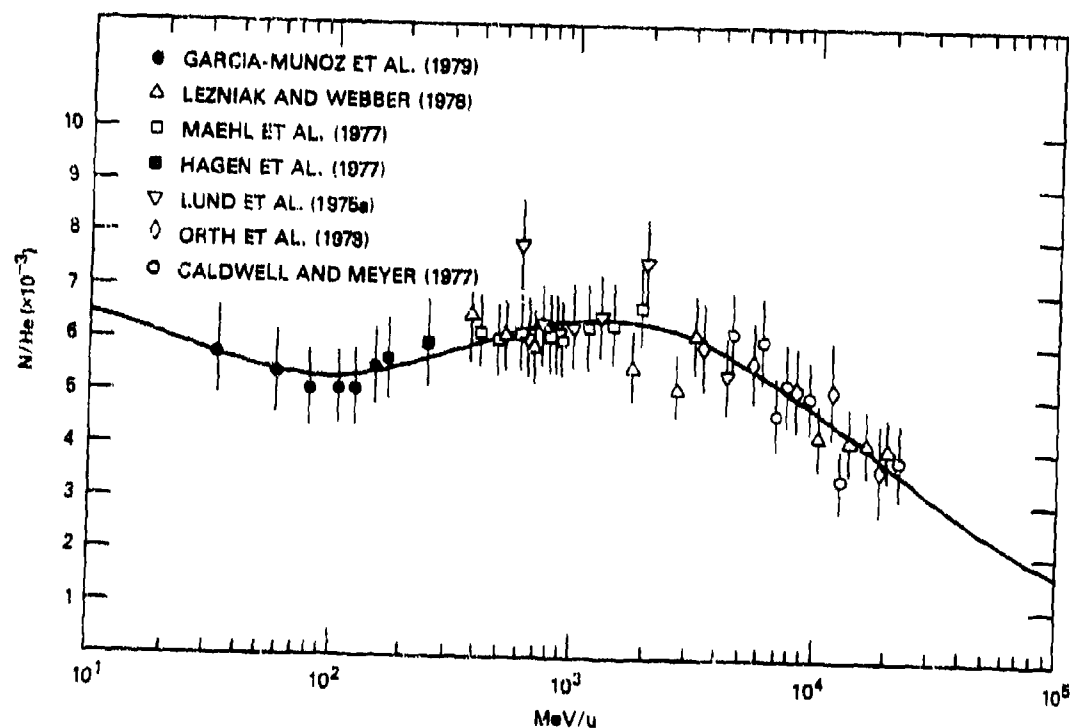


Fig. 2.12 — The N/He ratio is shown as a function of energy. The data points were transformed using the He/(C+O) ratio of Fig. 2.6. The smooth curve is an analytic functional fit through the data.

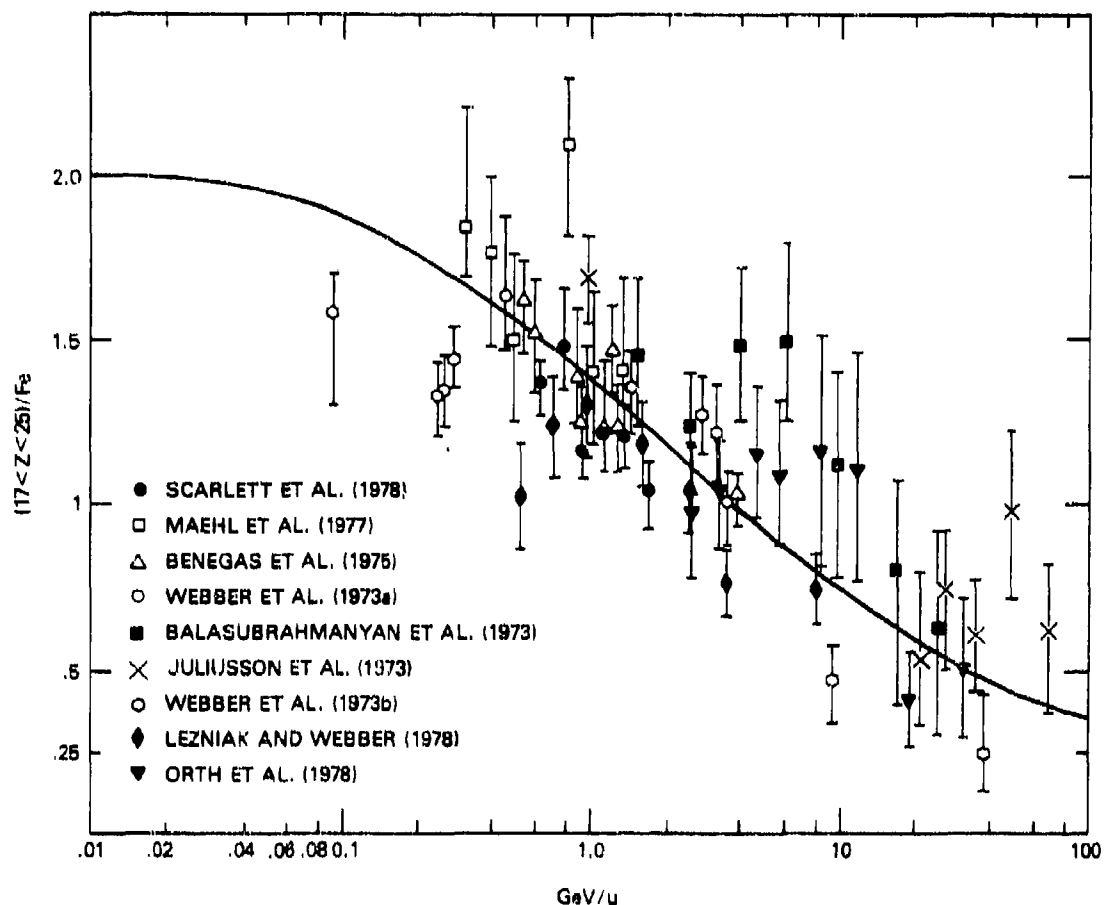


Fig. 2.13 — The sub-iron to iron ratio is shown as a function of energy. Some of the data points had to be corrected to this ratio from similar measured ratios. The smooth curve is an analytic fit through the data.

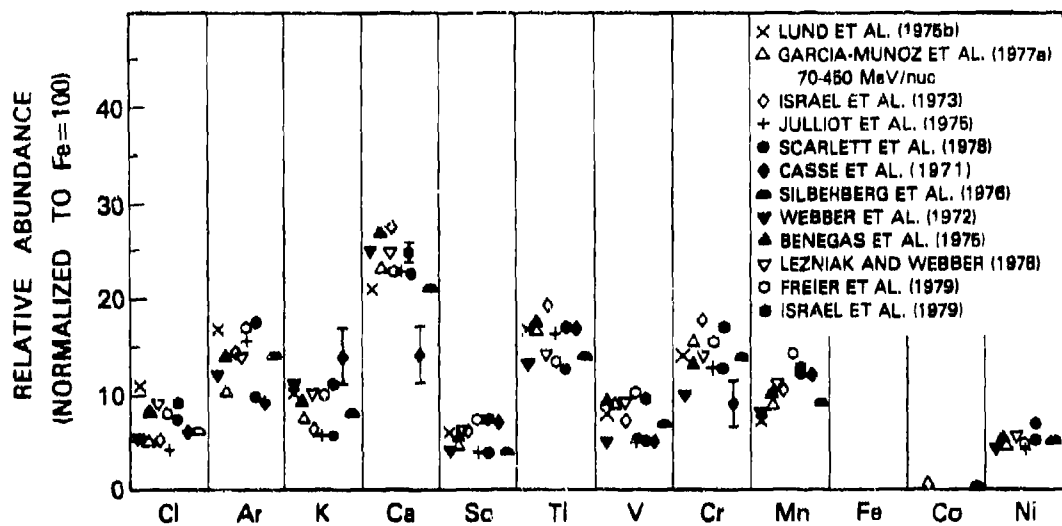


Fig. 2.14 — The abundances of the element chlorine through nickel are shown relative to iron. These data were used to establish the charge ratios shown in Tables 2.1 and 2.2 and the total arriving abundances in Fig. 2.1.

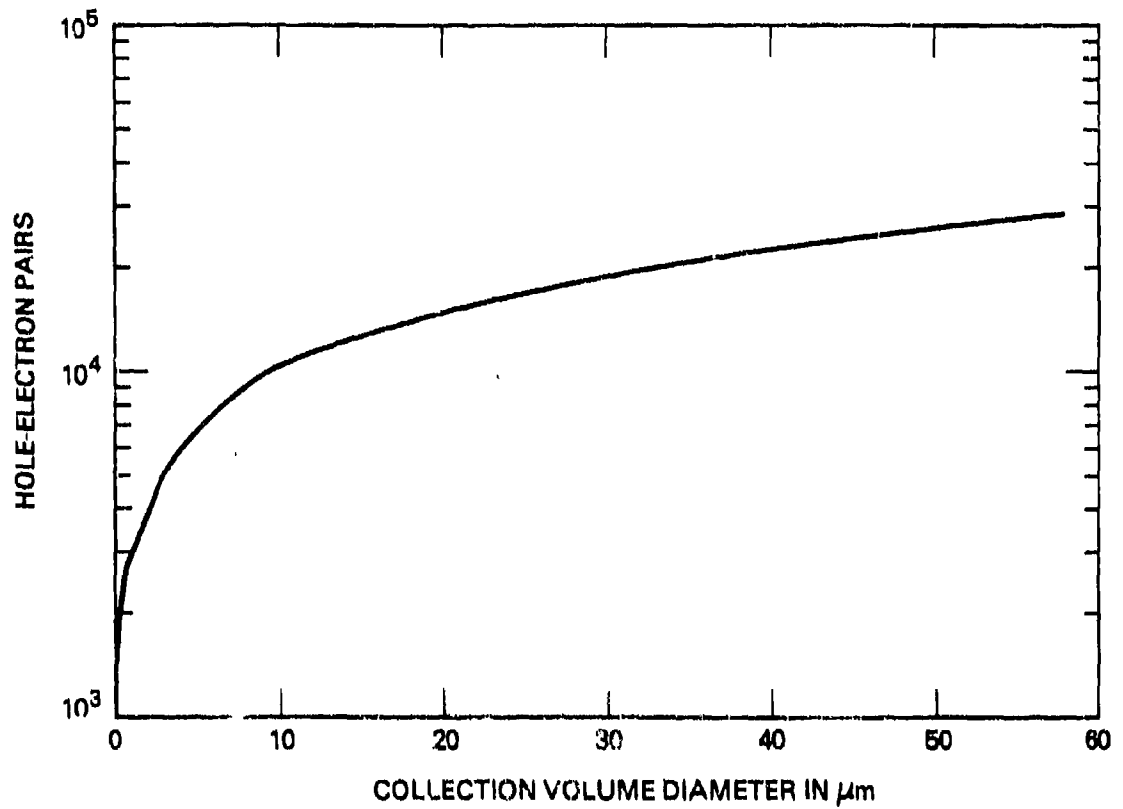


Fig. 2.15 — This figure shows the number of hole-electron pairs typically generated by an electron coming to rest in a collection volume of silicon as a function of the mean diameter of that volume.

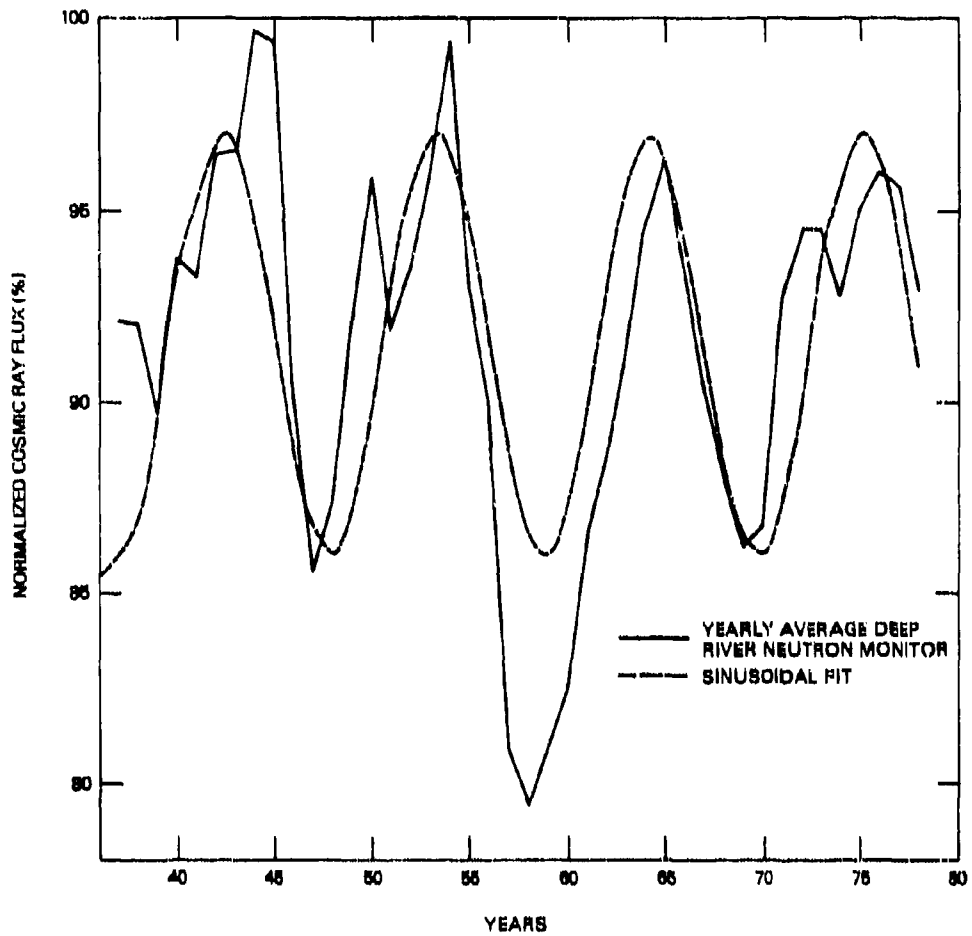


Fig. 2.16 — The 11-year solar cycle is shown as measured by the ground level cosmic ray intensity at the Deep River neutron monitor (located in northern Ontario, Canada). These data are taken from Rao (1972) and Ahluwalia (1979). The smooth curve is a sinusoidal fit to the data. The large depression in 1958 reflects the extraordinary level of solar activity during the 19th solar cycle. The depressions in 1951 and 1974 could be a 22-year repetitive feature, but the data are not sufficient to conclude this.

3.0 Particles from the Interplanetary Medium

There are two known components of the energetic charged particle environment which appear to originate in the interplanetary medium. We shall now discuss what is known about these components and how they contribute to the particle environment.

3.1 Co-rotating Events

The best established component from the interplanetary medium is the co-rotating particle stream. These streams are correlated with high-speed solar-wind streams and interplanetary magnetic field structures co-rotating with the sun. The particles are thought to be selected from the high energy tail of the solar wind and accelerated to higher energies in one of several ways (see the review by Gloeckler, 1979).

These events are infrequent and produce modest increases in the particle flux up to ~ 20 MeV/u, therefore, they affect only the lowest energies of interest in this study. These events are the source of part of the fluctuations in the low energy cosmic ray spectra discussed in section 2.0.

3.2 The Anomalous Component

A much more important contribution to the energy spectra comes from the anomalous component. This component was discovered by Garcia-Munoz et al. (1973) and independently by Hovestadt et al. (1973) and McDonald et al. (1974). Figure 3.1 (taken from Gloeckler, 1979) shows these unusual spectral features. The helium spectrum, instead of dipping to a minimum at about 10 MeV/u as do the proton and carbon spectra, is almost flat from 2 MeV/u to 200 MeV/u. Notice, that the helium flux actually exceeds the proton flux from 4 MeV/u to 30 MeV/u!

The oxygen spectrum, while following the carbon spectrum down to ~ 30 MeV/u, has a huge peak from 1 MeV/u to 20 MeV/u. Several explanations have been offered for these unusual spectral features. The most widely accepted theory, due to Fisk et al. (1974), suggests that these particles come from neutral interstellar gas that can freely enter the heliosphere. This gas becomes singly ionized as it approaches the sun. Once ionized it is accelerated in collision regions between fast and slow moving streams of solar wind. Because of the very good vacuum in interplanetary space, these particles will remain singly ionized regardless of the energy they acquire.

The Fisk theory predicts that only atoms with first ionization potentials higher than hydrogen will display anomalous spectra and that the anomalous particles will be singly ionized. The first prediction has largely been borne out by experiments that have shown anomalous spectra for He, N, O and Ne, but not for H, Li, Be, B, C and F. Tests of the second prediction, that the particles are singly ionized, have so far been only indirect and inconclusive. An experiment being prepared at the Naval Research Laboratory (Adams, et al. 1980b) will use the earth's magnetic field to test this prediction.

The anomalous component is not always present in the vicinity of the earth. It appeared between 1971 and 1972 and disappeared again with the return of solar maximum in 1978. It is unclear, from data taken during the last solar minimum, whether the anomalous component was present then.

One theory of solar modulation (Jokipii et al., 1977) suggests that the anomalous component will appear near earth only once every other solar minimum, i.e. not again until ~ 1994. It remains to be seen whether the anomalous component reappears ~ 1983 or not for another 11 years.

The anomalous component is observed even more strongly in the outer solar system by Voyager and Pioneer spacecraft and remains present beyond ~ 10 earth radii even now. Probably, a small part of the flux observed at higher energies near the earth originates in the anomalous component even during solar maximum.

If the anomalous component is singly ionized, it will be able to penetrate much more deeply into the earth's magnetosphere than galactic cosmic rays at the same energy. It could, therefore, make a much more important contribution inside the magnetosphere than it does in the interplanetary medium.

From Figure 3.1, it is clear that the largest contribution to the particle spectra of interest here is to the helium spectrum. The enhancements in the N and O spectra are at energies below 30 MeV/u in the interplanetary medium. Secondly, if the particles are singly ionized, geomagnetic filtering could make the anomalous component more important in the magnetosphere. Since the charge state of these particles has not been established, we don't know how the earth's magnetic field affects them. Until their charge state has been established, we will assume that they are fully ionized for the convenience this offers in treating them.

Our lack of knowledge of the charge state introduces a second uncertainty. Assuming that the anomalous component is singly ionized, Blake and Friesen (1977) have suggested that anomalous nuclei entering the atmosphere might be stripped in the lower geocorona, thus becoming stably trapped for periods up to a year or more. This could add heavy ions, unexpectedly, to the trapped radiation. Also, this component might persist long after the anomalous component became undetectable in the interplanetary medium in 1978. Since no experimental tests of this theory have been performed, we will assume for the present that these effects do not occur.

The contribution of the anomalous component to the helium spectrum can be included by ass'ing a constant flux extending down from the peak flux of the spectrum to 10 MeV/u. For the oxygen spectrum, we use the smooth curve fit through the anomalous oxygen peak in Figure 3.1. The equation for this curve is:

$$f(E) = 6 \times 10^{-2} \exp[-(\ln E - 1.79)^2 / 0.70] \text{ particles/m}^2 \text{ ster.sec.MeV/u} \quad (3.1)$$

with E in MeV/u.

This equation should be used in the energy interval $10 \text{ MeV/u} < E < 30 \text{ MeV/u}$ to replace that segment of the cosmic ray oxygen spectrum (see Section 2.0). This will include the anomalous component in the cosmic ray oxygen

spectrum. In a similar manner, the anomalous component can be added to the cosmic ray nitrogen spectrum. Using the N/O ratio reported by Klecker et al. (1977), the cosmic ray nitrogen spectrum is replaced by:

$$f(E) = 1.54 \times 10^{-2} \exp[-(\ln E - 1.79)^2 / 0.70] \text{ particles/m}^2 \text{ ster. sec. MeV/u} \quad (3.2)$$

in the $10 \text{ MeV/u} \leq E \leq 30 \text{ MeV/u}$ energy interval.

We recommend that helium, nitrogen and oxygen cosmic ray spectra be altered to include the anomalous component only for periods of solar minimum. The next such period is 1983-1989.

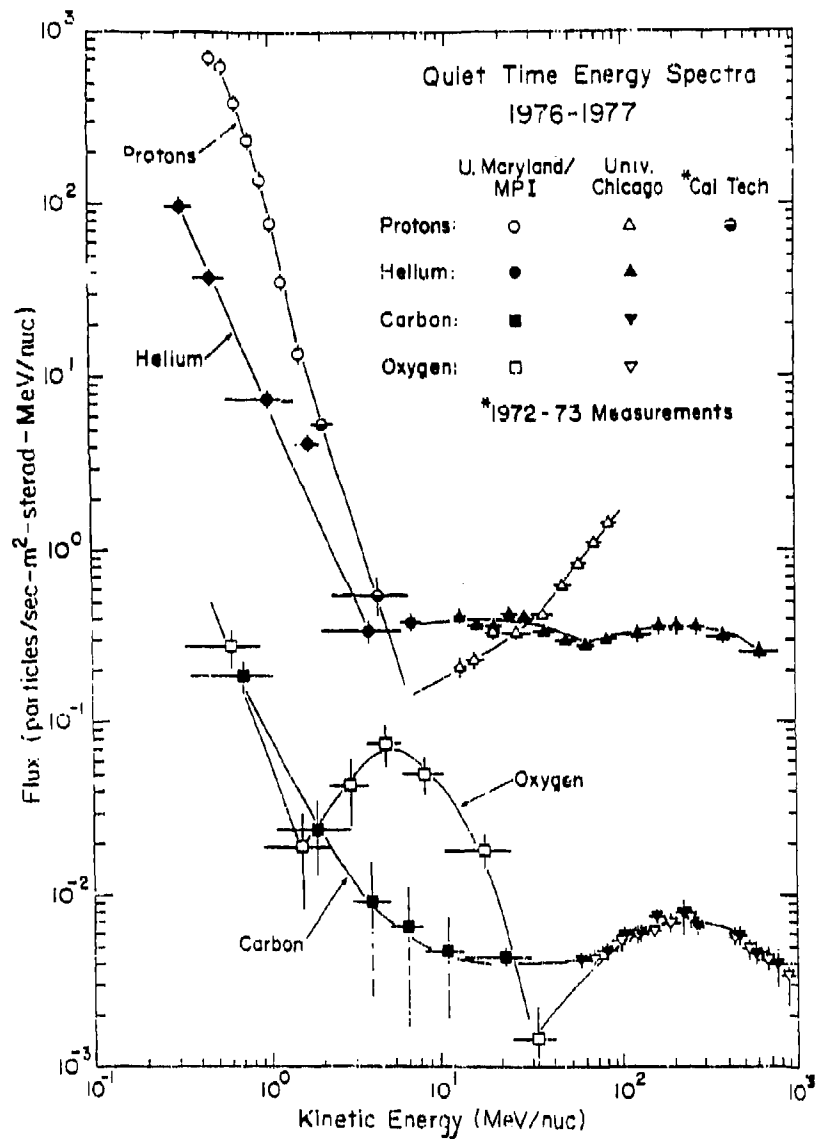


Fig. 3.1 — The quiet-time spectra of hydrogen, helium, oxygen and carbon in the interplanetary medium during the last solar minimum, 1972-1978, (taken from Gloeckler, 1979). It is instructive to compare the helium spectrum given here with that in Fig. 2.4. The solar minimum spectrum (upper solid curve) in Fig. 2.4 decreases gradually from 200 MeV/u to a minimum at ~ 15 MeV/u. In contrast, the helium spectrum in this figure remains nearly constant below 200 MeV/u, rising slightly below ~ 50 MeV/u and even exceeding the proton flux below ~ 30 MeV/u. This difference is due to the additional flux provided by the anomalous component during the last solar minimum.

4.0 Solar Flare Particles

Solar flares are sudden outbursts on the visible surface (photosphere) of the sun which release huge amounts of energy. Most of this energy is radiation in UV and X-rays. A part of this energy, mostly from hard X-rays goes into very rapid heating of the solar corona above the flare. This produces large currents and moving magnetic fields in the corona that accelerate ambient coronal material to very high energies quickly. (For a review of solar flare particle acceleration, see Ramaty et al. 1980).

Many of these coronal particles escape the sun and spray out into the interplanetary medium. As the particles move into the interplanetary medium they tend to be guided along the existing spiral magnetic field pattern in the ecliptic plane. As a result, both the intensity and the spectrum observed at earth depend on the relative positions of the earth and the flare on the sun. For example, a solar wind velocity of 430 Km/sec produces a spiral field that connects the earth directly to points on a solar longitude line ~ 54° west of the center of the sun as viewed from earth. For flares at other solar longitudes, the earth will, in general, receive a smaller flux of solar particles; the flux will build up more slowly; and it may contain fewer high energy particles. The actual degree of "well connectedness" between the earth and the flare site depends on interplanetary conditions at the time of the flare and these conditions are highly variable and unpredictable. This effect may lead to variations as large as 100 in the observed flux from the same flare at different points around the earth's orbit (see Simnett, 1976).

4.1 The Sizes and Frequencies of Flares

Major solar flares occur at random, with a frequency that varies from one every two months to one every two years. The particle events near earth that result from these flares last from two hours to ten days. The result is that ~ 98 per cent of the time the particle environment in the interplanetary medium near earth is determined by galactic cosmic rays, possibly enhanced at low energies by small flares etc. (Section 2.0) and with a possible contribution from the anomalous component (see Section 3.0). During the remaining ~ 2 per cent of the time the particle environment is dominated at low and moderate energies, by solar particles. Figure 4.1 taken from King (1974), shows the proton fluence ($E > 30$ MeV) and the time of occurrence of all the major solar flares from 1956 to 1972. From this figure we can see that the frequency distribution has a period of ~ 11 years (the solar cycle) and that each active period displays one anomalously large event. Apart from these two events, the remaining events seem to be distributed as though the log (to base 10) of their sizes was normally distributed. This is called a log-normal distribution (see Brown, 1957). King has found the log-normal fluence, F , distributions ($\log 10F$) for the fluence, F , above any energy threshold for these events. The means and standard deviations of the distributions for four thresholds are shown in Table 4.1.

The frequency distribution of flares is best described by the Burrell distribution (see Burrell, 1971),

$$p(n,t,N,T) = (n + N)! (t/T)^n / [n!N!(1 + t/T)^{1+n+N}] \quad (4.1)$$

where p is the probability that exactly n flares will occur during a time t

given that N flares were observed during a time T . For the second active period in Figure 4.1, we have $N = 24$, $T = 7$ years.

Because of its size, the August 1972 event (actually a series of four flares), produced a fluence at earth nearly twice that of all the other flares in this active period combined. King, therefore, treats this flare separately. If a satellite mission is long enough for the risk of such an event, $p(l,t,1,7)$ in Eq. (4.1), to be unacceptable, then it must be included in the particle environment model. When anomalously large events are considered they always dominate ordinary events in total fluence for the mission.

A solar particle event may last several hours or days, during this time the flux varies enormously. Besides knowing the integral fluence for the event, it is useful to know the maximum flux. Using data provided by King (1974) we have a log-normal distribution to the peak proton fluxes above three energy thresholds. The values of the means and standard deviations are shown in Table 4.1:

TABLE 4.1 The Parameters of Log-normal Distributions for Ordinary Solar Flares. Parameters are shown for: (a) the Integral omni-directional fluence for the entire solar event in protons/cm²; and (b) the peak omni-directional flux in protons/cm² sec.

	$E > 10$ MeV	$E > 30$ MeV	$E > 60$ MeV	$E > 100$ MeV
Integral Fluence mean $\pm \sigma$	$8.27 \pm .59$	$7.28 \pm .75$	$6.63 \pm .95$	5.77 ± 1.24
Peak Flux mean $\pm \sigma$	$3.27 \pm .64$	$2.37 \pm .82$	$1.88 \pm .78$	

4.2 Solar Proton Spectra

From Table 4.1 we can see that the ordinary solar flare proton spectra vary enormously in amplitude and spectral shape. The mean log fluence for ordinary events has been fit to give a differential spectrum of the form:

$$F_{\text{mean}} = 3.3 \times 10^5 (e^{-E/20.2} + 307e^{-E/3}) \text{ protons/cm}^2 \text{ ster. MeV} \quad (4.2)$$

for $E > 10$ MeV/u.

This is the typical spectrum of particles that we expect to arrive in the interplanetary medium near earth as the result of an ordinary flare, integrated over the period of the flare. A "worst case" spectrum can be obtained by fitting the mean $+ 1 \sigma$ for each threshold in Table 1. If the log-normal distributions were uncorrelated, this would produce a case which would be exceeded with a probability of only 0.014. The distributions are, of course, correlated to some degree so the probability is somewhat higher, but not larger than 0.34. An extensive study of the correlations between the spectra would be required to determine this probability. For now, we will assume that the spectra have two independent parameters and take the probability to be 0.12.

We have also fit the "worst case" spectrum, as shown below:

$$F_{\text{worst}} = 7.6 \times 10^5 (e^{-E/30} + 165 e^{-E/4.0}) \text{ protons/cm}^2 \text{ster.MeV} \quad (4.3)$$

for $E > 10$ MeV. As eq. (4.2) above, this is the most intense spectrum (with a 90 per cent confidence level) that we expect to find in the interplanetary medium near earth as the result of an ordinary flare. Both F_{mean} and F_{worst} are shown in Figure 4.2.

The same fits have been done for the peak flux distributions (i.e., the particle flux at the peak of the flare's intensity), they are shown below and in Figure 4.3 for the mean (typical) and worst (90 per cent) cases.

$$f_{\text{mean}} = 1.95 (e^{-E/27.5} + 173 e^{-E/4}) \text{ protons/cm}^2 \text{ster.sec.MeV} \quad (4.4)$$

and

$$f_{\text{worst}} = 17.1 [e^{-E/24.5} + 63.6 e^{-E/4}] \text{ protons/cm}^2 \text{ster.sec.MeV} \quad (4.5)$$

These are the mean and worst-case spectra to be expected during the most intense part of the flare.

For anomalously large events, King (1974) suggests the event time-integrated spectrum in the interplanetary medium near earth:

$$F_a = 2.37 \times 10^7 \exp[(30 - E)/26.5] \text{ protons/cm}^2 \text{ster.MeV} \quad (4.6)$$

This spectrum is compared with eqs. (4.2) and (4.3) in Figure 4.2.

Figure 4.4 taken from Lockwood et al. (1975), shows the existing data on the peak flux spectrum for the August 4, 1972 event. It gives a feeling for the kind of uncertainty that exists in the measurements of the spectrum of a large flare. For the purpose of this model, we recommend extending the 20:00 UT Explorer 41 spectrum to 150 MeV and matching it to a P-9 power law at that point,

That is:

$$f = \frac{dP}{dE} \times 9.3 \times 10^5 e^{-P/0.10} \text{ protons/cm}^2 \text{ster.sec. MeV} \quad (4.7)$$

for $E < 150$ MeV.

and,

$$f = \frac{dP}{dE} \times 17.6 P^{-9} \text{ protons/cm}^2 \text{ ster.sec.MeV} \quad (4.8)$$

for $E \geq 150$ MeV,

where

$$P = [(E/1000)^2 + 1.86 \times 10^{-3} E]^{1/2} \quad (4.9)$$

with E in MeV. This gives the particle energy spectrum to be expected in the interplanetary medium, near earth, during the most intense part of an anomalously large flare. It is compared to eqs. (4.4) and (4.5) in Figure 4.3

4.3 Solar Energetic Particle Composition

The elemental composition of particles from solar flares is highly variable showing, in some cases, enormous enhancements in heavy elements. The data on several large solar flares between October 30, 1973 and December 1, 1977 have recently been surveyed by Mason et al. (1980). The average composition they found at ~ 1 MeV/u for 37 days during major flares is given in Table 4.2, normalized to hydrogen.

TABLE 4.2 Solar Energetic Particle Composition*

Element	H	He	C	O	Ne	Mg	Si	S-Ca	Cr-Ni
Mean	1	.022	1.6 ⁴	3.2 ⁴	5.1 ⁵	4.8 ⁵	3.8 ⁵	2.5 ⁵	4.4 ⁵
Mean + 1 σ	1	.031	3.5 ⁴	8.7 ⁴	1.6 ⁴	1.5 ⁴	1.3 ⁴	9.5 ⁵	2.0 ⁴
Mean - 1 σ	1	.020	1.4 ⁴	2.3 ⁴	3.0 ⁵	2.8 ⁵	1.8 ⁵	1.1 ⁵	1.4 ⁵
Richest day	1	.074	.8 ³	3.2 ³	6.8 ⁴	7.7 ⁴	8.1 ⁴	4.8 ⁴	1.1 ³

*Notation in this table has been compressed 1.15 means 1.1×10^{-5} or .000011

These results are consistent with a more limited survey carried out by Webber (1975) for $E > 20$ MeV.

Mason et al. find that: (1) the average composition does not depend strongly on particle energy or flare size; (2) all extreme examples of composition anomalies are for small flares.

Comparing Table 4.2 with the cosmic ray composition described in Section 2.0, we see that solar flares have a $H/(C + O)$ ratio about ten times larger than cosmic rays. The $He/(C + O)$ ratio is ~ 45 in solar flares compared to 21 in cosmic rays while the $Fe/(C + O)$ ratio appears to be ~ 1.5 times larger in flares than cosmic rays. This is due to spallation; the $Fe/(C + O)$ ratio at cosmic ray sources is larger than in flares. The elements Li, Be, B and the odd Z elements above nitrogen are much less abundant in solar flare particles than cosmic rays. This is because spallation has filled in these nuclei in cosmic rays.

Table 4.2 also gives a feeling for the variability of the daily average composition during enhanced periods associated with large flares. The mean $+ 1 \sigma$ line gives the limit on heavy ion richness that is exceeded by only one in every six daily averages. Correspondingly, the mean -1σ line gives composition limit for heavy ion poor flares; only one in six days were poorer in heavy ions. It should be noted that the error bounds are not equidistant on either side of the mean, the distribution has a much larger wing to the heavy-ion-rich side and the distribution is not gaussian shaped. To give a feel for the worst case, the last line of the table gives the results for the richest day of the 37 days included in the survey. Mason et al. also show that these enrichments are highly correlated from element to element.

The survey of Mason et al. covers 11 periods of flare activity. Cook et al. (1980) report results for $Z > 2$ measured in the 4.6 to 8.7 MeV/u energy range from four flares in 1978. Their results show that one flare, April 29, 1978 was unusually rich in all heavy elements. The $\text{He}/(\text{C} + \text{O})$ ratio was 10, a factor of 4.5 richer than the average flare and a factor of 2 richer than cosmic rays.

The available data on solar flare composition is still quite limited at low energies and very sparse at the higher energies of interest here. The variations in composition from flare to flare are large and distributed in a broad non-gaussian manner. The result is that the uncertainty in the flux of any elemental species is due almost as much to the variations in the composition of energetic particles as to the variations in flare sizes.

To obtain a worst case composition for a given confidence level, we have chosen to treat the composition as though it were normally distributed with different standard deviations above and below the mean, using the standard deviations from Table 4.2, interpolating to neighboring elements as needed. The abundances of the elements P, Cl, K, Ti, Mn, and Co were estimated from the solar system abundances compiled by Cameron (1980).

Table 4.3 gives our recommendation for the mean composition and the worst case composition at the 90 per cent confidence level (i.e., there is only one chance in ten of having a richer flare). Elements with mean relative abundances below 10^{-7} were treated as absent in the composition.

TABLE 4.3 Mean and Worst Case Compositions

	Mean Case	Worst Case		Mean Case	Worst Case
H	1	1	P	2.3×10^{-7}	1.1×10^{-6}
He	2.2×10^{-2}	3.3×10^{-2}	S	1.8×10^{-5}	8.4×10^{-5}
Li	0	0	Cl	1.7×10^{-7}	8×10^{-7}
Be	0	0	Ar	3.9×10^{-6}	1.8×10^{-5}
B	0	0	K	1.3×10^{-7}	6×10^{-7}
C	1.6×10^{-4}	4.0×10^{-4}	Ca	2.3×10^{-6}	1×10^{-5}
N	3.8×10^{-5}	1.1×10^{-4}	Sc	0	0
O	3.2×10^{-4}	1.0×10^{-3}	Ti	1×10^{-7}	5×10^{-7}
F	0	0	V	0	0
Ne	5.1×10^{-5}	1.9×10^{-4}	Cr	5.7×10^{-7}	3.2×10^{-6}
Na	1.6×10^{-6}	6.1×10^{-6}	Mn	4.2×10^{-7}	2.3×10^{-6}
Mg	4.8×10^{-5}	1.8×10^{-4}	Fe	4.1×10^{-5}	2.3×10^{-4}
Al	3.5×10^{-6}	1.4×10^{-5}	Co	1×10^{-7}	5.5×10^{-7}
Si	3.8×10^{-5}	1.6×10^{-4}	Ni	2.2×10^{-6}	1.2×10^{-5}
	Z>28			0	0

Besides the atomic nuclei, flares accelerate electrons. As discussed in Section 2.4, electrons will only be important if they are overwhelmingly more abundant than nuclei at energies greater than 20 MeV. Ramaty et al. (1980) argue, based on the existing data, that the electron to proton ratio at energies greater than 10 MeV is $\sim 10^{-2}$, clearly solar flare electrons are not a problem and will be ignored in this model.

4.4 Recommendations

Large solar flares are transient phenomena, contributing to the particle environment only about 2 per cent of the time. If a few per cent operating time can be lost during flares, then their contribution to the particle environment can be ignored in formulating a worst case to be withstood.

If flares must be considered, then we recommend the following procedure: (1) determine whether there is an unacceptable risk of an anomalously large event from Eq. 4.1 with $N = 1$, $T = 7$; (2) if anomalously large events must be considered, assume the event integral spectrum, Eq. 4.6, and peak flux spectrum Eqs. 4.7, 4.8, and 4.9 for protons; (3) if anomalously large events are unlikely, use Eq. 4.1 to estimate the number of ordinary events to be expected; (4) Eqs. 4.3 and 4.5 give the worst case event fluence and peak

flux proton spectra to be considered; (6) in any case, Table 4.3 should be used to obtain the worst case composition. Multiplying the proton spectra by the numbers in this table will give estimates of the spectra for the other elements.

When spacecraft inside the magnetosphere are studied, the geomagnetic cutoff should be taken into account (see Section 5.0), using the model for a disturbed magnetosphere.

Some thought should be given to the problem of modulating the peak flux spectrum with the geomagnetic cutoff transmittance function. If the orbital period is ~ 100 minutes then the flare peak will be (at least partially) averaged over the orbit. For long-period orbits, the flare peak will not be averaged and a position for the satellite must be assumed.

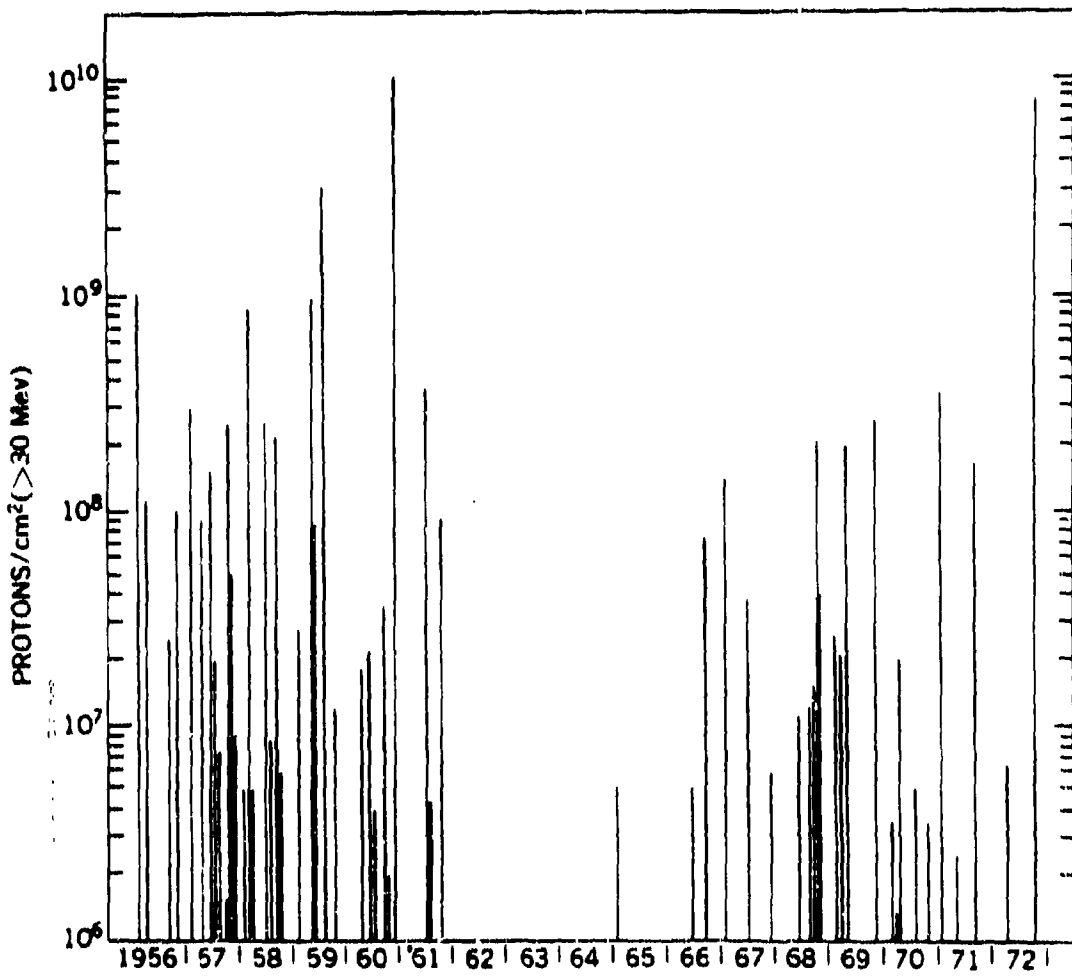


Fig. 4.1 — Event-integrated proton fluxes above 30 MeV for the major solar events of the 19th and 20th solar cycles (King, 1974).

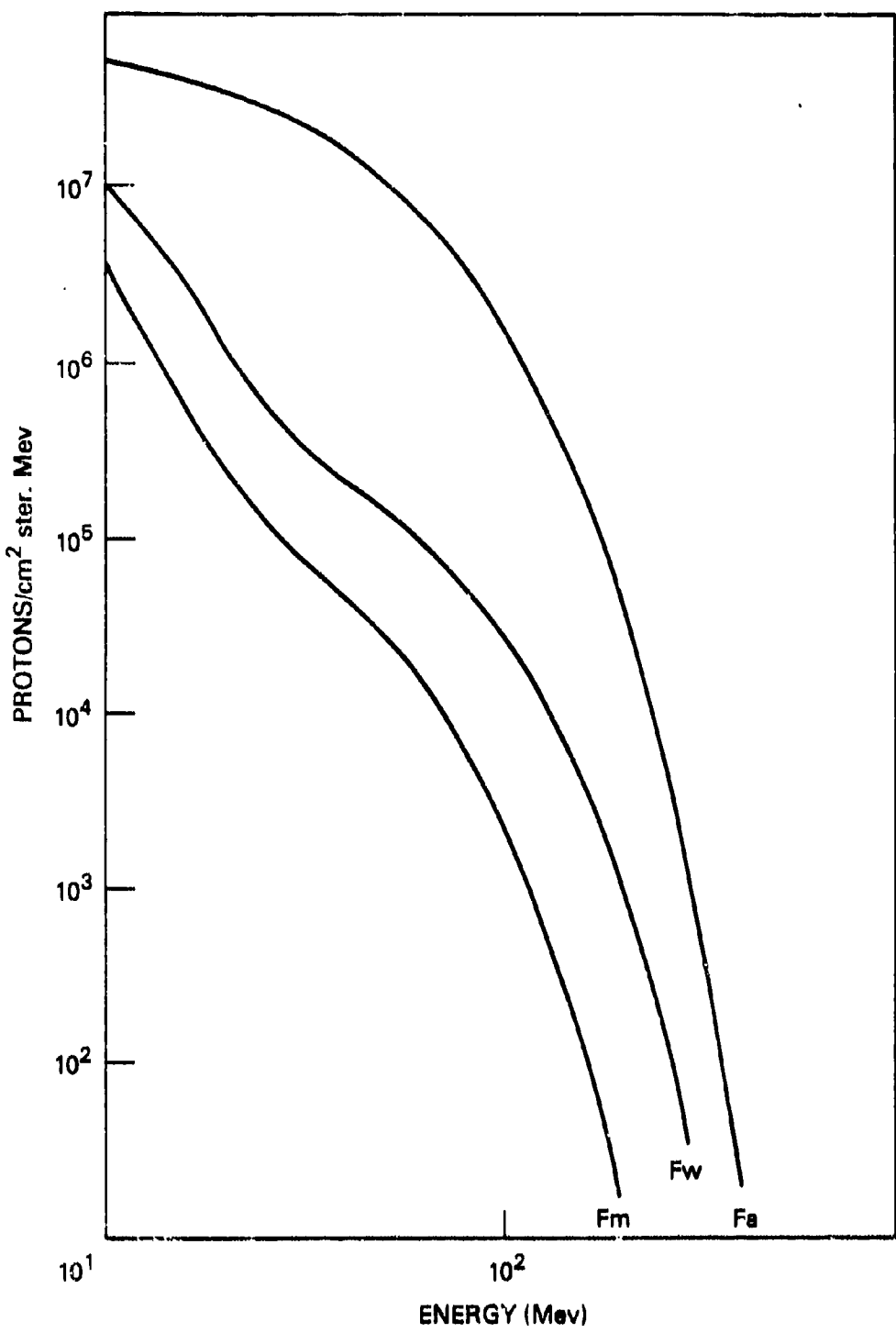


Fig. 4.2 — The event-integrated proton differential energy spectra for: F_m , a typical ordinary event; F_w , a worst-case ordinary event (90 percent confidence level); and F_a , an anomalously large solar event.

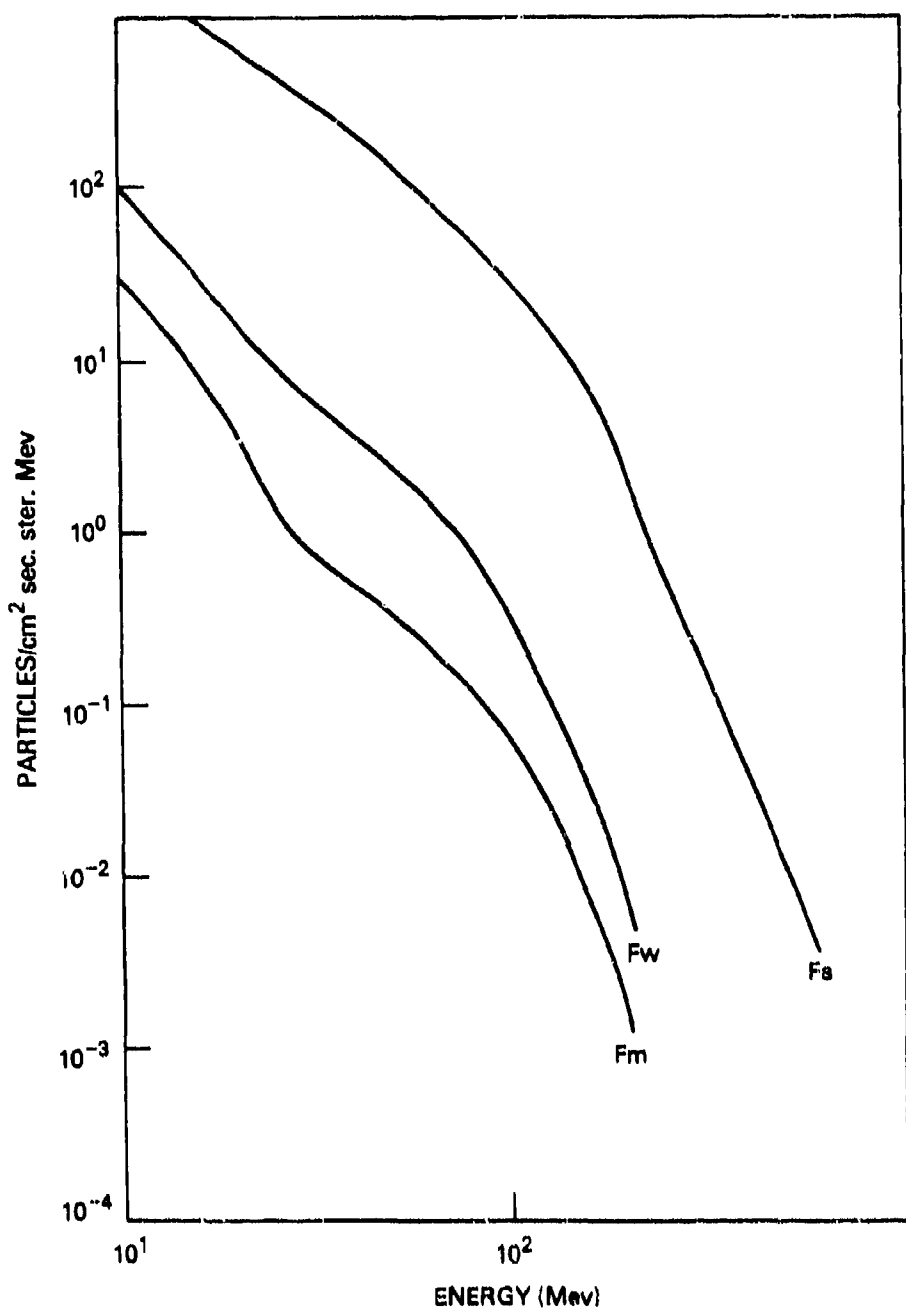


Fig. 4.3 — The peak proton flux differential energy spectra for: F_m , a typical ordinary event; F_w , a worst-case ordinary event (90 percent confidence level); and F_a , anomalously large event.

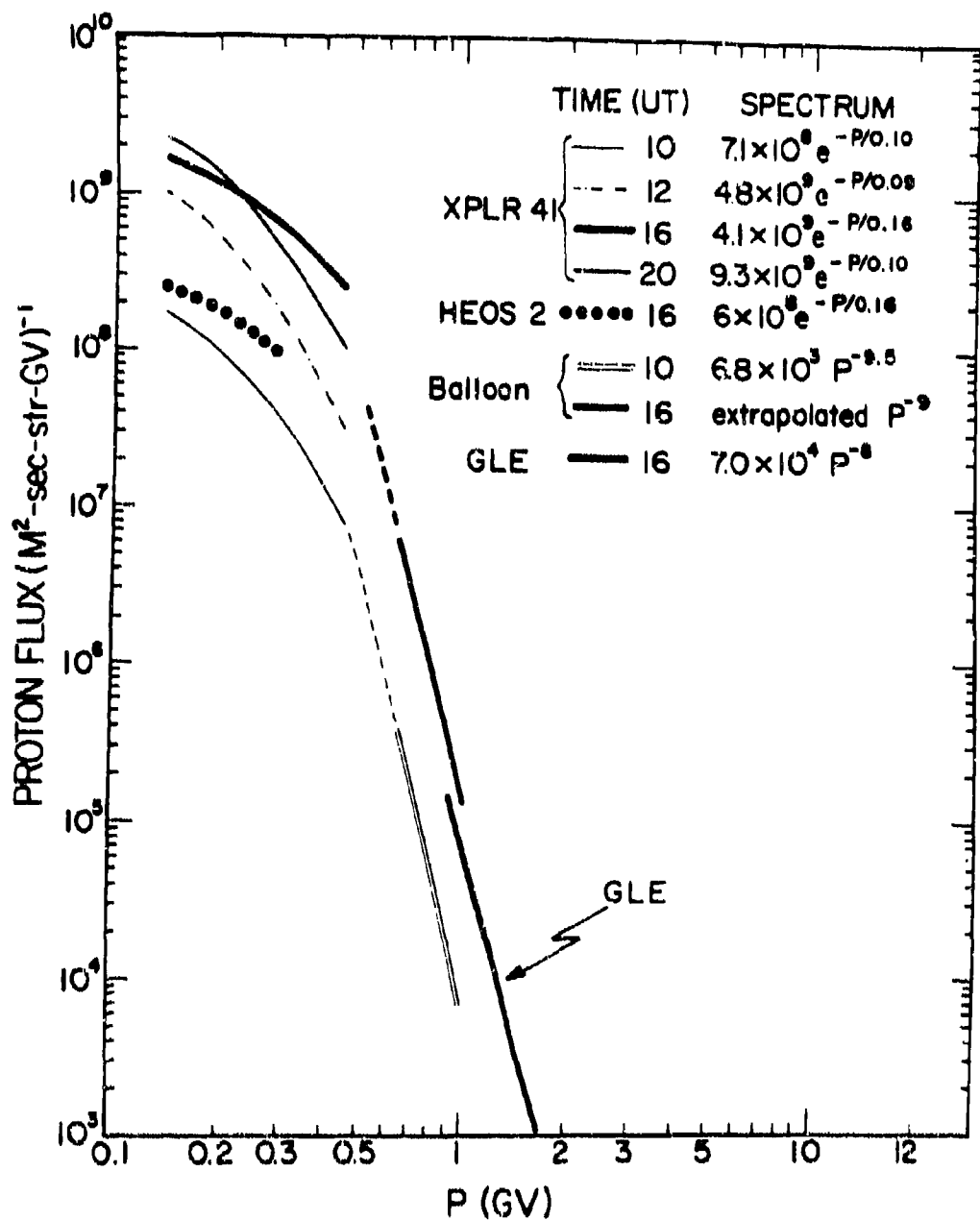


Fig. 4.4 — Differential solar proton magnetic rigidity spectra during the August 4 event (from Lockwood et al. 1975).

5.0 The Geomagnetic Cutoff

The earth's magnetic field must be penetrated by cosmic rays in order for them to reach a spacecraft in earth orbit. The number of magnetic field lines a cosmic ray must cross to reach a given point within the magnetosphere approximately determines the minimum energy it must possess. To cross more magnetic field lines more energy will be required. This penetrating ability is determined uniquely by the cosmic ray's momentum divided by its charge. This quantity is called magnetic rigidity (see Rossi, 1964, Appendix F). To penetrate the earth's magnetic field, a particle must have sufficient magnetic rigidity (momentum per unit charge) to avoid being turned away. There is a minimum magnetic rigidity a cosmic ray must possess to arrive from a given direction at a given point in the magnetosphere. Regions in the outer magnetosphere and near the poles can be reached at much lower magnetic rigidities than are required to reach points near the earth's equator. In general, for each point in the magnetosphere and for each direction from that point, there exists a magnetic rigidity below which cosmic rays cannot arrive. This value is the geomagnetic cutoff. For magnetic rigidities above this value, cosmic rays arrive freely, as though no magnetic field were present.

5.1 Methods for Computing the Cutoff

The geomagnetic cutoff was first calculated by C. Stormer (1930), using a dipole approximation for the earth's magnetic field. He showed that the cutoff rigidity at the earth's surface is given by:

$$P = \frac{60}{r^2} [1 - (1 - \cos \gamma \cos^3 \lambda)^{1/2}]^2 / [\cos \gamma \cos \lambda]^2 \quad (5.1)$$

for positively charged particles, where

P = magnetic rigidity in GeV/ec,

r = radial distance from the dipole center in earth radii

λ = latitude in dipole coordinates and,

γ = the angle which trajectory makes with magnetic west.

The magnetic rigidity, P, is related to the particles energy by:

$$E = (M_0^2 + P^2 Z^2 / A^2)^{1/2} = M_0 \quad (5.2)$$

where E is the kinetic energy in GeV/u (1 GeV/u = 1000 MeV/u),

P is the magnetic rigidity in GeV/ec

A is the particle's mass in amu

Z is the particle's charge and

$M_0 = 0.931$ GeV

Stormer's theory does not account for the presence of the solid earth, so in some directions at each location, this theory predicts a cutoff that is lower than the actual cutoff. The problem of the earth's shadow was first addressed by Vallarta (1948), again in the context of the dipole model. Vallarta showed that there existed a range of magnetic rigidities above the Stormer cutoff where the earth's shadow casts a broken pattern of allowed and forbidden bands of magnetic rigidity. There is the penumbral shadow of the earth. The width of the shadow varies from 10 per cent to 100 per cent above the Stormer cutoff at the earth's surface for zenith angles $< 45^\circ$. For larger zenith angles, the effect increases as the arrival direction approaches the horizon. The density of the penumbral shadow is also highly variable.

While these early investigations revealed the basic features of the geomagnetic cutoff, they were limited in their accuracy because they depended upon a dipole field model fit to the true geomagnetic field.

Shea and Smart (1975) have made detailed calculations of the geomagnetic cutoff using a realistic field model (IGRF-1965, 1969). This model describes the earth's field in an 80 term spherical harmonic expansion. For this reason, no analytic solution exists to the Stormer problem. Shea and Smart have calculated the geomagnetic cutoff by detailed ray tracing backwards from the point of interest, to determine if the trajectory leads back to outer space. Figure 6.1 (taken from Lund, 1980) shows such a computed trajectory for a cosmic ray whose magnetic rigidity is barely adequate to bring it into the atmosphere over Sinkiang Province in Western China. Such a calculation must be carried out for each point, each direction and each magnetic rigidity of interest using a high speed computer. This technique has provided very realistic maps of the geomagnetic cutoff as well as detailed examinations of the penumbral shadow. The authors define, for each point and direction: (1) a cutoff, below which no open trajectories are found, the Stormer cutoff; (2) a cutoff above which there are no closed trajectories, the main cutoff and; (3) the effective cutoff, a value between the main and Stormer cutoffs weighted according to the density of the penumbral shadow.

The size of the computational task required to employ this technique is such that it can only be used for selected sites and directions. Shea and Smart (1975) provide calculations of the vertical geomagnetic cutoff at an altitude of 10 Km on a world-wide grid of points spaced apart 15° in longitude by 5° in latitude.

To obtain the cutoff in other directions and at other points on earth, Shea et al (1973) recommend that the Stormer theory be used to interpolate the computed vertical cutoffs from the world grid. These authors show excellent agreement between transmittance functions for cosmic ray experiments at Palestine, Texas, calculated both by ray tracing and by Stormer theory interpolation.

Smart and Shea (1977) show that using eq. 5.1 with the "best fit" eccentric dipole model, which they suggest, it is possible to interpolate from the world grid (Shea and Smart, 1975) in three dimensions provided that radial interpolations are to altitudes small compared to an earth radius.

Heinrich and Spill (1979) have used these ideas to calculate the vertical geomagnetic cutoffs at various altitudes. The authors also calculated the vertical transmittance functions for several 223 Km circular satellite orbits, see Figure 5.2. The technique of Heinrich and Spill (1979) appears to be the best for calculating the transmittance function for an orbit.

The transmittance function calculated by Heinrich and Spill needs to be extended to include cutoffs from all directions, including vertical. This can be done [as Smart and Shea (1977) have suggested] with Stormer theory, (see eq. 5.1) extrapolating from the 400 Km altitude world grid recently prepared by these authors (Smart, 1980). To estimate the cutoff at higher altitudes, it is necessary to scale by $1/r^2$ from these calculations since none exist at higher altitudes.

There remains one problem, how to account for the earth's umbral shadow. On the earth's surface this is simple, cosmic rays can arrive from above, not below. At satellite altitudes the problem is not so simple, for the highest energies, the portion of the geometry factor that is occulted falls off with altitude, h , as

$$\Omega = 2\pi \{ 1 - [(R_e + h)^2 - R_e^2]^{1/2} / (R_e + h) \} \quad (5.3)$$

where R_e is the earth's radius. At lower magnetic rigidities, the earth's umbral shadow is distorted by the earth's field and swept off to an easterly direction so that particles may arrive below the optical horizon in the west. This distortion increases at lower rigidities as the cutoff is approached. Besides the change of direction of earth occultation at low rigidities, the occulting solid angle also falls off more rapidly with altitude than described by eq. 5.3 (Smart, 1980). The details of how the earth's umbral shadow changes with altitude and rigidity are unknown; Smart (1980) has suggested that the problem might be solved by ray tracing at a range of altitudes and rigidities.

5.2 The Effect of Magnetic Storms

So far in this discussion we have only dealt with the quiescent magnetosphere. When a solar flare occurs, it usually causes a magnetic storm at earth. This storm disrupts the magnetosphere altering the geomagnetic cutoff, usually depressing it. Figure 5.3 shows the fractional depression $\Delta P/P_0$ in geomagnetic cutoff as a function of quiescent cutoff P_0 , in two magnetic storms; Nov. 15, 1960 (Webber, 1962) and April 1, 1973 (Debrunner and Flückiger, 1977). The effect seems to be the result of ring currents induced by the sudden commencement of the storm (see Flückiger et al. 1979, Dorman, 1974). These currents reduce the equatorial magnetic field by $\sim 10^3 \gamma$ (where $\gamma = 10^{-5}$ gauss), allowing penetration to any given point in the magnetosphere by lower energy cosmic rays than is normally possible.

As a model for this effect, we recommend the function shown as the solid curve in Figure 5.3. Specifically,

$$\Delta P/P_0 = .54 \exp(-P_0/2.9 \text{ GV}) \quad \text{with } P_{\text{storm}} = P_0 - \Delta P \quad (5.4)$$

5.3 Recommended Procedure

Based on the foregoing discussion, we recommend for:

- 1) The quiescent cutoff. Use of Shea and Smart's 400 Km world grid of effective cutoffs, interpolating to other latitudes, longitudes and altitudes using Eq. 1 with the eccentric dipole recommended by Smart and Shea (1977). The earth's shadow should be taken as shrinking with altitude according to Eq. 2. The transmittance function is best computed by the orbit integration technique of Heinrich and Spill (1979).
- 2) During solar flares. Calculate the quiescent cutoff as described above and use Eq. 5.4 to obtain the depressed cutoff for flare conditions. There are several simple but less accurate alternatives to the above procedure. The simplest is to use the rule of thumb (Smart and Shea, 1967).

$$P_0 = 15.96/L^{2.005}$$

where L is the McIlwain L parameter (McIlwain, 1961) and P_0 is the vertical cutoff in GV. P_0 may then be taken as the average cutoff for the directions not occulted by the earth (see Eq. 5.3). A better technique is to use the $1/L^2$ rule to extrapolate the 400 Km world grid. This essentially is what was done by Heinrich and Spill (1979).

The principal sources of error are the uncertainty in the cutoff and the darkness of the penumbral shadow at points reached by extrapolation. This probably leads to no more than a ± 20 per cent error in the cutoff. A second source of error is the size we assume for the umbral shadow; this could be overestimated by a factor of 2. This error would be about the same as a ± 10 per cent error in magnetic rigidity at 400 Km and grow smaller at higher altitudes. The actual error in particle flux resulting from these errors in rigidity depends on where the cutoff comes on the differential energy spectrum, but even at high cutoff values these errors translate into no more than a ± 30 per cent error in the particle flux.

The uncertainty in the actual value of the geomagnetic cutoff may be ~ 50 per cent at low cutoffs during a magnetic storm. This translates into only a ± 50 per cent error in the flux, and since this condition is transient, it is only important for solar flares. The flux uncertainty during a solar flare is $>> 50$ per cent.

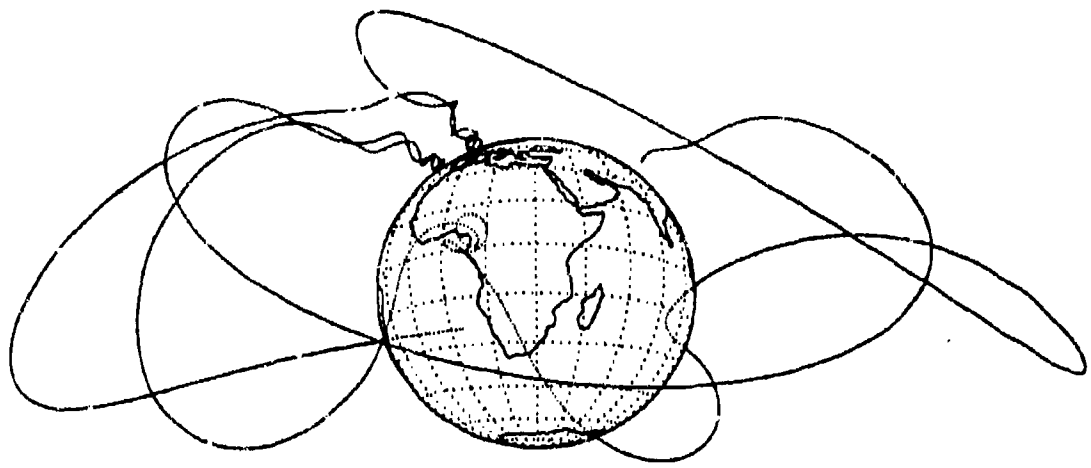


Fig. 5.1 — This figure shows the computed trajectory of a cosmic ray in the earth's magnetic field. Such complex trajectories are not unusual for cosmic rays in the penumbral shadow near the Stormer cutoff (Lund, 1980).

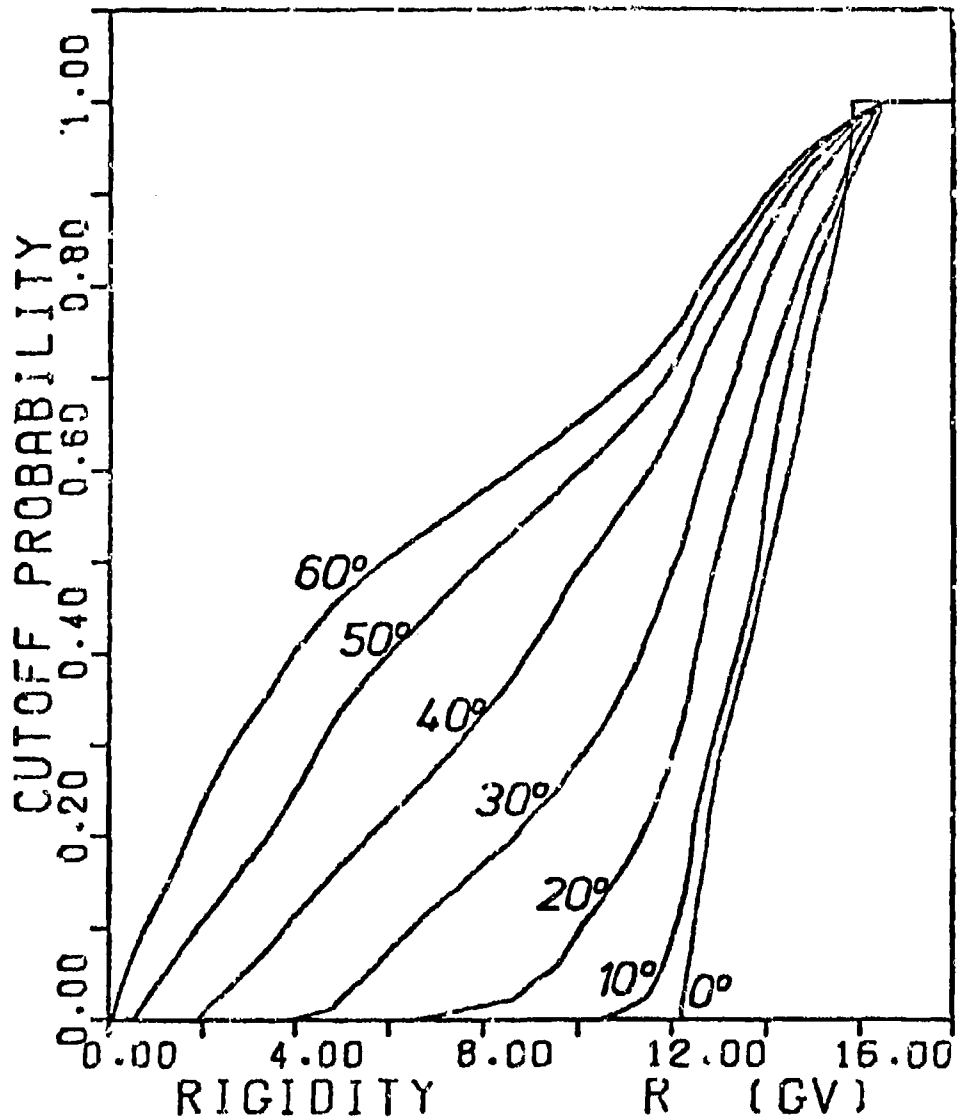


Fig. 5.2 — The geomagnetic transmittance function for 223 Km circular orbits of various inclinations. The symbol R is used here for magnetic rigidity taken from Heinrichs and Spill (1979).

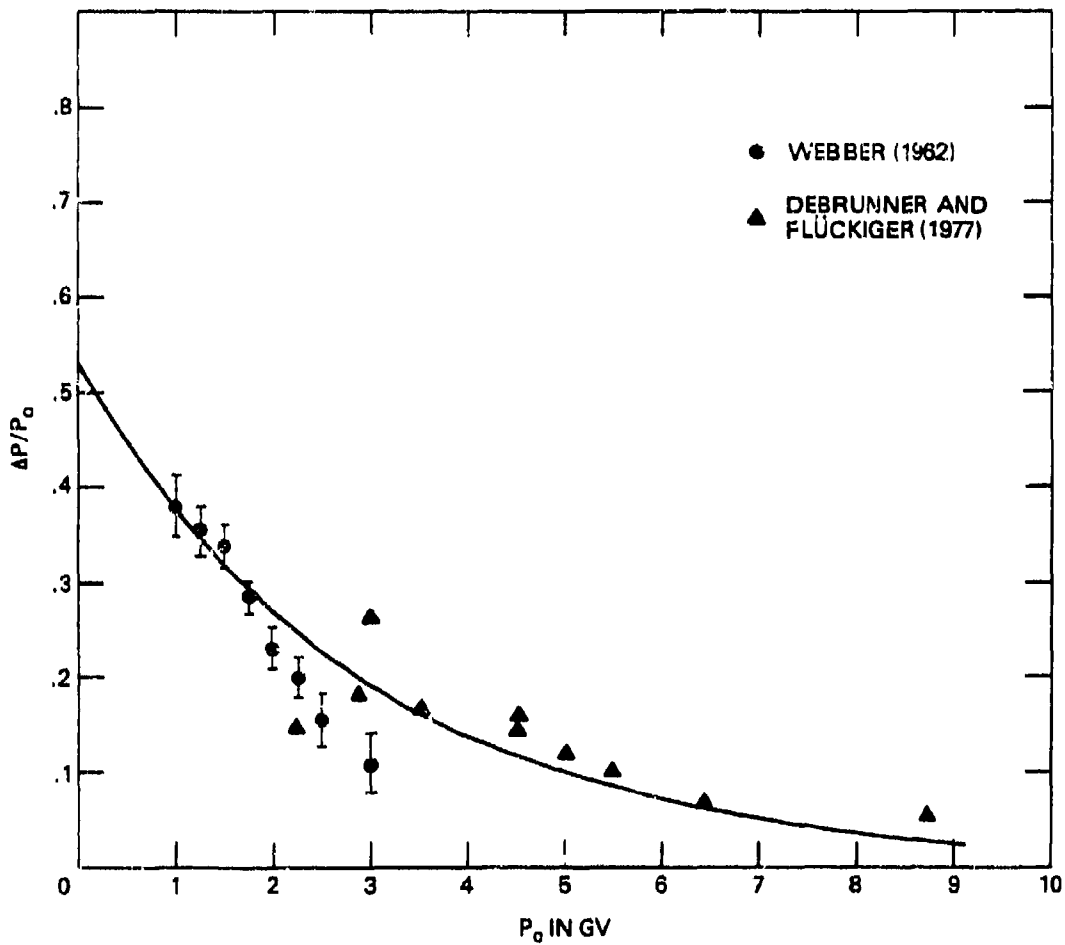


Fig. 5.3 — The fractional depression of the geomagnetic cutoff, $\Delta P/P_0$, as a function of quiescent cutoff, P_0 . The data are for magnetic storms, Nov. 15, 1960, and April 1, 1973. The solid curve is the fractional cutoff depression function we recommend using to describe the geomagnetic cutoff for major solar flares.

6.0 Particles from the Magnetosphere

6.1 Protons

Protons are the most abundant particles in the magnetosphere that can easily produce soft upsets. The trapped proton environment has been comprehensively studied and is well described by the computer model, AP-8 (Sawyer and Vette, 1975). We recommend that this model be used for the trapped proton environment. In addition to protons, the magnetosphere contains helium nuclei as well as heavier nuclei, especially carbon, nitrogen and oxygen. While these nuclei are less abundant than protons they are much more effective in producing soft upsets.

6.2 Alpha Particles

Helium nuclei (mostly alpha particles) have been detected throughout the magnetosphere. The principal source of these nuclei appears to be the solar wind (Blake, 1973 and Hovestadt et al. 1978). The solar wind particles are transported down into the magnetosphere and accelerated by radial diffusion. This process was described theoretically by Cornwall (1972) and has recently been shown to describe well the helium ion population in the magnetosphere (Spjeldnik and Fritz, 1978, and Fritz and Spjeldnik, 1979). The bulk of the helium nuclei are, however, at energies too low to penetrate the walls of the spacecraft.

The only measurements of geomagnetically trapped alpha particles at energies above ~ 2 MeV/u have been reported by Rubin et al (1977) and Panasyuk et al. (1977). The results of Rubin et al on the helium to proton ratio are shown in Figure 6.1. Also shown for comparison are the low energy measurements of Fennell et al. (1974) and Blake et al (1973). The data of Rubin et al cover the range of $1.85 \leq L \leq 2.65$ at low altitudes, i.e. $3 \leq B/B_0 \leq 8.5$. The data point of Fennell et al is at $2.6 \leq L \leq 2.7$, $1.3 \leq B/B_0 \leq 2.3$, while that of Blake et al. is on the geomagnetic equator at $L = 1.95$. The results of Panasyuk et al. (1977) cover the range from $2.0 \leq L \leq 2.55$ and $1.4 \leq B/B_0 \leq 2.35$. Their data cover the broad energy band $4.25 \leq E \leq 15$ MeV/u. For this range, they report $5 \times 10^{-4} \leq \alpha/p \leq 1.5 \times 10^{-3}$. These results are consistent with those shown in Figure 6.1.

These results may be taken as typical of quiet periods in the inner zone, although there was one magnetic storm during the period (Rubin et al. 1977).

The declining trend in the α/p ratio in Figure 6.1 can be expected to continue to higher energies. This is because the protons are principally from cosmic ray albedo neutron decay (CRAND) while the helium nuclei have diffused in from some external source, presumably, the solar wind.

Rubin et al (1977) show that the α/p ratio varies about a factor of 2 between L values of 1.85 and 2.65 with a peak at $L = 2.45$. For purposes of this particle environment model, we have chosen to ignore the L value dependence of the α/p ratio and adopt the dashed curve in Figure 6.1 as the energy dependent α/p ratio for $L < 2.6$. Specifically,

$$\alpha/p = 2.5 \times 10^{-3}; E < 5 \text{ MeV/u} \quad (6.1)$$

$$\alpha/p = 8.3 \times 10^{-3} \exp(-E/4.15); 5 \text{ MeV/u} \leq E \leq 10 \text{ MeV/u} \quad (6.2)$$

and

$$\alpha/p = 0.957 \exp(-E/1.4); E > 10 \text{ MeV/u} \quad (6.3)$$

There are no quiet time measurements of helium nuclei above 10 MeV/u at $L > 2.65$ so we must use the data at lower energies. Fritz and Spjeldnik (1979) have computed α/p ratios at the same energy per amu that best fit the data over a range of L values. Based on their results, we adopt the conservative value of $\alpha/p = 2.5 \times 10^{-3}$ for $L > 2.5$. While the calculations of Fritz and Spjeldnik extend only to 2 MeV/u, we have made the assumption that this ratio is the same at energies of 2 MeV/u or higher.

It should be noted that above $L = 2.5$, the proton flux with $E > 5$ MeV falls off very rapidly so, in practice, most of the helium nuclei with $E > 15$ MeV/u will still be found below $L = 2.5$.

There have been a few reports of α/p ratio measurements during solar flares and magnetic storms. These results differ considerably from the quiet time model presented above. Verzariu (1973) reported results following the solar flare of March 6, 1970. This flare had a proton fluence (> 30 MeV) of $1.3 \times 10^{6}/\text{cm}^2$, (compared to $8.1 \times 10^9/\text{cm}^2$ for the August 1972 flares). Verzariu reports a proton flux increase of ~ 10 , for a total α flux increase of ~ 50 . This condition decayed back to pre-flare levels over a few days.

Transient events of this type usually disturb the outer magnetosphere much more than the inner zone. Scholer et al. (1979) describe magnetospheric conditions during a large geomagnetic storm ($Dst = -230$) associated with a solar flare. They report that the α/p ratio increased by a factor of ~ 7 at $L = 2.48$ during the storm main phase. The proton flux appears to have increased by ~ 10 at the same time, leading to an α flux increase ~ 70 . The authors also report precipitating particles, including heavy ions, down to $L = 2.7$.

The enhanced α/p ratios reported by Verzariu and Scholer et al. are 2.3×10^{-3} and 2.5×10^{-3} respectively. These seem to be covered by our conservative choice of α/p ratio for this model.

In addition to the short term (few day) enhancements cited above, Van Allen and Randall (1971) report evidence that solar flare α particles may be durably trapped in the magnetosphere. They report an enhancement of ~ 40 in the 0.2 to 2 MeV/u α flux at $3.0 < L < 3.5$. The enhancement decayed away with a time constant of ~ 45 days. The proton flux at the same time increased by ~ 4 , implying an α/p ratio increase of ~ 10 . The authors also examined other α flux increases in the innerplanetary medium and found one additional example of durable trapping but several cases when α 's were

not durably trapped. They concluded that special conditions were required for α 's to become durably trapped in the magnetosphere. Spjeldnik and Fritz (1981a) have recently reported an additional example of stable trapping where the particles were presumably from solar flares. These authors report an α flux increase of ~ 30 at $L = 2.5$ for $E \sim 0.5$ MeV/u and a decay time > 160 days following the solar flares of August, 1972. At the same time, no appreciable increase was seen in the proton flux.

These results on durable trapping of solar flare particles must be extrapolated to the higher energies of interest here. There is no way of knowing how many α -particles were injected by these flares at higher energies. We can only guess that the flux increases may have been comparable. The decay times observed at these low energies will surely be much longer at energies above 10 MeV/u and based on the analysis of Spjeldnik and Fritz (1981a), we conclude that the decay time at $L = 2.5$ for equatorially mirroring α 's may be many years! Decay times will be more rapid for α 's mirroring off the equator because of the increased energy loss in the residual atmosphere. From this line of reasoning, it appears possible that the energetic α flux above 10 MeV/u and inside $L = 2.5$ may originate in solar flares.

Based on the scanty data available at energies above 10 MeV/u, it is difficult to draw any conclusions. Nevertheless, taking an optimistic view, as we said we would do in the introduction, we will assume that the results of Rubin et al. (1977) and Panasyuk et al. (1977) represent a typical sampling of the α flux. We therefore conclude that the α/p ratio model we suggest (Eqs. 6.1, 6.2, and 6.3) is sufficiently conservative to describe the conditions in the inner magnetosphere most of the time. We feel the α flux is best described by multiplying our α/p ratio by the proton flux predicted by Ap-8 (Sawyer and Vette, 1976).

6.3 Heavy Nuclei

C, N, and O have been observed in several experiments. It is by no means clear that the particles in all these observations were trapped in the magnetosphere, but in each instance the particles were forbidden direct access by the geomagnetic cutoff, so they did not come in directly from outside.

Van Allen et al. (1970) report the detection of heavy nuclei, presumably C, N, and O in the range $3.0 < L < 3.5$, and $0.15 < B < 0.2$. They found that a ratio $CNO/\alpha = 2.8 \times 10^{-3}$ above 0.3 MeV/u. Hovestadt et al. (1978) report substantial fluxes of C, O and heavier ions between $L = 2.5$ and 4. They report a CNO/α ratio of 3×10^{-2} for $0.4 \text{ MeV/u} < E < 1.5 \text{ MeV/u}$. The CNO flux is dominated by carbon with C:N:O proportions of 2.7:0.28:1. In contrast with these results, Blake et al. (1980) report a CNO/α ratio of 6.8×10^{-5} at $L = 3.25$, $0.35 < B < 0.25$ and $E > 0.25$ MeV. This is in clear disagreement with the results of Van Allen et al. (1970) and it is difficult to reconcile with the results of Hovestadt et al. (1978) which were obtained near the geomagnetic equator. It appears that more measurements will be required to resolve these differences.

As with the helium data, these measurements are at energies too low to cause soft errors. There is one measurement at higher energies, reported by Mogro-Campero (1972). The author was not able to measure the CNO/He ratio, but reports 2×10^{-5} CNO nuclei/cm² ster.sec. MeV/u at $L = 4$ with $13 < E < 33$ MeV/u which exceeded the interplanetary flux by ~ 100 . If these

particles are trapped in the magnetosphere as the authors argue, they represent a large flux. Comparing Mogro-Campero's CNO flux with the scanty data available on helium nuclei, we conclude that the CNO/ α ratio probably exceeds 1 and that the CNO flux may be comparable to the proton flux at $L = 4$, $13 \leq E \leq 33$ MeV/u.

In addition to those heavy nuclei believed trapped, in the magnetosphere, another population of unknown origin has been observed by Chan and Price (1975) and Biswas et al. (1975). The results are based on a single experiment performed outside Skylab from Nov. 1973 to Feb 1974 with a stack of plastic track detectors. For this reason, the experiment provided only the integral fluence for the 420 Km, 50° Skylab orbit. The orbit-averaged flux is shown in Figure 6.2 (Biswas and Durgaprasad, 1980 and Chan 1976). The figure compares the measured oxygen spectrum with the galactic cosmic ray spectrum (GCR) modulated by the geomagnetic cutoff of the Skylab orbit. Also shown is the anomalous component oxygen spectrum assuming the oxygen is singly ionized. As can be seen, the flux exceeds that expected from both these sources.

It is possible that the particles were trapped in the earth's magnetic field. If so, they would have been collected only when the spacecraft passed through the South Atlantic anomaly ($1.3 < L < 1.7$). About 1.4 per cent of the orbit time was spent in the anomaly. This implies that the trapped particle spectrum would be the same as that shown in Figure 6.2 with the flux multiplied by ~ 72 . This leads to a flux of $\sim 3 \times 10^{-4}$ CNO nuclei/cm² ster.sec.MeV/u, for $13 < E < 33$ MeV/u and $1.3 < L < 1.7$, more than an order of magnitude higher than that reported by Mogro-Campero, but much less than the proton flux at these L values. Comparing the orbit averaged proton flux with the measured average oxygen flux, we have $O/p \sim 1 \times 10^{-6}$ at 20 MeV/u.

A large number of explanations have been suggested for these results [see Biswas and Durgaprasad (1980) and Price (1979)]. In our judgment, the most likely of these has been put forward by Blake and Friesen (1977). These authors suggest that the particles of the anomalous component are singly ionized and that, because of their large rigidity at low energies, these ions penetrate deep into the magnetosphere at low energies. Some of these ions arrive close to the atmosphere near their geomagnetic cutoff and consequently travel in the local mirror plane for trapped particles. Because of the large cross section for stripping ($E > 10$ MeV/u), these particles become stripped rapidly. Once stripped, they have a much lower magnetic rigidity and because they are moving in the local mirror plane, become more or less stably trapped. This leads to a special trapped population of oxygen, nitrogen, neon and a few other elements which comprise the anomalous component. This population is also unusual because its equatorial pitch angle distribution would be double peaked near 36° and 145°, so that the flux is nearly independent of B/B_0 , i.e. all particles mirror at low altitudes.

The Blake and Friesen theory is further supported by the composition results shown in Table 6.1 (Biswas and Durgaprasad, 1980).

TABLE 6.1: ELEMENTAL COMPOSITION OF HEAVY IONS IN THE MAGNETOSPHERE

Element	Anomalous Comp.	Relative Composition	
		Magnetosphere	Galactic CR
C	.23 ± .09	.21 ± .019	1.13 ± .03
N	.22 ± .09	.21 ± .041	.27 ± .02
O	1.0	1.0	1.0
Ne	.07 ± .04	.08 ± .02	.18 ± .01
Mg	.002 ± .002	.006 ± .004	.20 ± .01
Si	< .02	.004 ± .002	.14 ± .006
S	----	< .004	.035 ± .003
Ar	---	< .003	.013 ± .002
Fe group	---	.05 ± .02	.084 ± .001

As Table 6.1 shows, the heavy ions in the magnetosphere have a composition which matches the anomalous component much more closely than the galactic cosmic rays, or for that matter, the solar composition.

In addition to the elements detected by the plastic track detectors outside Skylab, a second experiment was performed outside Skylab using a glass detector. Kretschmer (1975) reports the spectrum of low energy iron group nuclei measured in this detector. The spectrum was measured only up to 10 MeV/u. Assuming these particles are trapped, the trapped spectrum for $L < 1.4$ would be:

$$F = 1.3 \times 10^{-3} E^{-1.68} \text{ iron nuclei/cm}^2 \text{ ster.sec.MeV/u} \quad (6.4)$$

for $1 \leq E \leq 10$ MeV/u, and probably declining above that energy more like the oxygen spectrum, eqs. 6.5 and 6.6. Spjeldnik and Fritz (1981) have reported $Z > 9$ particles stably trapped at $2 \leq L \leq 3.5$ and $B/B_0 \leq 1.5$ at energies ~ 1 MeV/u.

While the Blake and Friesen theory explains the Skylab experiment, it cannot explain Mogro-Campero's OGO-5 data. The particles in this experiment have equatorial pitch angles $> 24^\circ$ (70 per cent of them $> 45^\circ$) while the Blake and Friesen theory would predict pitch angles $\sim 16^\circ$.

It would appear, based on these two experiments, that we have a relatively large component of energetic trapped heavy ions in the magnetosphere. During quiet times in the inner zone, the proton flux might be the dominant cause of soft errors, but beyond $L \sim 2.5$ the heavy ion flux becomes increasingly important.

Besides these "quiet time" measurements, Spjeldnik and Fritz (1981b) have reported two events in which heavy ions were injected deep

into the magnetosphere by solar flares. The event associated with the flares of August 1972 resulted in a 10^3 increase in $Z > 4$ ions at $L = 2.5$ and $E \sim 0.26$ MeV/u. At the same time, no appreciable increase was observed in the proton flux at $L = 2.5$. The injected flux decayed with a half-life of ~ 25 days.

In addition, Spjeldnik and Fritz (1981c) report that $Z > 9$ nuclei were injected by the same flare. They found an increase of $> 10^3$ at $L = 2.5$ from an indetectably low flux prior to the flares. Assuming these nuclei were predominantly silicon, they had energies in the range $0.4 < E < 3.9$ MeV/u. The flux decayed at $L = 2.5$ with a half-life of ~ 30 days. This decay time seemed to the authors, too short to have been controlled by charge exchange or energy loss processes.

The question now is what does this imply for the higher energies of interest here. We can only guess that such injections must have occurred at higher energies. If the injections at $E \geq 10$ MeV/u were as large as those reported at lower energies (and they may well have been), then heavy ions were probably the principal cause of soft errors arising from trapped radiations in the entire inner magnetosphere.

At higher energies, the decay times for heavy ion injections could be many years, for particles mirroring near the geomagnetic equatorial plane. With the little we currently know about these trapped energetic heavy ions, a worst case model cannot be constructed. We simply have no idea what the conditions are following a large flare or how long they persist. We can only hope that what has been seen in the two experiments (Mogro-Campero, 1972 and Chan and Price, 1975) is typical and can be extrapolated to other parts of the magnetosphere and other times.

With so little experimental data, any model for heavy ions in the magnetosphere is highly speculative. We will, nevertheless, suggest a model that we hope will prove to be sufficiently conservative.

For $L < 3$ we suggest the differential energy spectrum for oxygen (the dashed line in Figure 6.2) be adopted, with the ordinate multiplied by 72. Specifically,

$$\phi = 5.4 \times 10^{-4} \text{ oxygen nuclei/cm}^2\text{ster.sec.MeV/u} \quad E < 16 \text{ MeV/u} \quad (6.5)$$

and

$$\phi = 1.96 \times 10^2 E^{-4.62} \text{ oxygen nuclei/cm}^2\text{ster.sec.MeV/u} \quad E > 16 \text{ MeV/u} \quad (6.6)$$

We take this to be the trapped flux from $1.2 < L < 3.0$ for all values of B/B_0 . To obtain the spectra for other elements, just multiply the oxygen spectrum by the measured relative abundances for the magnetosphere in Table 2.

For $L < 3$, Mogro-Campero reports the ratio O/C $\sim 0.5 \pm 0.4$. This is more typical of galactic cosmic ray abundances (see Table 3).

No differential energy spectrum was measured in this experiment, hence we can only assume that the spectrum falls with increasing energy as the

Alfven criterion for stable trapping is approached. The Alfven criterion is:

$$\frac{R \text{ grad } B}{B^2} < 1 \quad (6.7)$$

where R is the magnetic rigidity and B is the magnetic field flux density.

This is the same factor that limits the proton spectrum at high energies, so we use the proton spectrum at L = 3.0 as a model. From Sawyer and Vette (1976):

$$\phi_p \sim E^{-5.2} \quad (6.8)$$

hence we propose to use

$$\phi = 1.6 E^{-5.2} \text{ oxygen nuclei/cm}^2 \text{ster.sec.MeV/u for } E > 13 \text{ MeV/u} \quad (6.9)$$

for the differential energy spectrum of oxygen. The spectra of the other elements are obtained from the galactic cosmic ray abundances shown in Table 6.1.

Besides nuclei, there are intense fluxes of electrons trapped in the magnetosphere, especially in the outer Van Allen belt. In section 2.2 we discussed the ways in which electrons could cause soft upsets in microelectronics and concluded that we need only be concerned about the case where the electron flux above 20 MeV far exceeds the elemental flux. There is a substantial flux of electrons above 20 MeV in the inner radiation belt, but the proton flux there is much greater. The electrons are the dominant component in the outer belt, but they are all at energies below 20 MeV (see Vette et al, 1966). Based on these results, we conclude that trapped electrons will not be an important cause of soft upsets on satellites.

6.4 Other Particles in the Magnetosphere

Besides stably trapped particles, the magnetosphere contains quasi-trapped particles that cannot complete a drift around the earth without loss and splash albedo cosmic ray particles. A few experiments have been carried out to measure each of these components (see Kuznetsov et al. 1979, and Friedlander and Hoppe, 1977). The results give fluxes that are very low in comparison with other components encountered on practical satellite orbits, therefore they will be ignored.

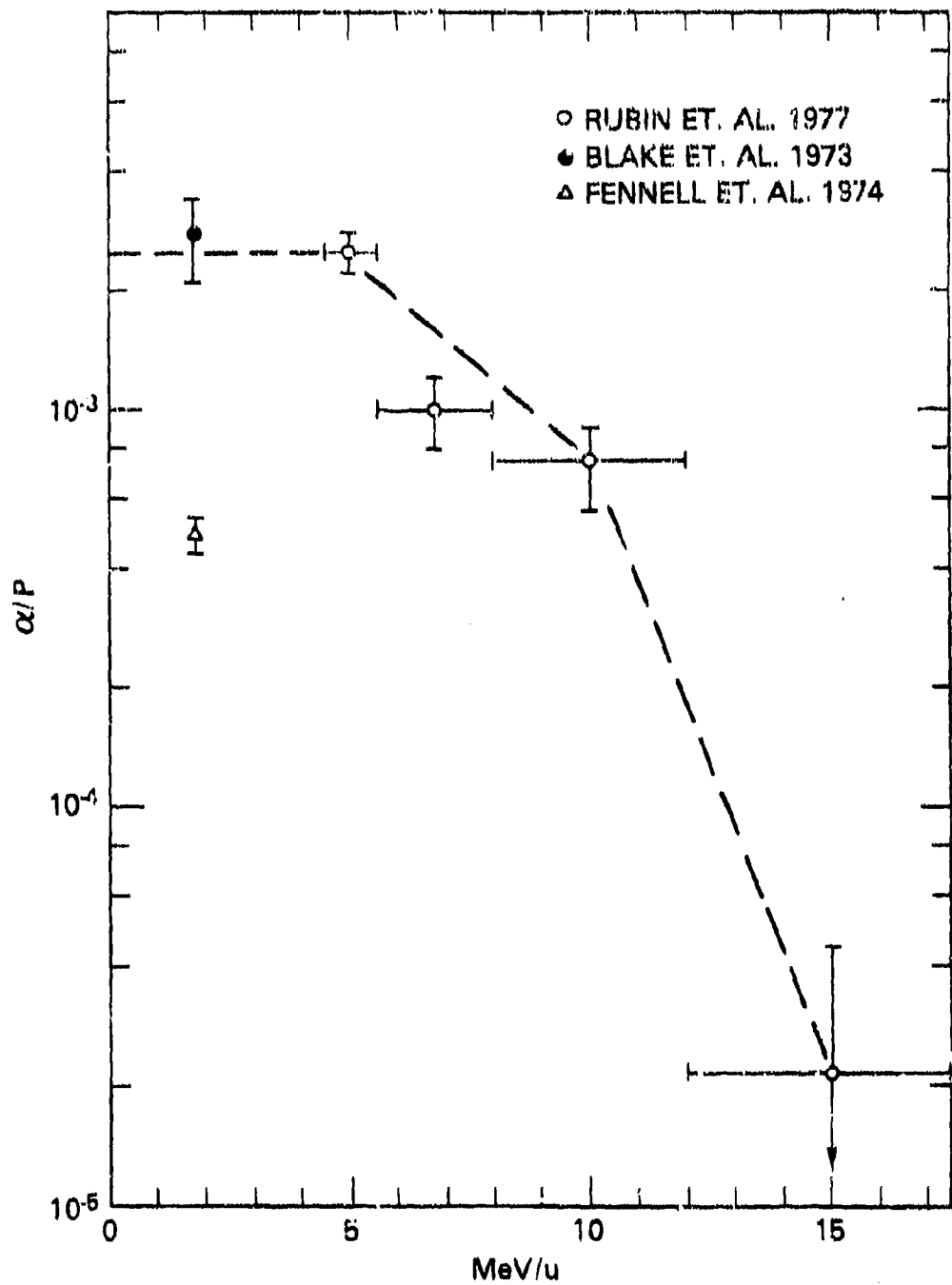


Fig. 6.1 — Measurements of the α/p ratio for $1.85 < L < 2.7$. The dashed line is the recommended α/p ratio as a function of energy for $L < 2.6$. It may be used to scale the orbit integrated proton spectra obtained with the AP-8 model (Sawyer and Vette, 1976).

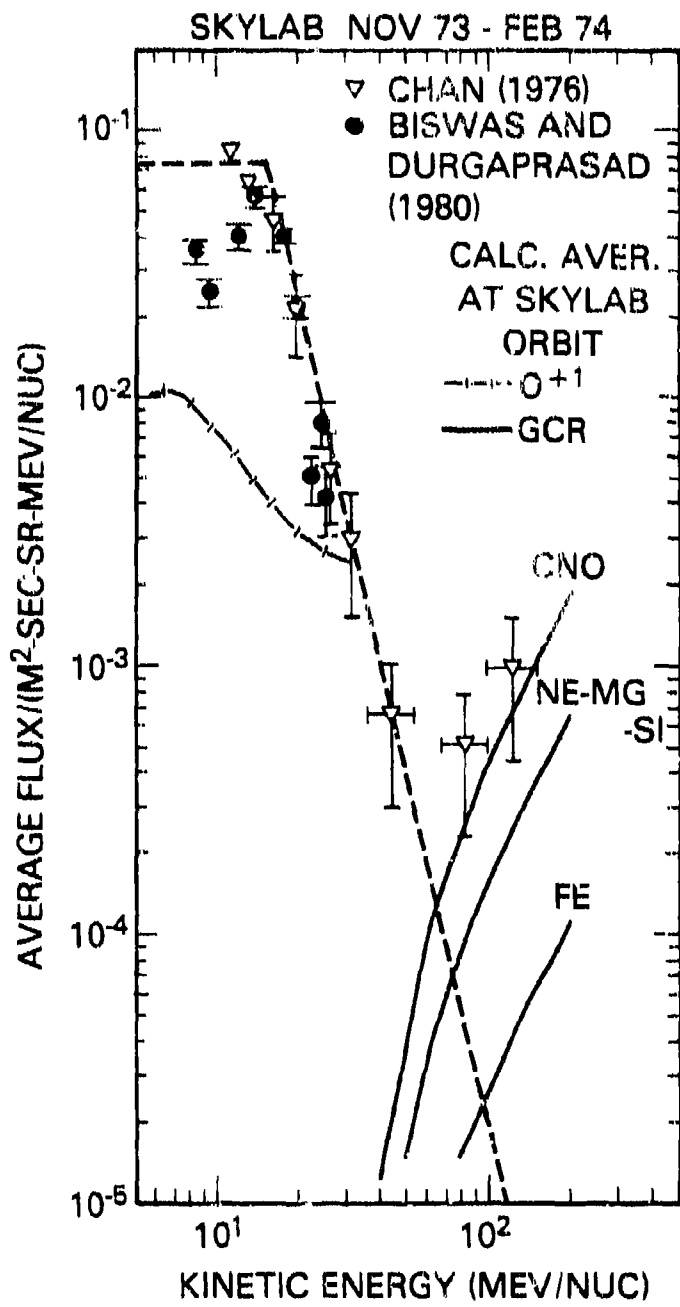


Fig. 6.2 — The orbit-averaged flux of oxygen nuclei from the Skylab orbit as measured in a stack of plastic track detectors analyzed independently by Chan (1976) and Biswas and Durgaprasad (1980). Also shown are the galactic cosmic ray spectra (GCR), geomagnetically modulated for the Skylab orbit and the anomalous oxygen spectrum similarly modulated, assuming the oxygen nuclei are in the +1 charge state.

7.0 Cosmic Ray Effects on Space-Borne Microelectronics

In the preceding sections we have developed a model that describes the particle environment through which spacecraft travel. We have shown how one computes the geomagnetic cutoff and uses it to modulate the spectra of particles coming from outside the magnetosphere. Finally, we have suggested a model for protons trapped in the magnetosphere and shown how this model can be augmented to predict the trapped fluxes of helium and heavier nuclei. By following this procedure, one can arrive at an estimate of the differential energy spectra of the various nuclei actually incident on the spacecraft. The present section is devoted to a discussion of how these spectra are used to estimate the cosmic ray effects on satellite-borne microelectronics and what might be done to minimize those effects.

7.1 Cosmic Ray Transport Through the Spacecraft Walls

Since cosmic rays are isotropic, they may reach the electronics in the spacecraft from all directions. Some of these directions may involve penetrating as little as 25 mils of aluminum, while others may involve a few inches.

A complete treatment of the cosmic ray transport problem involves accounting for how the energy spectrum of each element is modified by energy loss and nuclear fragmentation in the spacecraft. Heinrich (1977) has carried out such a calculation for the interplanetary cosmic ray spectrum. He shows that the effect of shielding is to reduce the amplitude of the differential energy spectra and gradually shift the peak of the spectrum to higher energies. It is only for minor constituent nuclei, like fluorine, that fragmentation can actually increase the flux above the unshielded level. Even then, this increase is only at low energies and for a limited range of shield thickness.

While the interplanetary cosmic-ray spectral shape is little affected by transport through shielding, this is not true of cosmic rays modulated by the geomagnetic cutoff. The effect of the earth's magnetic field is to exclude the lowest energy cosmic rays. After such a spectrum passes through shielding, this low energy part of the spectrum will be restored by ionization losses in the shielding.

Several workers, publishing papers on soft errors, have presented calculations of shielded cosmic ray spectra which show enormous increases in the low energy cosmic ray intensity after propagation through a modest shield thickness. These calculations are grossly in error! In making such calculations care must be taken. It is not enough to shift the cosmic ray intensity to a lower energy. The energy interval over which that intensity is measured must also be transformed to the lower energy. When this is properly done, results similar to those of Heinrich will be obtained. The only possibility for building up the spectrum at low energies is in the case of the hydrogen spectrum. Here it is possible for protons to suffer large energy losses in nuclear collisions. A small number of low energy protons could be produced in nuclear reactions initiated by heavier ions. Such protons could produce a low energy build up in the shielded hydrogen cosmic ray spectrum.

7.2 The Effects of Intense Ionization

In the previous paragraphs, we saw how it is possible to obtain the cosmic ray spectra incident on the microelectronic devices. We will now discuss the effects of the intensely ionized paths left by these particles.

Wallmark and Marcus (1962) were the first to predict that cosmic rays could have adverse effects on microelectronics. These authors predicted two effects: false signals resulting from cosmic ray ionization and displacement damage resulting in the permanent failure of individual circuit elements. The first of these effects was observed in dynamic random-access memories (RAMs) initially by May and Woods (1979). These authors observed bits flipped by charged particles with no permanent damage to the memory cells. They called these events "soft errors". Following publication of their results, there has been a flurry of papers describing soft errors in a variety of devices.

May and Woods showed that the soft errors they observed were due to alpha particles from uranium and thorium in the device packages. Clearly, whatever a stopping alpha particle can do, a stopping iron nucleus can do much more easily! The first published results on tests with heavy ions were presented by Kolasinski, et al. (1979). These authors reported the results of tests on a variety of devices, many of which are candidates for spacecraft electronic circuits. Most of these devices were found to exhibit soft errors. In addition some of the devices exhibited latchup (a bit which is permanently latched in one state until released by cycling the power supplies). The mechanism for latchup in one of these devices, the HM-6508, has been identified (Pickel and Blandford, 1980b). It results from "turning on" a parasitic circuit which is operationally equivalent to a silicon-controlled rectifier. Once turned on, the circuit must be powered down to reset it. The "turn on" current comes from the hole-electron pairs generated by a stopping heavy ion.

There have been quite a number of efforts to model the mechanisms by which cosmic rays produce soft errors. May and Woods seem to have correctly identified the mechanism in dynamic RAMs. A soft error will result whenever a passing alpha particle produces enough ionization to supply the critical charge needed to fill an empty potential well in the transistor-capacitor circuit of a dynamic RAM memory cell. Besides this mechanism, there appear to be many others. For example, floating bit-lines can be discharged, and bistable flip-flops may be disrupted by cosmic-ray-induced voltage transients and regenerate in the opposite state. Pickel and Blandford (1980a) have discussed models for these and other mechanisms in detail.

Besides soft errors, Wallmark and Marcus (1960) predicted hard failures. Pickel and Blandford (1980a) have reported hard failures due to heavy-ion-induced insulator punctures in MNOS EAROMS. In addition, based on cosmic-ray track structure considerations, Bradford (1978) has predicted that permanent radiation damage will be produced by cosmic rays in VLSI circuits.

7.3 Efforts to Reduce Cosmic Ray Effects

There are a number of proposals to reduce the effects of cosmic rays on microelectronics. The most obvious is to test available devices in heavy ion beams and reject those that are affected. This program is being actively pursued by NASA, SAMSO, and their contractors. It is becoming clear, from their work, that certain circuit designs and device technologies are much less sensitive than others.

A second approach (first suggested by Pickel and Blandford, 1978) is to pursue an especially promising device technology, CMOS/SOS. Because hole-electron pairs in the sapphire substrates of these devices have a very low mobility, the hole-electron pairs generated in the substrates cannot readily diffuse into the circuits' potential wells. This makes it necessary for cosmic rays to produce the required charge in a much shorter path. This, in turn, calls for higher stopping power, and thus heavier ions are required to produce soft errors. Kolasinski et al. (1979) and Brucker et al. (1980) have found some very error-resistant devices of this type.

Another approach, tried with some success, is to adjust the device parameters. Peeples and Every (1980) show that soft error rates can be reduced by increasing supply voltages. Increasing voltages, however, increases the device hard-failure rate and is therefore of limited use in controlling soft errors.

Throughout the test results published to date there is a disturbing correlation. The more dense and lower power a device is made, the more sensitive it becomes to cosmic rays. The most advanced devices, 64K dynamic RAMs, 256K CCD's and VLSI circuits are highly desirable candidates for satellite applications, but they are also among the most sensitive devices to cosmic rays. A potential solution to the problem is a fault-tolerant space-borne computer. Designs for such computers have recently reported by Retzler (1980) and Masson (1980). While these designs appear capable of tolerating moderate error rates, they impose a large penalty in weight, power and cost.

It seems clear that regardless of technique employed to reduce soft errors, an accurate means must be developed to estimate soft error rates since large design-penalty trade-offs will hinge on this parameter.

7.4 Shielding Against Cosmic Rays

Spacecraft shielding is not generally effective against cosmic rays. There are, however, specific instances in which it can clearly reduce or increase the soft error rate.

Suppose a spacecraft is in a 13,000 km circular orbit with a low inclination. This spacecraft would sample the particles trapped between $L = 3$ and $L = 3.5$ while always having a geomagnetic cutoff (from eq. 5.5) of

$$P \sim 16/L^2 \sim 1.3 \text{ to } 1.8 \text{ GV}$$

i.e. 180 to 320 MeV/u. Now suppose the electronics are lightly shielded on

one side, say 25 mils of aluminum, and the components are sensitive to helium, or even carbon nuclei. Under these conditions, the trapped helium and CNO (carbon, nitrogen and oxygen) fluxes at low energies, for these altitudes, could be a major cause of soft errors. There are two reasons: first, helium fluxes at this altitude are comparable to Si(p, α)-produced secondary helium fluxes from trapped protons (see Peterson, 1980); second, provided the shielding of the electronics does not exceed about 0.8 inches in any direction, cosmic ray CNO pass through the electronics too fast to have the required stopping power. In this case, only trapped CNO can contribute. Now by increasing the shielding to, at least, 100 mils in all directions, the trapped He, C, N, and O nuclei will probably be excluded and the error rate reduced.

This example is a rather restricted case. A much more general case is for a spacecraft in interstellar space, or nearly so. Suppose that the electronics are sensitive only to stopping iron, and are required to have low soft error rates, even during an anomalously large solar flare. If the electronics can be made to tolerate such a flare, galactic cosmic rays will never produce an unacceptable soft error rate. The spectra of all flares fall steeply from the lowest energies, so that the addition of shielding is especially effective in reducing the flux at the electronics. Furthermore, since iron has a relatively short range [(56/262) X the range of a proton at the same velocity] the shielding will be especially effective in reducing the iron flux at the electronics. Clearly, in such a case, shielding can be beneficial.

Shielding does not always help. Consider a low altitude, 400 km circular orbit with a low inclination such that the spacecraft never goes beyond $L = 3$. Further, suppose that the electronics are only sensitive to stopping iron. Because of this, the trapped protons encountered in the South Atlantic anomaly cannot produce soft errors, because the worst they can do is to produce recoil silicon. There are, of course, heavier nuclei trapped in the radiation belts, even iron, but these are probably rare and low in energy. A minimum of 100 mils of aluminum will probably stop all of these rare nuclei. Such a satellite would not be troubled by soft errors provided it is not too well shielded. The lowest geomagnetic cutoff encountered on the orbit is 320 MeV/u (from eq. 5.5). At this energy an iron nucleus has a range of 880 mils in aluminum. If there is a direction, any direction, looking outward from the electronics through that much material, a cosmic ray iron arriving along such a direction could stop in the electronics and cause an error. All it takes is a structural beam "aimed" at the electronics. Because nearby objects subtend greater solid angles, the electronics may shield themselves. The habit many designers have of placing components in a neat little row can build up a large shielding thickness along that row, especially if it's a row of, say, tantalum capacitors!

From these examples the reader can see that, while shielding can be important, its effects depend on specific mission requirements, orbits and device sensitivities. Indeed, estimating soft error rates is not a simple business!

7.5 The Relative Importance of the Various Components in the Near-Earth Particle Environment.

From what has been said up to now, it is probably clear that given the right set of circumstances (i.e. orbit, tolerable error rate, shielding, and device sensitivity), any of the components we have described could be the dominant source of soft errors. In the real world, however, there are "popular orbits," actual devices and typical missions. In the following paragraphs we will discuss how the environment affects some of these

Consider a 28.5° inclination circular orbit at 300-500 km. This is a typical Eastern Test Range minimum-energy orbit for shuttle sortie or shuttle-deployed free flier payloads. For electronics sensitive to any secondary particle that a proton can produce (see Petersen, 1980), the South Atlantic anomaly will be the problem area, and shielding will not help much against the protons. In this part of the magnetosphere, the proton spectrum is very hard (see Sawyer and Vette, 1976). A little shielding would help against heavier trapped nuclei, but their flux in this orbit may be too low to matter anyway.

If the electronics in this payload cannot be upset by proton-produced secondaries then something like stopping iron nuclei will be necessary and the soft error rate will be dramatically lower. The cosmic ray cutoff for this orbit is ~ 1000 MeV/u. At that energy, it takes 5 inches of aluminum to stop a cosmic ray iron nucleus. Even then only about 20 per cent of them will survive to come to rest without fragmenting in a collision with an aluminum nucleus. Assuming the electronics are shielded with much less than 5 inches of aluminum or equivalent, the only things left to worry about are trapped heavy nuclei, especially iron. They can probably be dealt with by 100 mils or so of shielding. All that remains then is cosmic ray re-entrant albedo, i.e. cosmic rays that skip off the atmosphere, thus evading the geomagnetic cutoff and arriving at the spacecraft with a lower energy than 1000 MeV/u. These events are very rare and can probably be neglected. There is always the anomalous component, if it's singly ionized and if besides oxygen, it contains ions like iron. It could be a problem, but the charge state of the anomalous component is unknown. For the present we don't know if it could contribute, so we can be optimistic and ignore it.

Solar flares could, in principle, cause soft errors in this payload, but they are subject to almost the same geomagnetic cutoff as cosmic rays. If the electronics are so lightly shielded that cosmic rays don't affect them, flares will not either.

Next, consider a low altitude circular orbit of 300 to 500 km again, but this time inclined at 90°, i.e. polar. For electronic components that are sensitive to trapped protons, the problems in the South Atlantic anomaly will be worse. Instead of only brushing through the northern side of the anomaly, as in the previous example, this payload will pass through the heart of the anomaly. The error rate experienced in the anomaly will depend critically on altitude. The proton flux considered here, scales approximately as altitude to the 5th power! At a 300 km altitude, it is almost possible to sneak through under the anomaly.

The southern part of the anomaly, at L values between 2 and 2.5, probably contain enough energetic helium to contribute directly to the error

rate. This is south of the most intense part and the error rate will be lower here, whatever the cause. Extra shielding, 100 mils or so could help here, but it's probably not worth the weight and bother.

While it may be possible to sneak through under the anomaly, there is no way to "sneak through" under the polar clefts. When the spacecraft passes over the magnetic poles, the geomagnetic cutoff goes practically to zero. Depending on the orbital altitude and the sensitivity of the electronics, cosmic rays coming in over the poles may cause a higher error rate than the South Atlantic anomaly. For electronics not sensitive to proton-produced secondaries, cosmic rays will surely be the major cause of soft errors, regardless of altitude.

If this payload is designed to operate during a major flare, its electronics will easily tolerate cosmic rays and the South Atlantic anomaly. The payload should be as heavily shielded as possible, if the electronics are even sensitive to very heavy nuclei. As noted earlier, the shielding is especially effective in stopping these nuclei and reducing their intensity in the steeply falling spectrum of a solar flare.

As a final example, we consider a payload in synchronous orbit with 0° inclination. The geomagnetic cutoff at synchronous orbit is

$$P \sim 16/(6.6)^2 \approx 0.364 \text{ GV}$$

or $\sim 15.2 \text{ MeV/u}$. At this energy, protons and helium nuclei have a range of 50 mils of aluminum; for heavier nuclei it will be even shorter. Clearly, there is no realistic way to shield the electronics so lightly that cosmic ray heavy ions do not stop in the circuits. For cosmic rays and solar flares, it's just as though the spacecraft were in interplanetary space.

As Heinrich (1977) has shown, even 10 g/cm^2 (= 1.5 inches of aluminum) doesn't do much to alter the cosmic ray spectra above 10 MeV/u . Clearly, shielding effectively against galactic cosmic rays is hopeless. Some researchers (Bernart and Stekly, 1964) have suggested using a strong magnetic field coupled with shielding to protect against cosmic rays. We judge such a proposal as heavy, expensive and, worst of all, dubious, since such an artificial magnetic field in space would develop its own magnetosphere filled with trapped particles. The cure could be worse than the disease!

Since this satellite is unprotected by the magnetosphere, it is exposed to solar flare particles. A decision has to be made here. It's much easier to design for a tolerable error rate from cosmic rays than from a major solar flare. If the mission can tolerate being shut down during a major flare, the design problem will be much easier. This may represent a loss of only ~ 2 per cent of the mission time and this has to be traded against the 80-90 per cent data recovery rates that are typical of many space missions. In short, losing data during major flares doesn't cost much in mission time.

There are some payloads that must continue to operate correctly during flares, uninterrupted military missions and scientific experiments to study flares, for instance. For these payloads one must reckon with the model in section 4.0. The mean, worst case, and anomalous case flare spectra are shown in figures 4.2 and 4.3. All these spectra, unlike galactic cosmic rays, are monotonically and rapidly decreasing functions of energy. By comparing the spectra in figure 4.3 with the cosmic ray proton spectrum, figure 2.2, we see that the peak flare flux falls below the cosmic ray background between 200 MeV/u and ~ 1000 MeV/u depending on flare size. Since flares are not generally as rich in the heavier elements as cosmic rays, this crossover may occur at somewhat lower energies when comparing iron spectra.

Now let us assume that the spacecraft designer, faced with the problem of controlling the soft error rate during a flare, resorts to circuits that are relatively "cosmic-ray hard" i.e. only very heavy stopping nuclei are capable of causing errors. He may be able to use components that are so insensitive to soft errors that the problem can be controlled in that way alone. This solution, however, may not be possible within the weight, power and cost constraints. If components which are just sensitive to stopping very heavy nuclei must be used, then shielding can help. Suppose an anomalously large flare occurs with a peak spectrum of the kind shown in figure 4.3. The stopping power of an iron nucleus reaches its peak at about 2 MeV/u. Under 25 mils of aluminum, the flux of iron at this energy will be 6.1×10^5 particles/m² ster. sec. MeV/u. If 100 mils of shielding is provided, the flux behind the shield, again at 2 MeV/u will be 5.8×10^4 particles/m² ster. sec. MeV/u. This is an order of magnitude improvement. Additional shielding will further reduce the flux at 2 MeV/u, but not as rapidly. It would be necessary to add several inches of aluminum to reduce the flare flux to near cosmic ray background levels. While this goal is unreasonable, some trade-off on shielding should be possible.

In these examples we have tried to show that galactic cosmic rays, solar flare particles, trapped protons and possibly even trapped heavy nuclei can be the dominant causes of soft errors under the right conditions. Unless the mission objectives can be economically accomplished with components that are practically "immune" to soft errors, it appears that an accurate estimate of soft error rates will be a critical parameter in deciding the various tradeoffs that must be made in mission planning.

8.0 Conclusions and Recommendations

The published data and their interpretation described in section 7.2 make it clear that intensely ionizing particles can produce soft errors and related phenomena. Furthermore it is well established (May and Woods, 1979) that there is a threshold; a critical charge that must be liberated by the ionizing particle in a very short path length. Below this threshold, soft errors do not occur. For fixed device dimensions and characteristics this threshold becomes a threshold on stopping power, which varies approximately as (the particle's charge)²/(the particle's velocity)². Because electrons are picked up from the medium by a stopping ion, there is a maximum stopping power reached by each ion just before coming to rest. If the threshold is higher than the maximum stopping power of an ion, then it cannot produce a soft error; a more highly charged, i.e. heavier ion will be required.

The critical charge is a key device parameter that helps determine a device's sensitivity to soft errors. For satellite applications, an effort must be made to select devices that are insensitive, i.e., have a high critical charge. This means in turn, that only heavy or very heavy ions can produce errors in such devices.

8.1 Galactic Cosmic Rays

We have made a comprehensive search of the published data on cosmic rays and developed an analytic model for the cosmic ray environment. This model describes the differential energy spectra for cosmic rays at all energies greater than 10 MeV/u and for all nuclei in the periodic table up to nickel. We judge that the model fits the data to ± 20 per cent for hydrogen, helium and the more abundant elements up to neon at energies below 10⁴ MeV/u. For higher energies and less abundant elements the fits are probably accurate to ± 50 per cent. In one important case, the available data were not adequate to define the model well. This is the differential energy spectrum of iron, figure 2.7. There are no data on the spectrum at solar maximum for energies below 900 Mev/u. Secondly the data below 200 Mev/u are very sparse, and only two experiments give results below 100 Mev/u. To emphasize the importance of the iron spectrum below 100 Mev/u, we note that iron nuclei with energies between 50 and 100 Mev/u are just stopping as they exit aluminum shielding with thicknesses in the range of 25 to 120 mils. It is just these stopping iron nuclei that are the most effective in producing soft errors.

Except for the data on the iron spectrum, the galactic cosmic ray data base we used is reasonably complete. The errors in the analytic model we suggest, are generally smaller than some of the other sources of error in the problem.

The model includes the effects of solar modulation, by sinusoidally interpolating between the solar maximum and solar minimum analytic-model spectra. When flux levels must be predicted in the future, such a model has to be employed. If we take our model for solar cycle variations, and compare it with the past, Figure 2.14, we see that it is, at best, only a crude fit to the data. From this figure, it is clear that a major source of error in these predictions is our inability to predict future levels of solar modulation.

The prediction of future levels of solar modulation has received very little attention by the scientific community and yet it appears to be the major source of error in our model of galactic cosmic rays. Comparing the analytic fit to the solar maximum and minimum helium spectra at 50 Mev/u, figure 2.3 with the solar modulation fit and data, figure 2.14, we see that our predictions could be wrong by a factor of 5 at solar maximum, and a factor of 2.5 at solar minimum. The overall accuracy of the model predictions is probably no better than \pm 100 per cent at low energies. Also it should be noted that these low energy cosmic rays are just stopping as they enter the electronic components, i.e. the ones most effective in causing soft errors.

8.2 The Anomalous Component

This little-understood feature in the cosmic ray spectra of certain elements was discussed in Section 3.0. Its presence in the interplanetary medium near earth was obvious from 1972 until 1978. Whether this feature will reappear during the 1983-1989 time frame is unknown. Indeed, since it never went away in the outer solar system, it may always be with us at some level here, near earth. The greatest mystery about the anomalous component is whether it is singly ionized. If it is singly ionized, its presence inside the magnetosphere would be much more widespread. Since the anomalous component is a feature of the low energy part of the cosmic ray spectrum, these nuclei will be most effective in causing soft errors. Their wide spread access to the inner magnetosphere could change the soft error rates on some satellites dramatically. Clearly the charge state of the anomalous component should be established as soon as possible because of its impact on the predictions of soft error rates.

8.3 Solar Flares

About 2 per cent of the time, a major solar flare is in progress, with an associated solar particle event in the interplanetary medium. When these events occur, they will be the dominant source of soft errors for satellites that are not well shielded by the earth's magnetic field. Not all satellites will have to operate during such events, but many will have to continue reliable operation under the heaviest of solar weather conditions.

Section 4.0 addressed the problems to be faced in planning for solar flares. The fundamental problem with flares is the uncertainty we have about their frequency, size distribution, and composition variability. There is a substantial research effort in the field of solar physics being supported by NASA. Several of these research programs are aimed at energetic solar particle measurements, but mostly at energies too low to affect satellite electronics directly. The Office of Naval Research is sponsoring two solar particle experiments from the University of Chicago, but we are unaware of any other research in this area supported by the DoD.

Solar flares have been recognized as the cause of other problems for satellites, in particular, and communications in general, and are the subject of ongoing research. The unanswered questions of special relevance to the soft error problem are: 1) how can we best predict the size and frequency of flares, 2) how can we best characterize their energy spectra, and, 3) perhaps most important, how can we best describe the solar flare composition and its variability.

Besides the major solar flares, there are small flares and particle flux enhancements occurring much more frequently. The uncertainty this introduces into the flux levels at low energies was discussed in section 2.1 based on unpublished IMP satellite data supplied us by Dr. Robert Pyle of the University of Chicago. There have been no publications, to our knowledge, discussing the variability of low energy fluxes. The data base for such a study has, no doubt, already been collected by a number of groups doing research in these areas. All that remains is to analyze the existing data.

8.4 Trapped Particles

There exists a standard model for the trapped proton environment (Sawyer and Vette, 1970). At present, this model describes a static magnetosphere with two states corresponding to solar maximum and minimum conditions. Obviously, the magnetosphere is dynamic with both short term and long term variations in the trapped particle population. No model has been constructed to describe these variations, primarily because the data base does not exist. In spite of this deficiency, studies of the trapped population have been very limited in recent years. Unless this trend is reversed, it is doubtful that a data base, suitable for such a model, will ever be collected.

Besides protons, there are other nuclei trapped in the magnetosphere. Helium, carbon, and oxygen nuclei have all been identified and, no doubt all heavier elements in the periodic table appear to be present as well. While there have been a number of experiments studying these nuclei at very low energies, only four experiments have been performed to examine the fluxes at energies above 10 MeV/u. It is our opinion that the results of these experiments are in disagreement with a steady-state radial diffusion model that has the solar wind as a source, though, this model seems to explain most results reasonably well at lower energies. From the results of these four experiments, it appears that trapped heavy nuclei may contribute to the soft error problem, at least, in some parts of the magnetosphere though possibly only for lightly shielded satellites.

In light of the mysterious origin of these nuclei, the exceedingly scanty experimental data, and their potential impact on spacecraft design, it will be necessary to carry out additional experiments to confirm the earlier results and extend the measurements to obtain a firmer basis for assessing the contribution of trapped heavy ions to the soft errors observed on satellites.

Some final words of caution need to be mentioned about the particle environment in general. We have paid very little attention to nuclei heavier than iron, yet cosmic rays have been detected with charges up to ~ 96 (the element Curium or thereabouts). While these nuclei are rare, they do exist in cosmic rays and they are probably capable of upsetting microelectronic circuits normally thought of as immune to soft errors. Claims of immunity to cosmic ray effects for electronic circuits must, therefore be regarded with some skepticism.

As we explained in the introduction, when the data base is inadequate to describe the environment, a credible worst-case model might be so conservative that it would result in undue preparation for conditions that never occur. We have chosen, instead, to be optimistic and present the

mildest environment that the data will support. The user should then be reasonably guaranteed of actually experiencing an environment close to that predicted. He can be confident that his preparations and precautions were not wasted effort. It is, of course, possible that actual conditions could be far more severe than predicted. Until experiments actually show that speculations concerning these conditions are correct, spacecraft designers must simply take a chance.

9.0 Acknowledgements.

This report has been eight months in preparation. During that time, the authors have been assisted by many others in this work.

We would like to thank Ms. Lorraine Beahm for her assistance in drawing and checking many of the figures for this report. We would also like to acknowledge the generous assistance Mr. Peter Graney and Mr. John Rogers, high school students, and Midshipman Jeff Asher of the U. S. Naval Academy who volunteered their time to do much of the library research and data plotting required in this report.

The authors would like to thank Ms. Jo Lyon for her patience in typing the many drafts of this report.

Finally we would like to acknowledge the advice and encouragement of Dr. N. M. Shapiro throughout the preparation of this report.

REFERENCES

Adams, J. H., Jr., Shapiro, M. M., Silberberg, R. and Tsao, C. H., presented at the Conf. on Cosmic Ray Astrophysics and Low-Energy Gamma-Ray Astronomy, Minneapolis, Sept. 1980a.

Adams, J. H., Jr., Shapiro, M. M., Silberberg, R. and Tsao,, C. H., "Proceedings of the Tenth International Conference on Solid State Nuclear Track Detectors," 1, 1011, 1980b.

Ahluwalia, H. S., 16th Int'l. Cosmic Ray Conf., 12, 182, 1979.

Anand, K. C., Daniel, R., R., Stephens, S. A., Bhowmik, B., Krishna, C. S., Aditya, P., K. and Puri, R. K. Canad. J. Phys. 46, 1064, 1968.

Atallah, K., Cleghorn, T. F., Modlinger, A. and Schmidt, W. K. H. Proc., 13th Int'l. Cosmic Ray Conf., 1, 208, 1973.

Badhwar, G. D., Deney, C L. and Kaplon, M. F., J. Geophys. Res. 74, 369, 1969.

Balasubrahmanyam, V. K., Boldt, E and Palmeira, R. B. R., J. Geophys.Res. 72, 27, 1967.

Balasubrahmanyam, V. K., Ormes, J. F. and Ramaty, R., Proc. 13th Int'l. Cosmic Ray Conf., 1, 163, 1973.

Balasubrahmanyam, V. K., Hagge, D. E., Ludwig, G. H. and McDonald, F. B. Proc. Int. Conf. Cosmic Rays (London) 1, 427, 1965.

Balasubrahmanyam, V. K., Hagge, D. E., Ludwig, G. H. and McDonald, F. B., J. Geophys. Res. 71, 1771, 1966.

Benegas, J. C., Israel, M. H., Klarmann, J. and Maehl, R. C., Proc. 14th Int'l. Cosmic Ray Conf., Munich, 1, 251, 1975.

Bernet, R. E. and Stekly, Z. J. J., Second Symposium on Protection Against Radiations in Space, p. 199, Gatlinburg, Tennessee, 1964.

Bhatia, V. S., Paruthi, S. and Kainth, G. S., J. Geophys. Res. 82, 2419, 1977.

Biswas, S. and Durgaprasad, N., Space Science Reviews, 25, 285, 1980.

Biswas, S., Durgaprasad, N., Nevatia, J., Venkatnaradan, V. S., Goswami, J. N., Jayanthi, U. B., Lal, D. and Mattoo, S. K., Astrop. and Space Sci., 35, 337, 1975.

Biswas, V. S., Lavakare, P. J., Ramadurai, S. and Sreenivasan, N., Proc. Indian Acad. Sci. 65a, 104, 1967

- Blake, J. B., JGR, 78, 5822, 1973.
- Blake, J. B., Fennell, J. F., Schulz, M and Paulikas, G. A., JGR, 78, 5498, 1973.
- Blake, J. B., Fennell, J. F. and Hovestadt, D., JGR, 85, 5992, 1980.
- Blake, J. B. and Friesen, L. M., 15th International Cosmic Ray Conf. 2, 341, 1977
- Bradford, J. N., IEEE Trans., NS-25, 1144, 1978.
- Brown, J. A. C., "The Lognormal Distribution," Cambridge University Press, 1957.
- Brucker, G. L., Chater, W. and Kolasinski, W. A., IEEE Trans., NS-27, to be published,, 1980.
- Burrell, M. O., NASA TN D-6379, Marshall Space Flight Center (1971).
- Caldwell, J. H., Ap. J., 218, 269, 1977.
- Caldwell, J. H. and Meyer, P., Proc. 15th Intl. Cosmic Ray Conf., 1, 243, 1977.
- Caldwell, J. H., Evenson, P., Jordan, S. and Meyer, P., Proc. 14th Intl. Cosmic Ray Conf., 3, 1000, 1975.
- Cameron, A. G. W., Harvard-Smithsonian Center for Astrophysics Preprint Series No., 1357 (1980).
- Casse, M., Koch, L., Lund, N., Meyer, J. P., Peters, B., Soutoul, A. and Tandon, S. N., Proc. 12th Intl. Cosmic Ray Conf. (Hobart) 1, 241, 1971.
- Chan, J. H., Doctoral Dissertation, Univ. of California, Berkeley, September 1976.
- Chan, J. H. and Price, P. B., Phys. Rev. Letters, 35, 539, 1975.
- Cleghorn, T. F., Freier, Phyllis S. and Waddington, C. J., Astrophys. Space Sci. 14, 422, 1971.
- Comstock, G. M., Astropophys. J., 155, 619, 1969.
- Cock, W. R., Stone, E. C. and Vogt, R. E., submitted to Ap. J. Letters, 1980.
- Cornwall, J. M., JGR, 77, 1756, 1972.
- Cumming, A. C., Stone, E. C. and Vogt, R. E., Proc. 13th Intl. Conf. Cosmic Rays, 1, 335, 1973.
- Debrunner, H. and Fluckiger, E., 15th Intl. Cosmic Ray Conf., 11, 251, 1977.
- Dorman, L. I., "Cosmic Rays; Variations and Space Explorations," North Holland Publishing Co., Amsterdam, 1974.

- Durgaprasad, N., Fichtel, P. S. and Guss, D. E., J. Geophys. Res. 72, 2765, 1967.
- Dwyer, R., Ap. J. 224, 691, 1978.
- Fan, C. Y., Gloeckler, G. and Simpson, J. A., Phys. Rev. Letters 17, 329, 1966.
- Fan, C. Y., Gloeckler, G. and Simpson, J. A., Proc. Ninth Intl. Cosmic Ray Conf., 1, 380, 1965.
- Fennell, J. F., Blake, J. B. and Paulikas, G. A., JGR, 79, 521, 1974
- Fermi, E., Phys. Rev. 75, 116ⁿ, 1949.
- Fisk, L. A., Kozlovsky, B. and Ramaty, R., Ap. J. (Letters), 190, L35-L37, 1974.
- Fisk, L. A., J. Geophys. Res., 81, 4646, 1976.
- Fluckiger, E., Debrunner, H. Smart, D. F. and Shea, M. A., 16th Intl. Cosmic Ray Conf., 4, 273, 1979.
- Forbush, S. E., Phys. Rev., 52, 1254, 1938.
- Fritz, T. A., and Spjeldvik, W. N., JGR, 84, 2608, 1979.
- Friedlander, M. W., and Hoppe, M., JGR, 82, 734, 1977.
- Freier, P. S. and Waddington, C. J., J. Geophys. Res. 70, 5753, 1965.
- Freier, P. S. and Waddington, C. J., Phys. Rev. 175, 1641, 1968.
- Freier, P. S., Long, C. E., Cleghorn, T. F. and Waddington, C. J., 12th Intl. Conf. on Cosmic Rays, 1, 252, 1971.
- Freier, P. S., Young, J., Waddington, C. J., Fickle, R., Gilman, C. and Scarlett, W. R., Proc. 16th Intl. Cosmic Ray Conf., (Kyoto) 1, 316, 1979.
- Garcia-Munoz, M. and Simpson, J. A., Acta. Phys. Acad. Sci. Hung. 29, Suppl. 1, 317, 1970.
- Garcia-Munoz, M., Mason, G. M. and Simpson, J. A., 12th Int. Conf. Cosmic Rays, Hobart, 1, 209, 1971.
- Garcia-Munoz, M., Mason, G. M. and Simpson, J. A., Ap. J. (Letters) 182, L81-L84, 1973
- Garcia-Munoz, M., Mason, G. M. and Simpson, J. A., Astrophysics. J. 202, 265, 1975.
- Garcia-Munoz, M., Mason, G. M. and Simpson, J. A., Proc. 15th Intl. Conf. Cosmic Ray Conf., 1, 224, 1977a.

- Garcia-Munoz, M., Mason, G. M. and Simpson, J. A., Ap. J. 217, 859, 1977b.
- Garcia-Munoz, M., Mason, G. M., Simpson, J. A. and Wefel, J. P., Proc. 15th Intl. Cosmic Ray Conf., 1, 230, 1977c.
- Garcia-Munoz, M., Margolis, S. H., Simpson, J. A. and Wefel, J. P., 16th Intl. Cosmic Ray Conf., 1, 310, 1979.
- Golden, R. L., Adams, J. H., Jr., Badhwar, G. D., Deney, C. L., Heckman, H. H. and Lindstrom, P. L., Nature, 249, 814, 1974.
- Gloeckler, George, Rev. of Geophys. and Space Physics, 17, 569-582, 1979.
- Hagen, F. A., Fisher, A. J. and Ormes, J. F., Ap. J. 212, 262, 1977.
- Hagge, D. E., Balasubrahmanyam, V. K. and McDonald, F. B., Canadian J. Phys. 46, S539, 1968.
- Heinrich, W., Radiation Effects, 34, 143-8, 1977.
- Heinrich, W. and Spill, A., JGR, 84, 4401, 1979.
- Hess, Wilmot, N. and Mead, G. D., "Introduction to Space Science," Gordon and Breach, New York 1968.
- Hofmann, D. J. and Winckler, J. R., Phys. Rev. Lett., 16, 109, 1966.
- Hovestadt, D., Gloeckler, G., Fan, C. Y., Fisk, L. A., Ipavich, F. M., Klecker, B., O'Gallagher, J. J. and Scholer, M., JGR Letters 5, 1055, 1978.
- Hovestadt, D., Vollmer, G., Gloeckler, G. and Fan, C. Y., Phys. Rev. Letters, 31, 650-653, 1973
- IGRF-1965, JGR, 74, 4407, 1969.
- Israel, M. H., Klarmann, J., Maehl, R. C. and Binns, W. R., Proc. 13th Intl. Cosmic Ray Conf. (Denver), 1, 255, 1973.
- Israel, M. H., Klarmann, J., Love, P. L. and Tueller, J., Proc. 16th Intl. Cosmic Ray Conf., (Kyoto) 1, 323, 1979.
- Jokipii, J. R., Levy, E. H., and Hubbard, W. B., Ap. J. 213, 861, 1977.
- Jokipii, J. R., Rev. Geophys. and Sp. Sci., 9, 27, 1971.
- Jones, F. C., Ap. J., 229, 747, 1979.
- Juliussen, E., Ap. J., 191, 331, 1974.
- Juliussen, E., Proc. 13th Intl. Cosmic Ray Conf., 1, 178-183, 1973
- Juliussen, E., Meyer, P., Muller, D., Phys. Rev. Lett. 29, 445, 1972.

Julliot, C., Koch, L. and Petrou, N, Proc. Munich Cosmic Ray Conf.,
12, 4118, 1975.

King, J. H., Journal of Spacecraft and Rockets 11, 401-8, 1974.

Klecker, B., Hovestadt, D., Gloeckler, G. and Fan, C. Y., Ap. J.
212, 290-299, 1977.

Kobetich, E. J. and Katz, R., Phys. Rev., 170, 391, 1968.

Kolasinski, W. A., Blake, J. B., Anthony, F. K., Price, W. E., and
Smith, E. C., IEEE Trans., NS-26, 5087, 1979.

Kratschmer, W., 14th Intl. Cosmic Ray Conf., 2, 827, 1975.

Kuznetsov, S. N., Logachev, Y. I., Ryumin, S. P. and
Trebekhovskaya, G. A., 16th Intl. Cosmic Ray Conf., Kyoto, 3, 161,
1979.

Leech, H. W. and O'Gallagher, J. J., Astrophysics, J. 221, 1110,
1978.

Lezniak, J. A. and Webber, W. R., Ap. J. 223, 676, 1978.

Lockwood, J. A., Hsieh, L. and Quenby, J. J., JGR, 80, 1725-34,
1975.

Lund, N., Bulletin of Am. Phys. Soc., 25, 563, 1980.

Lund, N. Rasmussen, I. L., Peters, B., Rotenberg, M., and
Westergaard, N. J., Proc. 14th Intl. Cosmic Ray Conf. 1, 263, 1975b.

Lund, N., Rasmussen, I. L. and Peters, B., and Westergaard, N. J.,
Proc. Munich Cosmic Ray Conf., 1, 257, 1975a.

Maehl, R. C., Ormes, J. F., Fisher, A. J. and Hagen, F. A.,
Astrophysics and Space Sci. 47, 163, 1977.

May, T. C. and Woods, M. H., IEEE Transactions, ED-26, p. 2, 1979.

Mason, G. M., Ap. J., 171, 139, 1972.

Mason, G. M., Fisk, L. A., Hovestadt, D. and Gloeckler, D., Ap. J.
239, 1070, 1980.

Masson, G. M., DNA/DARPA Workshop, "Single Events Radiation
Effects/Soft Errors," 1980.

McDonald, F. B., Teegarden, B. J. Trainor, J. H. and Webber, W. R.,
Ap. J. (Letters), 187, L105-108, 1974.

McDonald, F. B., Van Hollebeke, M.A.I., Trainor, J. H. Lal, N. and
Webber, W. R., 16th Intl. Cosmic Ray Conf. (Japan) 12, 330, 1979.

McIllwain, C. E., JGR, 66, 3681, 1961.

Mogro-Campero, A., JGR, 77, 2799, 1972.

Ormes, J. F., Fisher, A., Hagen, F., Maehl, R. and Arens, J. F., Proc. 14th Intl. Cosmic Ray Conf. (Munich) 1, 245, 1975.

Ormes, J. F. and Webber, W. R., J. Geophys. Res. 73, 4231, 1968.

Ormes, J. F. and Webber, W. R., Proc. 9th Int. Conf. Cosmic Rays (London) 1, 349, 1965.

Orth, C. D., Buffington, A., Smoot, G. F. and Mast, T. S., Ap. J., 226, 1147, 1978.

Panasyuk, M. I., Riezman, S., Sosnovets, E. N., and Filatov, Cosmic Research 15, 887, 1977.

Peeples, J. W. and Every, T. J., Proc. of the 18th Annual Intl. Reliability Physics Symposium, p. 1, 1980.

Petersen, E., IEEE Trans. NS-27, p. 1494-99, 1980.

Pickel, J. C. and Blanford, J. T., Jr., IEEE Trans., NS-25, 1166-71, 1978.

Pickel, J. C. and Blanford, J. T., Jr., IEEE Trans. NS-27, 1980a.

Pickel, J. C. and Blanford, J. T., Jr., DNA/DARPA Workshop, "Single Event Radiation Effects/Soft Errors," McLean, Va., 1980b.

Price, P. B., JGR Letters, 6, 711, 1979.

Price, P. B., Chan, J. H., O'Sullivan, D. and Thompson, A., 13th Intl. Cosmic Ray Conf., 1, 146, 1973.

Pyle, K. R., private communication, 1981.

Ramaty, R., Colgate, S. A., Dulk, G. A., Hoyng, P., Knight, J. W., Lin, R. P., Melrose, D. B., Orrall, F., Paizis, C., Shapiro, P. R., Smith, D. F., Van Hollebeke, M., Proc. of the Second Skylab Workshop on Solar Flares, Chapter 4, in press, Boulder, Colorado, 1980.

Rao, U. R., Space Sci. Rev. 12, 719, 1972.

Reames, D. V. and Fichtel, C. E., Phys. Rev. 162, 1291, 1967.

Retzler, J. P., DNA/DARPA Workshop, "Single Events Radiation Effects/Soft Errors," 1980.

Rossi, B., "Cosmic Rays," McGraw-Hill, New York 1964.

Rubin, A. G., Filz, R. C., Rothwell, P. L. and Sellers, B., JGR, 82, 1938, 1977.

Ryan, M. J., Ormes, J. F. and Balasubrahmanyam, V. K., Phys. Rev. Lett. 28, 985, 1972.

Fygg, T. A. and Earl, J. A., J. Geophys. Res. 76, 7445, 1971.

Sawyer, D. M. and Vette, J. I., Report NSSDC/WDC-A-R and S 76-06, Greenbelt, Md., 1976.

Scarlett, W. R., Freier, P. S. and Waddington, C. J., Univ. of Minnesota Cosmic Physics Report a1777, 1978.

Scarlett, W. R., Freier, P. S. and Waddington, C. J., Ap. Space Sci. 59, 301, 1978.

Scholer, M., Hovestadt, D., Hartmann, G., Blake, J. B., Fennell, J. F., and Gloeckler, G., JGR, 84, 79, 1979.

Shapiro, M. M. and Silberberg, R., Ann. Rev. Nucl. Sci., 20, 323, 1970

Shea, M. A. and Smart, D. F., Report No. AFCRL-TR-75-0185, Hanscom AFB, Mass., 1975.

Shea, M. A., Smart, D. F. and Mooney, W. R., 13th Intl. Cosmic Ray Conf., 2, 1075, 1973.

Silberberg, R. and Tsao, C. H., Ap. J. Suppl. 25, 315, 1973.

Silberberg, R., Tsao, C. H. and Shapiro, M. M. in Spallation Nuclear Reactions and their Applications, edited by B. S. P. Shen and M. Merker, 59, 49, 1976.

Simnett, G. M., Sp. Sci. Rev. 19, 579, 1976.

Simon, M., Spiegelhauer, H., Schmidt, W. K. H., Siohan, F., Ormes, J. F., Balasubrahmanyam, V. K. and Arens, J. F., 16th Intl. Cosmic Ray Conf. 1, 352, 1979.

Smart, D., private communication, 1980.

Smart, D. F. and Shea, M. A., 15th Intl. Cosmic Ray Conf. 11, 256, 1977.

Smart, D. F. and Shea, M. A., JGR, 72, 3447, 1967.

Smith, L. H., Buffington, A., Smoot, G. F., Alvarez, L. W. and Wahlig, W. A., Ap. J. 180, 987, 1973.

Soderstrom, K., Linsatam, S., Behrnetz, S. and Kristiansson, K., Ap. Space Sci. 21, 211, 1973.

Spjeldnik, W. N. and Fritz, T. A., JGR, 83, 654, 1978.

Spjeldnik, W. N. and Fritz, T. A., JGR, 86, 2317, 1981a

Spjeldnik, W. N. and Fritz, T. A., JGR, 86, 2349, 1981b.

Spjeldnik, W. N. and Fritz, T. A., JGR, (in press) 1981c

Stormer, C., Z. Astrophys. 1, 237, 1930.

Teegarden, B. J., McDonald, F. B. and Balasubrahmanyam, V. K. Acta. Phys. Acad. Sci. Hung. 29, Suppl 1, 345, 1970.

- Vallarta, M. S., Phys. Rev., 74, 1837, 1948.
Van Allen, J. and Randall, B. A., JGR, 76, 1830, 1971.
- Van Allen, J., Randall, B. A., and Krimigis, S. M., JGR, 75, 6085, 1970.
- Verma, R. P., Rengarajan, S. N., Tandon, S. N., Damle, S. V. and Pal, Yash, Nature (London), 1, 349, 1965.
- Verma, R. P., Rengarajan, S. N., Tandon, S. N., Damle, S. V. and Pal, Yash, Nature Phys. Sci., 240, 135, 1972.
- Vette, J. I., Lucero, A. B., and Wright, J. A., "Model of the Trapped Radiation, Vol. II: Inner and Outer Zone Electrons," NASA SP-3024, Washington, D. C., 1966.
- Verzariu, P., JGR, 78, 8367, 1973.
- Von Rosenvinge, T. T., Webber, W. R. and Ormes, J. F., Astrophys. Space Sci., 241, 96, 1973.
- Von Rosenvinge, T. T., Webber, W. R. and Ormes, J. F., Astrophys. Space Sci., 5, 342, 1969.
- Wallmark, J. T., and Marcus, S. M., Proc. of the IRE, pp. 286, 1962.
- Webb, G. M. and Gleeson, L. J., Ap. J., 70, 3, 1980.
- Webber, William, Canadian Journal of Physics, 40, 906, 1962.
- Webber, W. R., Proc. 13th Intl. Conf. Cosmic Rays, Denver, 5, 3568, 1973.
- Webber, W. R., 14th Intl. Cosmic Ray Conf., 5, 1597, 1975.
- Webber, W. R., Tenth Int. Conf. Cosmic Rays, 4, 883, 1967.
- Webber, W. R., Damle, S. V. and Kish, J., Astrophys. Space Sci., 15, 245, 1972.
- Webber, W. R., and Lezniak, J. A., JGR, 78, 1979, 1973c.
- Webber, W. R., Lezniak, J. A. and Kish, J., Proc. 13th Intl. Cosmic Ray Conf., 1, 248, 1973b
- Webber, W. R., Lezniak, J. A., Kish, J. C. and Damle, S. V., Nature Phys. Sci., 241, 96, 1973a.
- Webber, W. R. and Ormes, J. F., J. Geophys. Res. 72, 5957, 1967.
- Webber, W. R. and Ormes, J. F., Canad. J. Phys., 46, S883, 1968.
- Webber, W. R., Stone, E. C., Vogt, R. E., 16th Intl. Cosmic Ray Conf., 5, 357, 1979.

White, R. S., "Space Physics," Gordon and Breach, New York, 1970.

Wiedenbeck, M. E. and Greiner, D. E., Ap. J., 239, 139, 1980.

Ziegler, J. F. and Lanford, W. A., Science, 206, 776, 1979.

APPENDIX 1

THE ANALYTIC MODEL FOR THE CHARGED PARTICLE ENVIRONMENT

In the paragraphs that follow we will present a recipe for the near-earth charged particle environment. The recipe consists of a set of equations and tables for computing the differential energy spectra of the most important charged particle populations in the earth's vicinity. These equations were devised to fit the data and are intended to have no physical interpretation. This analytic recipe may be easily programmed for a digital computer of almost any size, and is intended to become a subroutine in a program which will be used to estimate the soft error rates in satellite-borne electronics.

Galactic cosmic rays consist of electrons and the nuclei of all the elements in the periodic table, the first 28 elements are the most important for cosmic ray effects on microelectronics. These particles are from outside the solar system and their flux at low energies is anti-correlated with solar activity (i.e. more cosmic rays at solar minimum). The differential energy spectra in particles per square meter - steradian - second - million electron volts per atomic mass unit (i.e. particles/m² ster.sec. MeV/u) are given in the following paragraphs.

The spectra for protons (hydrogen nuclei), α -particles (helium nuclei), and iron nuclei are given below:

$$F(E,t) = A(E)\sin[W(t-t_0)] + B(E) \quad (1)$$

where

$$W = 0.576 \text{ radian/years},$$

$$t_0 = 1950.6 \text{ A.D. date},$$

and, $t = \text{current date in years}$,

$$B(E) = 0.5 [f_{\min}(E) + f_{\max}(E)], \quad (2)$$

and

$$A(E) = 0.5 [f_{\min}(E) - f_{\max}(E)] \quad (3)$$

f_{\max} and f_{\min} differ only by the choice of constants in the equation,

$$f(E) = 10^m (E/E_0)^a \quad (4)$$

where E is in MeV/u

where,

$$a = a_0 \left\{ 1 - \exp[-X_1 (\log_{10} E)^b] \right\} \quad (5)$$

and

$$m = C_1 \exp[-X_2 (\log_{10} E)^2] - C_2 \quad (6)$$

The values of the constants a_0 , E_0 , b , X_1 , X_2 , C_1 and C_2 are given in Table 1 for each of the elements hydrogen (H), helium (He) and Iron (Fe) for the conditions of solar maximum and solar minimum.

TABLE 1. Constants used Eqs. (1-6) to Compute the Differential Energy Spectra of H, He and Fe at Solar Maximum and at Solar Minimum

Element	a_0	E_0	b	X_1	X_2	C_1	C_2
H-min	-2.2	1.175×10^5	2.75	.117	.80	6.52	4.0
H-max	-2.2	1.175×10^5	2.75	.079	.80	6.52	4.0
He-min	-2.25	7.94×10^4	2.3	.22	.83	5.0	5.0
He-max	-2.25	7.94×10^4	2.3	.155	.83	5.0	5.0
Fe-min	-2.70	1.1×10^5	2.3	.140	.65	7.0	8.0
Fe-max	-2.70	1.1×10^5	2.3	.117	.65	7.0	8.0

The differential energy spectra for carbon (C), oxygen (O), fluorine (F), neon (Ne), sodium (Na), magnesium (Mg), aluminum (Al), silicon (Si), phosphorus (P) and sulfur (S) are obtained by multiplying the helium spectrum [obtained from eq. (1)] by the appropriate scaling factor in Table 2.

TABLE 2: The Ratio of the Abundance of Various Nuclei to Helium

Element	Ratio	Element	Ratio
C	2.5×10^{-2}	Mg	4.7×10^{-3}
O	2.3×10^{-2}	Al	8.3×10^{-4}
F	4.1×10^{-4}	Si	3.5×10^{-3}
Ne	3.5×10^{-3}	P	2.0×10^{-4}
Na	7.0×10^{-4}	S	7.4×10^{-4}

The differential energy spectra for calcium (Ca), cobalt (Co) and nickel (Ni) are obtained by multiplying the iron spectrum [obtained from eq. (1)] by the scale factors listed in Table 3.

TABLE 3: The Ratios of the Abundance of Various Elements to Fe

Element	Ratio
Ca	2.3×10^{-1}
Co	6×10^{-3}
Ni	4.8×10^{-2}

The spectra of the elements lithium (Li), beryllium (Be) and boron (B) are obtained from the helium spectrum, F_{He} , modified by the equation:

$$F^* = \begin{cases} 0.0142 F_{He}, & E < 6000 \text{ MeV/u} \\ 0.67 E^{-0.443} F_{He}, & E \geq 6000 \text{ MeV/u} \end{cases} \quad (7)$$

to obtain the combined spectrum of (Li + Be + B). Eq. (7) is then multiplied by the ratios in Table 4 to obtain the individual elemental spectra.

TABLE 4: The Relative Fractions of Li, Be, and B in the Combined Total Abundance Li + Be + B

Element	Ratio
Li	0.33
Be	0.17
B	0.5

The spectrum of the element nitrogen (N) is obtained by modifying the helium spectrum, F_{He} as shown below:

$$F_N = \{ 6.4 \times 10^{-3} \exp[-.4(\log_{10}E - 3.15)^2] + 5.6 \times 10^{-3} \exp[-.9(\log_{10}E - 0.8)^2] \} F_{He} \quad (8)$$

where E is in MeV/u.

The spectra for the elements chlorine, (Cl), argon (Ar), potassium (K), scandium (Sc), titanium (Ti), vanadium (V), chromium (Cr) and manganese (Mn) are all obtained by modifying the iron spectrum F_{Fe} as shown below:

$$F^* = Q(E) F_{Fe} \quad (9)$$

$$Q(E) = 16[1 - \exp(-.126 E^{0.4})] E^{-0.33} \quad (10)$$

where E is in MeV/u.

Finally F^* the sub-iron spectrum [eq. (9)] is multiplied by the appropriate ratio in Table 5 to obtain the individual elemental spectra.

TABLE 5. The Fractional Abundance of each Element in the sub-iron group

Element	Ratio	Element	Ratio
C1	.07	Ti	.14
Ar	.13	V	.07
K	.09	Cr	.14
Sc	.05	Mn	.10

The recipe given above is correct for quiet periods in the interplanetary medium when only the galactic cosmic rays are present. These conditions are often disturbed, especially at low energies, by small solar flares, co-rotating events, etc. To allow for typical disturbed conditions, we recommend that, below 100 MeV/u, a worst-case spectrum be employed. With 90 per cent confidence, the particle flux should never be more intense than described by this case.

To construct the worst-case spectrum for protons, compute the "H-min" spectrum (using Eq. 4) and then compute $F_{H\text{-worst}}$ as shown below:

$$F_{H\text{-worst}} = [1897e^{-E/9.66} + 1.64]F_{H\text{-min}} \quad (11)$$

This applies for $E < 100$ MeV. For higher energies, you may use the galactic cosmic ray spectrum for the appropriate mission time t [in Eq. (1)].

In like manner, the solar minimum case helium and iron spectra [obtained from (eq. 4)] are multiplied by:

$$28.4 e^{-E/13.84} + 1.64 \quad (12)$$

for $E < 100$ MeV/u. The resulting spectra are employed as described previously to obtain the other elemental spectra, i.e. in the same way as F_{He} and F_{Fe} were used. Again this worst-case only applies for $E \leq 100$ MeV/u, above that energy, use the "pure" galactic cosmic-ray spectra.

In addition to galactic cosmic rays, some particles are believed to be accelerated in the interplanetary medium. The most important of these is called the anomalous component. The contribution of the anomalous component to the helium spectrum is important for cosmic ray effects on microelectronics. We recommend that, for the period 1982-1990, the cosmic ray helium spectrum be modified as follows:

1. Determine the maxima values of the cosmic-ray spectra from Eq. (4) using the He-max and He-min constants from Table 1.
2. Modify eq. (4) so that these maximum values apply for all energies below the energy at which the maxima occurs, i.e., for solar minimum:

$$f^*_{\text{He-min}} = \begin{cases} 0.4 \text{ for } & E < 195 \text{ MeV/u} \\ f_{\text{He-min}} [\text{from eq. (4)}] & E \geq 195 \text{ MeV/u} \end{cases} \quad (13)$$

Make the same kind of modification, $f^*_{\text{He-max}}$ for solar maximum.

3. Combine the resulting spectra as before using eqs. (1-3).

NOTE: This applies only to He, use the regular He spectra eqs. (1-6), for obtaining the spectra of the other elements.

Besides helium, the anomalous component contributes to the oxygen and nitrogen spectra at low energies. For the years 1982-1990, these contributions may be added to the galactic cosmic ray oxygen and nitrogen spectra as follows:

For oxygen, use:

$$f(E) = 6 \times 10^{-2} \exp[-(\ln E - 1.79)^2 / 0.70] \text{ particles/m}^2 \text{ ster.sec.MeV/u} \quad (14)$$

This spectrum crosses over the galactic spectrum at ~ 30 MeV. The two should be blended at that point with eq. (12) replacing the galactic spectrum at lower energies. Similarly for nitrogen:

$$f(E) = 1.54 \times 10^{-2} \exp[-(\ln E - 1.79)^2 / 0.70] \text{ particles/m}^2 \text{ ster.sec.MeV/u} \quad (15)$$

Again, this blends with the galactic cosmic ray spectrum at about 30 MeV/u and should replace it below this energy.

The spectra of the remaining elements are unaffected or affected at too low an energy to matter.

Solar flare particle events are sporadic occurrences lasting 1-5 days. When these events occur they can be the dominant cause of soft errors. For statistical treatment, they are broken into two classes, ordinary (OR) and anomalously large (AL). The probability of having more than a number of events, n , in a time, t , is given by:

$$P(n, t, N, T) = 1 - \sum_{i=0}^n (i + N)! (t/T)^i / [i! N! (1 + t/T)^{1+i+N}] \quad (16)$$

where T and t are in years, and N is the number of flares that have occurred in T years.

For ordinary events, eq. (16) becomes:

$$\text{POR} = P(n, t, 24, 7) \text{ for (1981-1983)}$$

and

(17)

$$\text{POR} = P(n, t, 6, 8) \text{ for (1984-1988)}$$

where there is a probability P_{OR} of having more than n ordinary events in t years. Similarly for anomalously large events:

$$P_{AL} = P(n, t, 1, 7) \quad (18)$$

If there is an unacceptable risk of an AL event then it will be the worst case flare for the mission.

A typical OR event-integrated proton differential energy spectrum is given by,

$$f_{tOR} = 3.3 \times 10^9 (e^{-E/20.2} + 307 e^{-E/3}) \text{ protons/m}^2\text{ster.MeV} \quad (19)$$

where E is in MeV.

Ordinary flares come in a broad range of sizes. With a ~ 90 per cent confidence level, an ordinary flare spectrum should not be worse than:

$$f_{WOR} = 7.6 \times 10^9 (e^{-E/30} + 165 e^{-E/4}) \text{ protons/m}^2\text{ster.MeV} \quad (20)$$

where E is in MeV.

The peak proton flux differential energy spectrum for ordinary events is, typically:

$$f_{tOR} = 1.95 \times 10^4 (e^{-E/27.5} + 173 e^{-E/4}) \text{ protons/m}^2\text{ster.sec.MeV} \quad (21)$$

where E is in MeV.

and no worse than:

$$f_{WOR} = 1.71 \times 10^5 (e^{-E/24.5} + 63.6 e^{-E/4}) \text{ protons/m}^2\text{ster.sec.MeV} \quad (22)$$

with a confidence of ~ 90 per cent.

Using the August 1972 flare as a model AL event, the flare integrated proton differential energy spectrum is:

$$F_{AL} = 2.37 \times 10^{11} \exp[(30-E)/26.5] \text{ protons/m}^2\text{ster.MeV} \quad (23)$$

with E in MeV (King, 1974).

The peak proton flux differential energy spectrum is:

$$f_{AL} = \begin{cases} 9.3 \times 10^9 (dP/dE) \exp(-P/0.10) & E < 150 \text{ MeV} \\ 1.76 \times 10^5 (dP/dE) P^{-9} & E \geq 150 \text{ MeV} \end{cases} \quad (24)$$

in $\text{protons/m}^2\text{ster.sec.MeV}$, where

$$P = [(E/1000)^2 + 1.86 \times 10^{-3}E]^{1/2} \quad (25)$$

and E is in MeV.

The composition of flare particles is also highly variable from flare to flare. Table 6 gives the composition relative to hydrogen for the elements through nickel. Both mean and (90 per cent confidence level) worst cases are given. To obtain the spectrum of any element in a flare just multiply the abundance from Table 6 by the appropriate flare proton spectrum.

TABLE 6. Mean and Worst Case Compositions

	Mean Case	Worst Case		Mean Case	Worst Case
H	1	1	P	2.3×10^{-7}	1.1×10^{-6}
He	2.2×10^{-2}	3.3×10^{-2}	S	1.8×10^{-5}	8.4×10^{-5}
Li	0	0	Cl	1.7×10^{-7}	8×10^{-7}
Be	0	0	Ar	3.9×10^{-6}	1.8×10^{-5}
B	0	0	K	1.3×10^{-7}	6×10^{-7}
C	1.6×10^{-4}	4.0×10^{-4}	Ca	2.3×10^{-6}	1×10^{-5}
N	3.8×10^{-5}	1.1×10^{-4}	Sc	0	0
O	3.2×10^{-4}	1.0×10^{-3}	Ti	1×10^{-7}	5×10^{-7}
F	0	0	V	0	0
Ne	5.1×10^{-5}	1.9×10^{-4}	Cr	5.7×10^{-7}	3.2×10^{-6}
Na	1.6×10^{-6}	6.1×10^{-6}	Mn	4.2×10^{-7}	2.3×10^{-6}
Mg	4.8×10^{-5}	1.8×10^{-4}	Fe	4.1×10^{-5}	2.3×10^{-4}
Al	3.5×10^{-6}	1.4×10^{-5}	Co	1×10^{-7}	5.5×10^{-7}
Si	3.8×10^{-5}	1.6×10^{-4}	Ni	2.2×10^{-6}	1.2×10^{-5}
		Z>28		0	0

There are several good mathematical models for the trapped proton environment. We recommend, "AP-8 Trapped Proton Environment for Solar Maximum and Solar Minimum" by Donald M. Sawyer and James I. Vette, Report no. NSSCS/WDC-A-R and S 76-06, Dec 1976, NASA-Goddard, Greenbelt, Md.

The α particle (helium nucleus) flux in the trapped radiation can be scaled from the proton flux by:

$$\alpha/p = \begin{cases} 2.5 \times 10^{-3} & E < 5 \text{ MeV/u} \\ 8.3 \times 10^{-3} \exp(-E/4.15) & 5 \leq E \leq 10 \text{ MeV/u} \\ 0.957 \exp(-E/1.4) & E > 10 \text{ MeV/u} \end{cases} \quad (26)$$

We suggest that this formula be used throughout the magnetosphere.

Based on the exceedingly scanty data available, trapped nuclei heavier than helium are probably only important, for this study, in the outer belt. For $L > 3$ (McIlwain's L value), and suggest that,

$$F_{CNO} = 3.8 \times 10^4 E^{-5.2} \text{nuclei/m}^2 \text{ster.sec.MeV/u} \quad (27)$$

with E in MeV/u, be used for carbon + nitrogen + oxygen.

The modulation of cosmic ray spectra by the earth's magnetic field requires a more thorough treatment than can be offered here, but some guidance will be provided. The geomagnetic cutoff is a value of magnetic rigidity below which cosmic rays will not reach a specified point in the magnetosphere from a specified direction. The magnetic rigidity, P, in GeV/ec may be computed from the particles' energy using:

$$P = \frac{A}{Z} [(E/1000)^2 + 1.86 \times 10^{-3} E]^{1/2} \quad (28)$$

where E is in MeV/u and A and Z are the atomic mass and charge of the nucleus in question.

The cutoff is most simply computed with:

$$P_C = 15.96/L^{2.005} \quad (29)$$

where L is McIlwain's L parameter

Detailed calculations of the cutoff are available from Shea and Smart (1975). Transmittance functions for satellite orbits may be computed using the techniques described in Heinrich and Spill, (1979).

The transmittance functions of Heinrich and Spill are useful in modulating the cosmic ray spectra. Some thought must be given to their use on solar flare spectra because the flare particle intensity changes on a time scale comparable to or shorter than an orbital period. Also the geomagnetic cutoff is suppressed to some extent during a flare. We recommend that the geomagnetic cutoff during a flare, P_F , be computed from the "quiet time" cutoff P_0 using:

$$\Delta P/P_0 = 0.54 \exp(-P_0/2.9) \quad (30)$$

and

$$P_F = P_0 - \Delta P \quad (31)$$

where P_F , P_0 and ΔP are in GeV/ec.